UNCLASSIFIED
SECURITY CLASSIFICATION OF THIS PAGE

REPORT DOCUMENTATION PAGE

Form Approved
OMB No. 0704-0188
Exp. Date: Jun 30, 1986

1a. REPORT SECURITY CLASSIFICATION: UNCLASSIFIED	1b. RESTRICTIVE MARKINGS: NONE
2a. SECURITY CLASSIFICATION AUTHORITY	3. DISTRIBUTION/AVAILABILITY OF REPORT: Approved for Public Release; Distribution Unlimited.
2b. DECLASSIFICATION/DOWNGRADING SCHEDULE	
4. PERFORMING ORGANIZATION REPORT NUMBER(S): TECHNICAL REPORT BRL-TR- 2763	5. MONITORING ORGANIZATION REPORT NUMBER(S)
6a. NAME OF PERFORMING ORGANIZATION: US Army Ballistic Research Laboratory; 6b. OFFICE SYMBOL (If applicable): SLCBR-TB	7a. NAME OF MONITORING ORGANIZATION
6c. ADDRESS (City, State, and ZIP Code): Aberdeen Proving Ground, Md 21005-5066	7b. ADDRESS (City, State, and ZIP Code)
8a. NAME OF FUNDING/SPONSORING ORGANIZATION: US Army Harry Diamond Laboratory; 8b. OFFICE SYMBOL (If applicable): SLCHD-NW	9. PROCUREMENT INSTRUMENT IDENTIFICATION NUMBER
8c. ADDRESS (City, State, and ZIP Code): 2800 Powder Mill Road, ADELPHI, MD 20783-1197	10. SOURCE OF FUNDING NUMBERS: PROGRAM ELEMENT NO. 62120; PROJECT NO. AH25; TASK NO.; WORK UNIT ACCESSION NO.

11. TITLE (Include Security Classification)
THE BRL-Q1D CODE: A TOOL FOR THE NUMERICAL SIMULATION OF FLOWS IN SHOCK TUBES WITH VARIABLE CROSS-SECTIONAL AREAS.

12. PERSONAL AUTHOR(S)
Opalka, Klaus O.; Mark, Andrew

13a. TYPE OF REPORT	13b. TIME COVERED	14. DATE OF REPORT (Year, Month, Day)	15. PAGE COUNT
Final	FROM _____ TO FY86	October 1986	86

16. SUPPLEMENTARY NOTATION

17. COSATI CODES		
FIELD	GROUP	SUB-GROUP
20	04	

18. SUBJECT TERMS (Continue on reverse if necessary and identify by block number)
Computational Fluid Dynamics; 1-D Hydrocode Computations; Implicit Beam-Warming Scheme; Explicit MacCormack Scheme; Blast-Wave Simulation; Blast-Wave Simulator

19. ABSTRACT (Continue on reverse if necessary and identify by block number)

The BRL-Q1D code is a computer program that uses quasi-one-dimensional, adiabatic, inviscid, numerical algorithms to solve the Euler equations. The governing equations are derived for arbitrary geometry and transformed into a uniform computational grid. An implicit Beam-Warming solver and an explicit MacCormack solver are employed. The input requirements, the code structure and the output options are discussed.

Various flow calculations with the BRL-Q1D code are verified against experiments. Calculations are performed using the experimental geometries and test conditions of a conventional shock tube, a small-scale blast-simulator model and the large blast simulator (LBS) at the Centre d'Etudes de Gramat (CEG), France. The comparison of the computational results with the experimental data validates the numerical flow simulation. In addition, two methods are discussed which are helpful for improving the computational prediction.

20. DISTRIBUTION/AVAILABILITY OF ABSTRACT: ☒ UNCLASSIFIED/UNLIMITED ☐ SAME AS RPT. ☐ DTIC USERS	21. ABSTRACT SECURITY CLASSIFICATION: UNCLASSIFIED
22a. NAME OF RESPONSIBLE INDIVIDUAL: Klaus O. Opalka	22b. TELEPHONE (Include Area Code): (301) 278-6036; 22c. OFFICE SYMBOL: SLCBR-TB-B

DD FORM 1473, 84 MAR — 83 APR edition may be used until exhausted. All other editions are obsolete.

SECURITY CLASSIFICATION OF THIS PAGE

UNCLASSIFIED

18. Subject Terms (continued)

Shock Tubes
Shock Tubes with Variable Cross-Sectional Areas
Blast Waves
Shock Overpressure
Pressure History
Dynamic Pressure

US ARMY
MATERIEL
COMMAND

AD

TECHNICAL REPORT BRL-TR-2763

THE BRL-Q1D CODE: A TOOL FOR THE NUMERICAL SIMULATION OF FLOWS IN SHOCK TUBES WITH VARIABLE CROSS-SECTIONAL AREAS.

Klaus O. Opalka
Andrew Mark

October 1986

US ARMY BALLISTIC RESEARCH LABORATORY
ABERDEEN PROVING GROUND, MARYLAND

Destroy this report when it is no longer needed.
Do not return it to the originator.

Additional copies of this report may be obtained from the National Technical Information Service, U. S. Department of Commerce, Springfield, Virginia 22161.

The findings in this report are not to be construed as an official Department of the Army position, unless so designated by other authorized documents.

The use of trade names or manufacturers' names in this report does not constitute indorsement of any commercial product.

TABLE OF CONTENTS

LIST OF ILLUSTRATIONS

LIST OF TABLES

1. INTRODUCTION

The ban on open-air nuclear testing forces the U. S. Army to look for alternative testing techniques in its effort to qualify military equipment as nuclear survivable. There are currently two techniques used to simulate the blast effects of nuclear explosions involving either high explosives in large quantities, or special shock tubes. The simulation of nuclear blasts with high explosives (HE) is very costly and limited to small yields ($\leq$20 kt). HE tests require much space and their set-up is very time consuming. For these reasons, the use of specialized shock tubes is becoming increasingly attractive. Such facilities, called large blast-wave simulators (LBS), are large enough to accommodate full-sized tactical equipment such as trucks, tanks and helicopters. A few LBS facilities exist abroad, the largest at the Centre d'Etudes de Gramat (CEG), France.[1*] The U. S. Army, in concert with other government agencies, is presently developing a concept of such a facility suitable to simulate both thermal and blast effects of nuclear explosions for the survivability testing of military equipment and for research studies.

During the concept-phase, questions are raised about the necessary size and the expected performance of such a facility, and to answer these questions, a parametric study was initiated. A numerical study seemed preferable to an experimental one, because the latter would take up too much preparation time, and yield too few data points. Among the many numerical fluid-dynamic schemes, the implicit Beam-Warming method[2] stood out for its apparent flexibility and numerical stability. Using this scheme, we developed a quasi-one-dimensional (Q1D) Eulerian code for simulating the flow in shock tubes with arbitrary cross-sectional areas. In this report, the BRL-Q1D code and its underlying theory are described. Computational results are compared with experiments to establish confidence in the performance and the applicability of the code.

2. THEORETICAL CONSIDERATIONS

The BRL-Q1D code incorporates two computational techniques. One is an implicit finite-difference technique developed by Beam and Warming,[2,3,4] the other is an explicit finite-difference technique according to MacCormack.[5] These techniques are applied to the quasi-one-dimensional Euler equations in their weak conservation form. The weak conservation form is retained as the Euler equations are transformed to a uniform, computational grid. Central spatial differencing casts the difference equations into a block-tridiagonal structure which is solved for the increments in the dependent variables at each successive time step.

2.1 GOVERNING EQUATIONS.

The differential Euler equations which describe the one-dimensional flow with variable area may be written in the following form.

$$\frac{\partial(\vec{q}A)}{\partial t} + \frac{\partial(\vec{E}A)}{\partial x} + \vec{H} = 0, \tag{2.1}$$

---

* *References are listed at the end of the report*

where the vectors $\vec{q}$, $\vec{E}$, and $\vec{H}$ are

$$\vec{q} = \begin{bmatrix} \rho \\ \rho u \\ e \end{bmatrix}, \quad \vec{E} = \begin{bmatrix} \rho u \\ (\rho u^2 + p) \\ u\,(e + p) \end{bmatrix}, \quad \vec{H} = \begin{bmatrix} 0 \\ -p\dfrac{\partial A}{\partial x} \\ 0 \end{bmatrix}. \tag{2.2}$$

This set of three scalar equations represents the conservation of mass, momentum, and energy, per unit volume, with the usual notation of ρ as density, u as velocity, e as total energy, and p as pressure. The cross-sectional area, A, may vary with x and/or t, where x is a linear dimension and t is time. As written, the equations are in weak conservation form because of the vector $\vec{H}$. If $A \neq f(x)$, $\vec{H}$ vanishes and the equations revert to the strong conservation form. Either form is shown by Peyret and Viviand[6] to capture shocks accurately in the grid.

The physical, independent variables, x and t, are transformed into a uniformly-spaced computational grid by a general transformation of the form

$$\xi = f(x,t)\,, \; and \quad \tau = t - t_0\,. \tag{2.3}$$

The resulting transformed version of Equation (2.1) is then

$$\frac{\partial \vec{Q}}{\partial \tau} + \frac{\partial \vec{E}}{\partial \xi} + \vec{h} = 0\,, \tag{2.4}$$

where it is noted that the weak conservation form is retained. In Equation (2.4) we define the transformed vectors as follows.

$$\vec{Q} = \vec{q}\tilde{A} = \begin{bmatrix} \rho\tilde{A} \\ \rho u\tilde{A} \\ e\tilde{A} \end{bmatrix}, \quad \vec{E} = \vec{q}\tilde{A}\xi_t + \vec{E}\tilde{A}\xi_x = \begin{bmatrix} \rho\tilde{A}\xi_t + \rho u\tilde{A}\xi_x \\ \rho u\tilde{A}\xi_t + (\rho u^2 + p)\tilde{A}\xi_x \\ e\tilde{A}\xi_t + u\,(e + p)\tilde{A}\xi_x \end{bmatrix}, \quad \vec{h} = \begin{bmatrix} 0 \\ -p\dfrac{\partial A}{\partial \xi} \\ 0 \end{bmatrix}, \tag{2.5}$$

where subscripts x and t imply partial differentiation and $\tilde{A} = A/\xi_x$. The system of Equation (2.4), together with the ideal-gas equation of state

$$p = (\gamma - 1) \cdot \left(e - \frac{\rho}{2}u^2\right), \tag{2.6}$$

where γ is the ratio of specific heats, constitutes the governing set of one-dimensional Euler equations with arbitrary geometry.

2.2 IMPLICIT NUMERICAL SCHEME

These equations are numerically applied to the variable-area shock-tube problem using the implicit "Delta" formation of Warming and Beam.[9] Implicit time differencing and central spacial differencing are employed to evaluate the derivative terms in Equation (2.4) while the source term, $\vec{h}$, is evaluated explicitly. Equation (2.4) then takes the following difference form.

$$\vec{Q}_j^{n+1} - \vec{Q}_j^{n} + \frac{\Delta\tau}{2\Delta\xi}\left(\vec{E}_{j+1}^{n+1} - \vec{E}_{j-1}^{n+1}\right) + \Delta\tau\,(\vec{h})_j^{n} + O(\Delta\tau^2, \Delta\xi^2) = 0 \tag{2.7}$$

where the subscript "j" refers to a specific grid point and the superscript "n" to a time step. The terms containing the vector $\vec{E}$ are non-linear functions of the conserved flow variables $\vec{Q}$, and the system of Equation (2.7) can be solved by iteration. However, as suggested by Lomax,[7]

Equation (2.7) can be solved directly with only one inversion when these terms are locally linearized. This can be shown to be equivalent to one iterative step[2] while the formal accuracy of Equation (2.7) is retained. Performing the local linearization and defining the increment in the variable $\vec{Q}$ by

$$\Delta \vec{Q}_j = \vec{Q}_j^{n+1} - \vec{Q}_j^n \,, \tag{2.8}$$

one obtains the "Delta" form of the algorithm in matrix notation:

$$\left[\mathbf{I} + \Delta\tau\delta_\xi \mathbf{A} \right]_j^n \cdot (\Delta \vec{Q})_j = - \Delta\tau\delta_\xi (\vec{E})_j^n - \Delta\tau (\vec{h})_j^n \,, \tag{2.9}$$

where the bold character indicates a $k \times k$ matrix and δ_ξ indicates central spacial differencing. The above notation is favored by Beam and Warming[3,4] and clearly points to the solution in terms of the flow variable increment $\Delta\vec{Q}$. The solution of the dependent variables at the next time step, therefore, is

$$\vec{Q}_j^{n+1} = \vec{Q}_j^n + \Delta \vec{Q}_j. \tag{2.10}$$

In Equation (2.9), $\mathbf{I}$ is the identity matrix and $\mathbf{A}$ is the Jacobian of the convective terms with respect to the flow variables, $\partial\vec{E}/\partial\vec{Q}$. The notation in Equation (2.9) requires the dot product to be carried out prior to the spacial differencing. Although the "Delta" formation leads to numerical efficiency and analytical simplicity, it should be pointed out that Briley and McDonald[8] were first in extensively applying the local-linearization concept and implementing the algorithm in its "Non-Delta" form. In the actual implementation of Equation (2.9), the left-hand term in brackets is a tridiagonal system which is easily solved.

2.3 EXPLICIT NUMERICAL SCHEME

The Beam-and-Warming Algorithm is generally preferred as the robust solution technique for stiff partial-differential equations. For the unsteady problems treated in the BRL-Q1D code, however, it was found that the MacCormack Explicit scheme captures the shock within the least number of grid points and consumes the lesser amount of machine time. For this reason, it is presented here as the preferred method where resolution of surface discontinuities is required.

The MacCormack explicit scheme is a second-order, non-centered, predictor-corrector scheme[5] that alternatively uses forward and backward differences for the two steps as follows. In the predictor step, $\vec{Q}$ is defined by

$$\vec{Q}_j^{\overline{n+1}} = \vec{Q}_j^n - \Delta\tau \left(\Delta_\xi \vec{E}_j^n\right) . \tag{2.11}$$

In the corrector step, the new $\vec{Q}$ is defined by

$$\vec{Q}_j^{n+1} = \vec{Q}_j^{\overline{n+1}} + \vec{Q}_j^n - \Delta\tau \left(\nabla_\xi \vec{E}_j^{\overline{n+1}}\right) + \epsilon \vec{D}_j^n \,. \tag{2.12}$$

In both equations, the barred superscripts refer to predicted values; in particular, $\vec{E}_j^{\overline{n+1}}$ implies that the flux vector is evaluated using elements of the predicted Q-vector. The symbols Δ and ∇ are used as the standard forward and backward difference operators, respectively. The quantity $\vec{D}$ represents a fourth-order dissipation term, the effect of which is governed by an empirical constant ϵ. The dissipation term is described in the following section.

2.4 STABILITY CRITERION AND DISSIPATION

The typical stability limitation for the system of Equation (2.9) is the Courant, Friedrichs and Lewy (CFL) stability criterion.[5] Application of this criterion prevents any small disturbance (i.e. sound wave) from traveling farther than one cell width in the grid in one time increment.

$$C_N = \left(|\vec{u}| + a\right) \frac{\Delta t}{\Delta x} \leq 1. \tag{2.13}$$

The CFL-criterion is used in the BRL-Q1D code to determine the time step Δt from the smallest cell width in the grid Δx using an empirically determined value for the Courant number C_N.

To control phase errors associated with the highest frequencies, a fourth-order dissipation term is explicitly added to Equation (2.1). This term is of the following form.

$$\left.\frac{\partial^4 Q}{\partial \xi^4}\right|_j \approx \frac{Q_{j+2} - 4Q_{j+1} + 6Q_j - 4Q_{j-1} + Q_{j-2}}{(\Delta\xi)^4} = (\Delta_\xi \nabla_\xi)^2 \, Q_j \,, \tag{2.14}$$

where Δ and ∇ represent forward- and backward-difference operators respectively. The final form of the computational algorithm which has been programmed is

$$\left[\mathbf{I} + \Delta\tau\delta_\xi \mathbf{A}\right]_j^n \cdot (\Delta \vec{Q})_j = -\Delta\tau\delta_\xi (\vec{E})_j^n - \Delta\tau (\vec{h})_j^n + \epsilon \, (\Delta_\xi \nabla_\xi)^2 \, \vec{Q}_j^n \,. \tag{2.15}$$

Since the order of the dissipation term is higher than the order of the truncation error of the model difference equation, formal accuracy is maintained. At boundary grid points the dissipation is of second order.

2.5 INITIAL AND BOUNDARY CONDITIONS

The variables in the governing equations were non-dimensionalized by the following relationships.

$$\hat{\tau} = \tau a_1 / L \,, \quad \hat{\rho} = \rho/\rho_4 \,, \quad \hat{p} = p/\rho_4 a_1^2 \,, \quad \hat{\xi} = \xi/L \,, \quad \hat{u} = u/a_1 \,, \quad \hat{e} = e/\rho_4 a_1^2 \,. \tag{2.16}$$

The subscripts 1 and 4 refer to the initial atmospheric and driver conditions, respectively. L is the reference length of the shock tube, and a is the sound speed. The computation is then initialized with the following conditions,

$$\hat{\rho}_4 = 1 \,, \quad \hat{p}_4 = \frac{T_{41}}{\gamma} \,, \quad \hat{e}_4 = \frac{T_{41}}{\gamma\,(\gamma-1)} \,, \tag{2.17}$$

$$\hat{\rho}_1 = \frac{T_{41}}{P_{41}} \,, \quad \hat{p}_1 = T_4 \frac{1}{\gamma\, P_{41}} \,, \quad \hat{e}_1 = \frac{T_{41}}{\gamma\,(\gamma-1)} \,. \tag{2.18}$$

where T_{41} and P_{41} are the initial temperature and pressure ratio across the diaphragm of the shock tube.

At the endpoints of the grid, boundary conditions were defined. The reflective boundary at the left-hand side of the grid (i. e. the closed end of the driver) was computationally modeled by means of image points, such that $\rho_1 = rho_3$, $u_1 = -u_3$, $u_2 = 0$, and $e_1 = e_3$. At the right-hand side of the grid (at the open end of the expansion tube) boundary conditions for outflow as well

as for inflow were considered. For outflow, the static pressure is specified; for inflow, the static pressure and the density are specified. The remaining flow variables are then computed from one-sided differences at the exit plane using backward differencing in space and forward differencing in time.

3. BRL-Q1D CODE DESCRIPTION

The BRL-Q1D code was developed to study the flow in complex shock tubes with arbitrary area changes. This development was done in view of simulating in a simple manner the multiple-driver CEG-LBS[1] in France and subsequently to study other LBS designs. This chapter discusses the input options and the basic structure of the code. The user's input instructions are given in the Appendix.

3.1 SHOCK-TUBE CONFIGURATIONS

A variety of shock-tube geometries can be accommodated by the code by combining and altering the basic components of the shock tube: Driver, diaphragm section, and expansion tube. Figure 1 illustrates some of the possible configurations.

3.1.1 Drivers

The driver may be shaped as a cylinder, a series of up to four cylinders, each with different diameter, or as a frustrum of a cone. The driver diameter is independent of the diameter of the expansion tube and may be larger, equal, or smaller. The cylindrical driver may be equipped with a series of baffles each of which is modeled as a parabolic constriction. The driver length may be chosen at the discretion of the user.

3.1.2 Diaphragm Section

The diaphragm section may be just the locus of the diaphragm, or a convergent/divergent nozzle with the diaphragm located in the throat area. A throttled diaphragm opening may be modeled with a parabolic area constriction about the diaphragm location. Instead of an instantaneously opening diaphragm, or in combination with it, the user may define a fast-opening and/or closing blast valve.

3.1.3 Expansion Tube

The expansion tube (or, driven tube) may be of any length, but is assumed to have a constant diameter which is used as a reference value. A blockage in the test-section area may be modeled as a parabolic area constriction. At the open end of the expansion tube, a rarefaction-wave eliminator (RWE) may be modeled as a linear area constriction which may be varied linearly with time.

3.2 GRIDDING TECHNIQUES

Three gridding methods are presently incorporated in the BRL-Q1D code; they are linear, multi-linear and non-linear gridding as illustrated in Figure 1.

(a) Conventional Shock Tube with 25% Blockage in Test Section

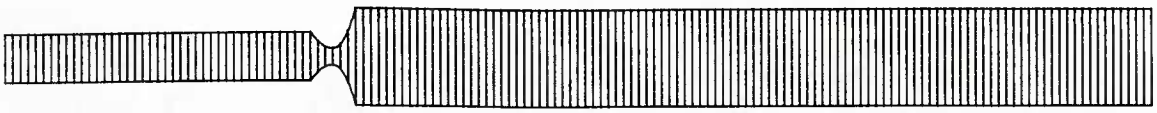

(b) Shock Tube with Valve (modeled as Parabolic Constriction) - Linear Grid

(c) Shock Tube with Baffled Driver and Converging/Diverging Nozzle

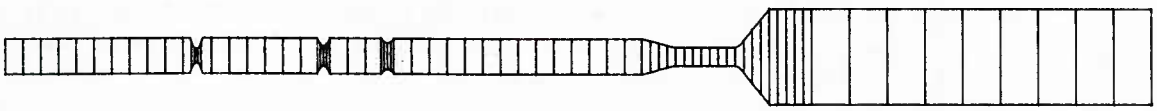

(d) Baffled Driver Detail - Multi-Linear Grid

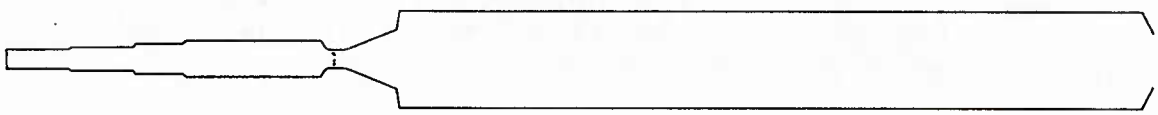

(e) Shock Tube with Stepped Driver, Nozzle and RWE

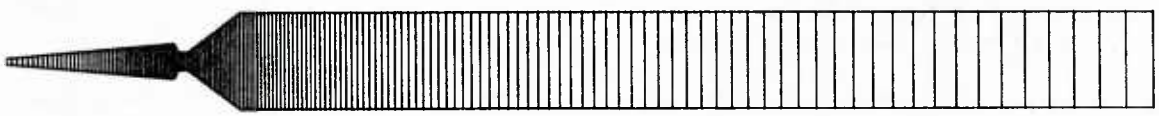

(f) Shock Tube with Conical Driver and Nozzle - Non-Linear Grid

Figure 1. Quasi-One-Dimensional Geometries and Numerical Grids

3.2.1 Linear Grid

The simplest method is a grid of constant cell width (Figure 1b). It is established by dividing the number of grid points into the total length of the shock tube. This method is sufficient for geometries with moderate and gradual changes of the cross-sectional area. A small number of grid points may be chosen for a "quick and dirty" calculation. But for an accurate, converging solution, a high number of grid points (>600) is required.

3.2.2 Multi-Linear Grid

The second method allows clustering the grid points in critical areas by superimposing a fine grid over the basic, coarse grid (Figure 1d). This method is to be used when there are more than one critical areas in the shock tube, e. g. when there are baffles in the driver, or when the driver length is short compared to the total length, and an RWE is defined at the other end of the shock tube. This method saves grid points but requires a greater number of time steps than the first method because the time step depends on the smallest cell size in the grid which has been generated by the clustering.

3.2.3 Non-Linear Grid

The third method allows clustering about a single critical area as e.g. the convergent/divergent nozzle (Figure 1f). Typically, the diaphragm location would be chosen as the cluster point. This method is particularly convenient when the initial pressure ratio across the diaphragm is high and the shock has to be stretched over a few cells to avoid instabilities (i.e. negative density) in the computation. But the user must make sure that there are no other critical areas far away from the clustering location which could be denuded of a sufficient number of grid points. To help the user with this judgement, a graph of maximum and minimum cell size versus the clustering parameters was developed.

3.2.4 Choosing the Clustering Parameters.

The clustering function used for the j-th grid point is

$$X_j = \frac{1}{\beta} \sinh \left[\ln C_2 + \frac{j-2}{j_{\max}-2} (\ln C_1 - \ln C_2) \right] + X_{clust} \tag{3.1}$$

where C_1 and C_2 are the following functions,

$$C_1 = \beta (1 - X_{clust}) + \sqrt{\beta^2 (1 - X_{clust})^2 + 1} \tag{3.2}$$

and

$$C_2 = -\beta X_{clust} + \sqrt{\beta^2 X_{clust}^2 + 1} \tag{3.3}$$

Since the clustering function is already programmed into the code, it was easy to execute a series of calculations with a single time step to find the value of the maximum cell size at the location farthest away from the cluster point, as well as the value of the minimum cell size at the cluster point as a function of the two input constants β and X_{clust}. These values were then normalized by the average cell size,

$$\overline{\Delta x} = L_{ref} / (j_{\max} - 2) \tag{3.4}$$

and plotted versus β for constant X_{clust} (Figure 2).

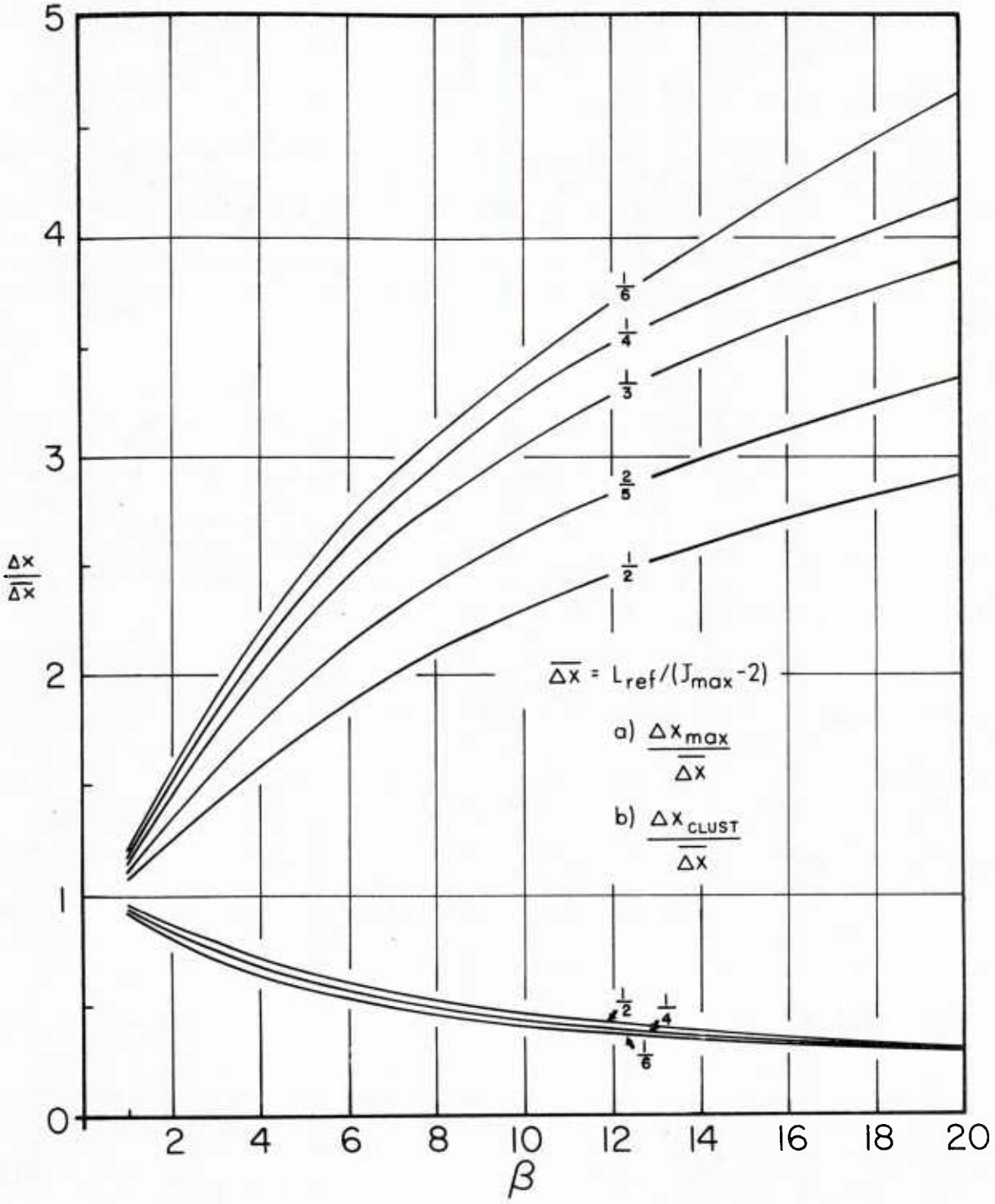

Figure 2. Grid-Cell Size as a Function of β and X_{clust}.

For given β and X_{clust}, the graph will yield the smallest and the largest cell size in the grid. Conversely, for a known cluster location and a predetermined critical cell size, the graph will yield the required β-factor. The critical cell size may be chosen at the clustering point (minimum), or at the point in the grid farthest away from it (maximum).

3.3 CODE STRUCTURE

The BRL-Q1D code is an algorithm for implicitly or explicitly solving the quasi-one-dimensional (Q1D) Euler equations with arbitrary geometry. The code was written in FORTRAN 77 to be executed on the CYBER system at the BRL. Another version of the code was adapted for execution on the Vax 11/780.

3.3.1 The Main Program

The main program has two functions: It instructs the user on how to use the code, and it coordinates the information flow by calling the appropriate subprograms. The user instructions are contained in a comment section which is located at the head of the main program. They are presented in the Appendix (page 55-61). Secondly, the main program serves as a calling program controlling the information flow which is charted in Figure 3.

At the start, the program reads the necessary input data which are contained on from six to twenty-one card images depending on the complexity of the shock-tube configuration. Several cases of flow computations may be stacked in sequence; the program will continue to read a new set of input data every time a computation has been finished. After the input data have been read they are normalized and reflected back to file OUTPUT (see pages 64-66 in the Appendix). Next, a finite-difference grid is layed-out according to the specified grid parameters. Then the cross-sectional areas and the initial flow conditions are defined at all grid point. The user then has the option of writing these initial conditions to file OUTPUT and/or to file TAPE15 for later plotting.

The time loop is entered and a new time step (Δt) is calculated. Now the flow variables are calculated for the new time at all interior points of the grid using either the implicit Beam-Warming, or the explicit MacCormack scheme. Then the flow variables are defined at the boundaries and the flow variables may be written to files OUTPUT and/or TAPE15 as chosen by the user. Finally, the time-dependent areas in the valve, or the RWE are redefined and control then returns to the beginning of the time loop.

There are two checks incorporated in the time loop in order to prevent involuntary abortion of the computation by the central processor. The first is a check on the size of the time step. We observed in some computations that the time step would go to zero because of excessive local flow velocities. When this happened, an overflow condition occurred which caused the job to abort. Therefore, a conditional loop exit based on the size of the time step was introduced which prevents this overflow condition from occurring and allows the computation to conclude normally. The second check is made on the flow density. A negative density is physically unreal and may be caused by too large a time step. Once a negative density occurs, the time loop is exited and the computation concludes normally.

Upon conclusion of the time loop, a set of blast-wave characteristics for the pressure history is determined which characterize the simulated blast wave relative to free-field blast waves. The pressure, density and velocity histories (versus time) are written to files OUTPUT and/or TAPE16 together with these blast-wave characteristics. Control then returns to the beginning of the main program where an attempt is made to read the next set of input data. If an end-of-record mark is encountered instead, the program stops executing.

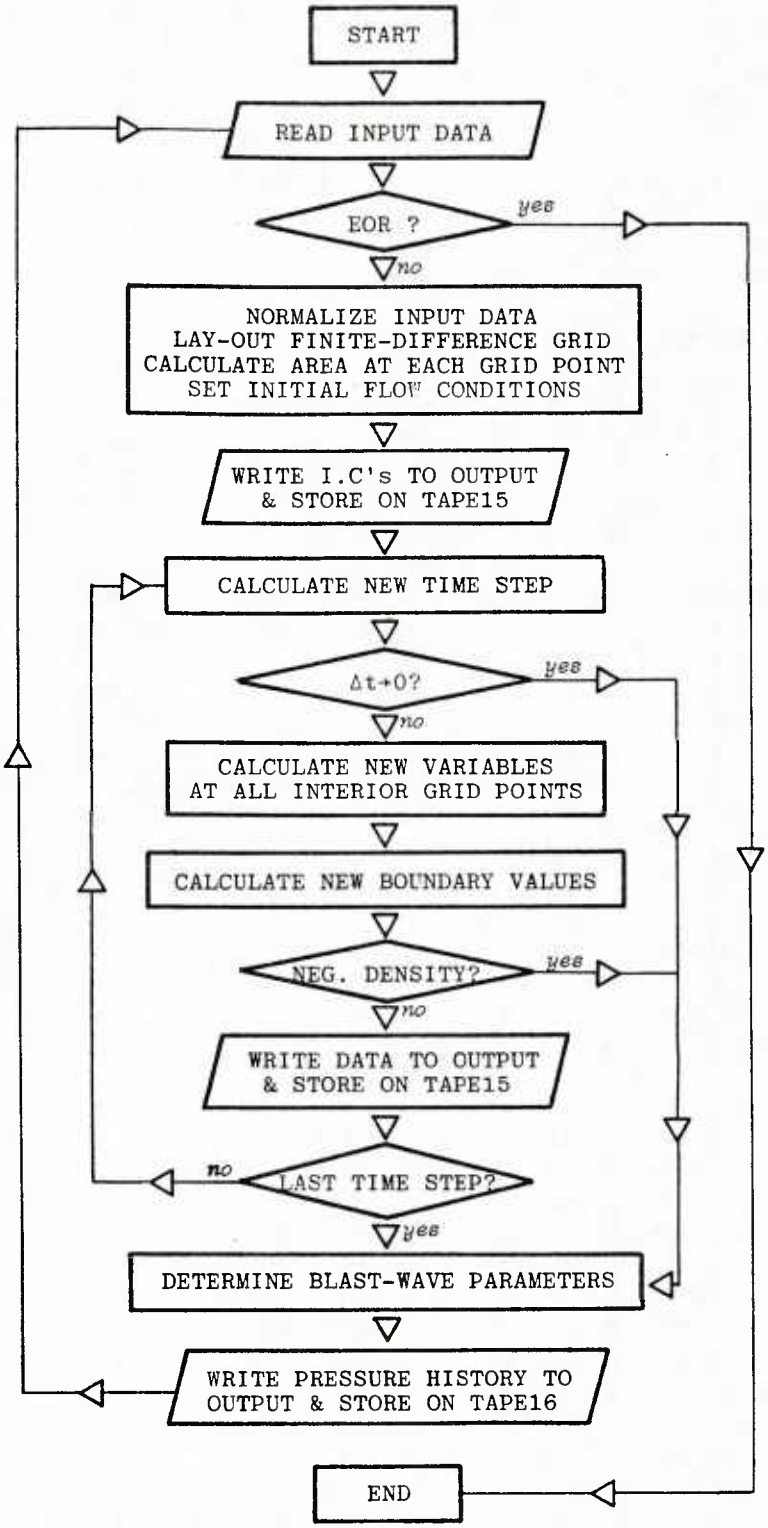

Figure 3. Basic Information-Flow Structure in the BRL-Q1D Code.

3.3.2 The Subprograms

There are presently 25 user-defined subprograms in the BRL-Q1D code, each of which performs one particular aspect of the computation. All but one subprogram are subroutines. The first eight subroutines are related to the input; they set up the computation. The next nine subroutines constitute the Q1D-algorithm proper; they carry out the computation. The last eight subprograms prepare and store the output data. The names and purposes as well as the calling routines of all these subprograms are as follows.

READIN	This SUBROUTINE reads the input data from card images stores them in common and echoes them to output.	MAIN
NORMAL	This SUBROUTINE normalizes the physical input data. areas: Ar → Ar/L_{ref}^2 lengths: X → X/L_{ref} diameters: D → D/L_{ref} time: t → ta_{amb}/L_{ref}	MAIN
MULTLIN	This SUBROUTINE defines a multi-linear grid-point distribution in the computational scheme, and transforms the x-coordinate from the physical to the computational (ξ-) plane, when MTRX = 2.	MAIN
METRIX	This SUBROUTINE defines the grid-point distribution in the computational scheme, and transforms the x-coordinate from the physical to the computational (ξ-) plane when MTRX $\neq$ 2.	MAIN
AREA	This SUBROUTINE determines the cross-sectional areas at all grid points.	MAIN
ARVA	This SUBROUTINE defines the areas in the blast valve as a function of time.	MAIN
ARWE	This SUBROUTINE defines the areas in the rarefaction -wave eliminator (RWE).	MAIN
DRIVOL	This subroutine computes the reference area and the driver volume.	MAIN
INITIA	This SUBROUTINE sets the initial conditions at each grid point. The dependent variables of Euler's conservation equations are stored in the Q-array: Q1 = $\rho \cdot Ar$ (mass) Q2 = $\rho \cdot u \cdot Ar$ (momentum) Q3 = $e \cdot Ar$ (energy)	MAIN
EIGEN	This SUBROUTINE finds the largest velocity gradient in the grid and determines the time step, Δt, from the CFL stability criterion for compressible flow.	MAIN

EULERI	This SUBROUTINE solves the Euler equations using the Beam-Warming implicit scheme which involves the inversion of the block tridiagonal matrix of the flow equations. This subprogram calls subroutines SMOOTH, FILTRX, BTRI and BC.	MAIN
MACCOR	This SUBROUTINE solves the Euler equations using the explicit MacCormack technique. This subroutine calls subprograms BCS, SMOOTH AND BC.	MAIN
SMOOTH	This SUBROUTINE does fourth order smoothing for interior grid points, $2 < j < j_{max}-1$, and second order smoothing at the grid points $j = 2$ and $j_{max}-1$.	EULERI MACCOR
FILTRX	This SUBROUTINE fills the block-tridiagonal A-matrix for the implicit solution.	EULERI
BTRI	This SUBROUTINE inverts the block tridiagonal matrix (Beam-Warming solution). Each block is a 3x3 element matrix.	EULERI
BCS	This SUBROUTINE determines the flow-field parameters at the right (=open) and left (closed) boundaries for MacCormack's predictor step.	MACCOR
BC	This SUBROUTINE defines the flow-field parameters at the right, open-end (with RWE) and left, closed-end boundaries of the shock tube at the n-th time step.	EULERI MACCOR
WRIT	This SUBROUTINE writes the geometrical shock-tube parameters and the gas parameters to file OUTPUT.	MAIN BC
WRITXP	This SUBROUTINE prints arrays, 10 numbers per line, mixed with lines of output denoting constant-value strings.	WRIT
PLOTX	This SUBROUTINE writes gas parameters versus X on file TAPE15 for later plotting.	MAIN
OUTSTA	This SUBROUTINE converts gas parameters at test station XSTA(J) to dimensional values and stores them in arrays for later plotting and/or printing.	MAIN
IMPULS	This SUBROUTINE finds the time of shock arrival, the shock overpressure and the positive-phase duration at test station XSTA(J). It determines the static and dynamic pressure impulses using Simpson's rule of integration and calculates the equivalent nuclear weapon yield for both impulses. This subroutine calls subprogram DVDINT.	MAIN
BASER4	This BLOCK DATA subprogram specifies the data base for a selected nuclear blast-wave reference.	IMPULS

DVDINT	This SUBROUTINE does divided-difference interpolation. The arguments have been tabulated in descending order.	IMPULS
OUTPOT	This SUBROUTINE writes the gas parameters which were determined at the test station by subprogram OUTSTA, to files OUTPUT and TAPE16 for later plotting.	MAIN

3.3.3 Code Execution

The BRL-Q1D code is typically executed on the CYBER 7600 at BRL which runs under the SCOPE 2 operating system of CDC. It requires 67,303 words octal in Small-Core Memory (SCM) and 575,550 words octal in Large-Core Memory (LCM). The CPU-time required for execution is less than 1/8 ms per grid point per time step when the code is compiled with optimization level 2. Two sample job streams are shown in the Appendix (page 62-63).

The output is stored on two tape files (TAPE15 and TAPE16) which may be stored on disc for later reference and serve as input to two plotting codes which are executed separate from, and subsequent to, the BRL-Q1D code. This separation was chosen to limit the SCM field length required for execution. Although a request for greater field length can be included on the job card, it is undesireable because it delays the job execution until the requested memory is made available by a human operator.

3.4 OUTPUT OPTIONS

The results of the Q1D computation are printed in tabulated form or stored on disc for subsequent plotting. Sample tabulations and plots are presented in the Appendix.

3.4.1 Tabulated Output

There are two types of printed output. For data analysis, the complete arrays of density, velocity and pressure are printed out at user-defined time steps together with the arrays of grid-point location (X), $\partial\xi/\partial x$ (XIX), areas (AR) and its derivatives, $\partial A/\partial x$ (ARX) and $\tilde{A}$ (ART). See the example in the Appendix (page 67-74). For plotting, these arrays are written to disk via local file TAPE15 at user-defined time steps.

The pressure history is printed in tabulated form at the end of the computation for user-defined time intervals. It contains a heading with useful summary data like shock-arrival time, peak static overpressure, positive-phase duration and static-overpressure impulse. In the table, the static (side-on) overpressure and impulse, the dynamic pressure and impulse, the flow velocity and the density are listed versus time. A sample listing is shown in the Appendix (page 75-76). The pressure history is also stored on disc for later plotting if the user so chooses. The local file for this record is TAPE16.

3.4.2 Plotted Output

Two plotting codes are available, PX1DPLT for plotting pressure, density or velocity versus distance, and PT1DPLT for plotting pressure and/or density versus time. Both plot codes are written in FORTRAN 77 using the DISSPLA-Version 8.2 plotting package.[10] Both codes contain a comment section with the necessary user instructions. They may be obtained from the authors upon request.

The density-versus-distance plot is very useful for studying the wave propagation in the shock-tube flow. The incident shock, the contact surface, the recompression shock and various shock reflections can be recognized easily in the sample plot shown in the Appendix (page 77). The data given in the heading serve the identification of the plot. Below the plot title are listed from 1 to 6 test stations ($XSTA_i$), the driver volume and pressure and the reference length of the shock tube. In the second, right-adjusted column are listed the case identifier and the plot number, the offset value, Δy, for multiple-curve plots, and comments on shock stretching and grid clustering when applicable. A sketch of the shock-tube configuration is drawn below these data and above the plot with or without grid indication.

A sample plot of a pressure history is shown in the Appendix (page 78). The heading data specify the shock-tube dimensions in column 1, the test conditions in column 2 and the blast-wave characteristics in column 3. The shock-tube dimensions listed under the heading include the case identification, the total (i.e., Reference) length of the facility (L-ref), the driver length (L-drv) and volume (V-drv), the length of the expansion tube (L-dvn) and the length of the RWE (L-rwe).

The test station and initial conditions are listed in column 2. The pressure history is recorded at the test section, X-sta, the location of which is given in metres from the exit of the divergent nozzle. The initial conditions include the driver pressure (P-drv), the ambient, atmospheric pressure (P-amb), the ambient Temperature (T-amb) and the temperature ratio across the diaphragm (T_4/T_1).

The third column lists the blast-wave characteristics, shock overpressure (P-so), shock-arrival time (t-a), positive-phase duration (PPD), the static-overpressure impulse (I-so), the peak dynamic pressure (Q-s) and the dynamic-pressure impulse (I-dyn). The values in parentheses are the related free-field data for PPD and weapon yield. They were obtained by interpolation from the reference data base as functions of the shock overpressure.

4. RESULTS AND DISCUSSION

This chapter presents the results of several computations of the flow in conventional shock tubes and in shock tubes with varying crossectional area.

4.1 SIMULATION OF FLOW IN CONVENTIONAL SHOCK TUBES

Figure 4 shows a comparison of four computations with experimental data from the BRL-24" shock tube.[11,12] The test conditions are listed in Table I. Also listed are three blast-wave characteristics which were gained from the pressure curves in Figure 4. These are the shock overpressure, p_{so}, the positive-phase duration, t_+, and the static-overpressure impulse, I_{so}.

From the comparison of the computational and experimental values of these blast-wave characteristics we learn that the computation predicts a higher shock overpressure than the experimental value. At the same time, the computational driver empties faster leading to shorter positive-phase durations. This is to be expected from the computation because the inviscid Euler equations do not account for flow losses.

The positive area under the static-overpressure curve in Figure 4 was then integrated to find the static-overpressure impulse. In the code, this was done numerically, using the trapezoidal rule. For the experimental records, it was done graphically. The computational and experimental values are close, although differences should be expected because of the different,

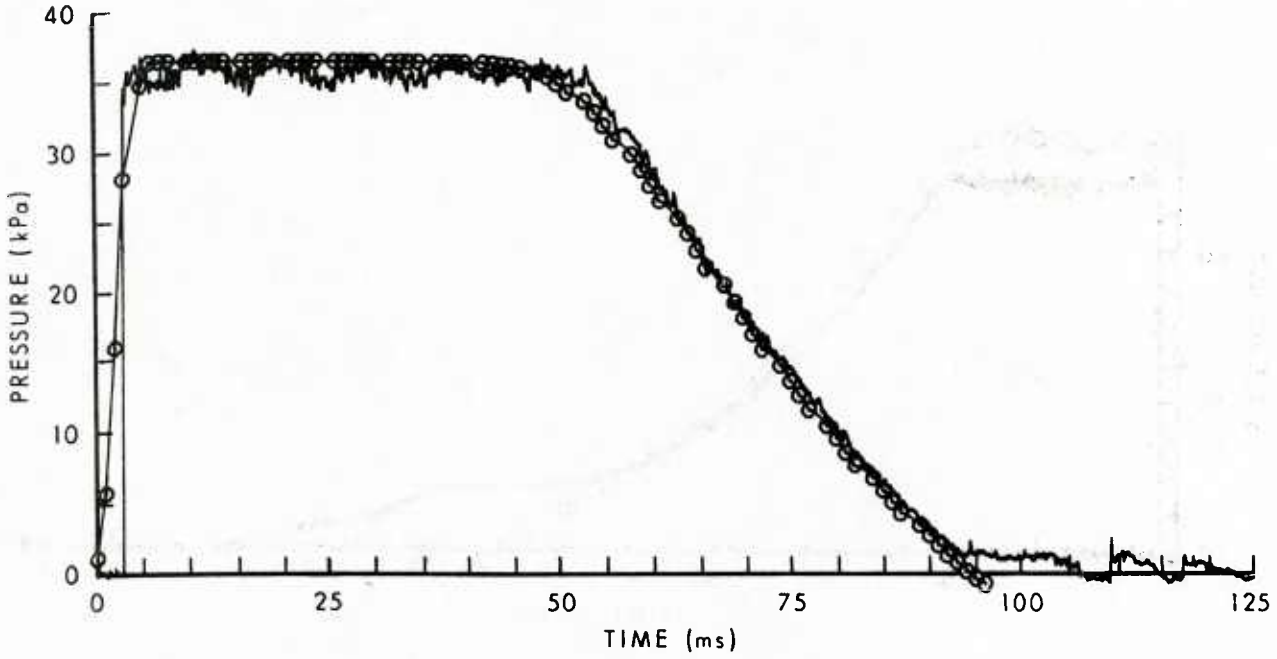

(a) Driver Pressure 1.87 atm (p_{so} = 35.9 kPa)

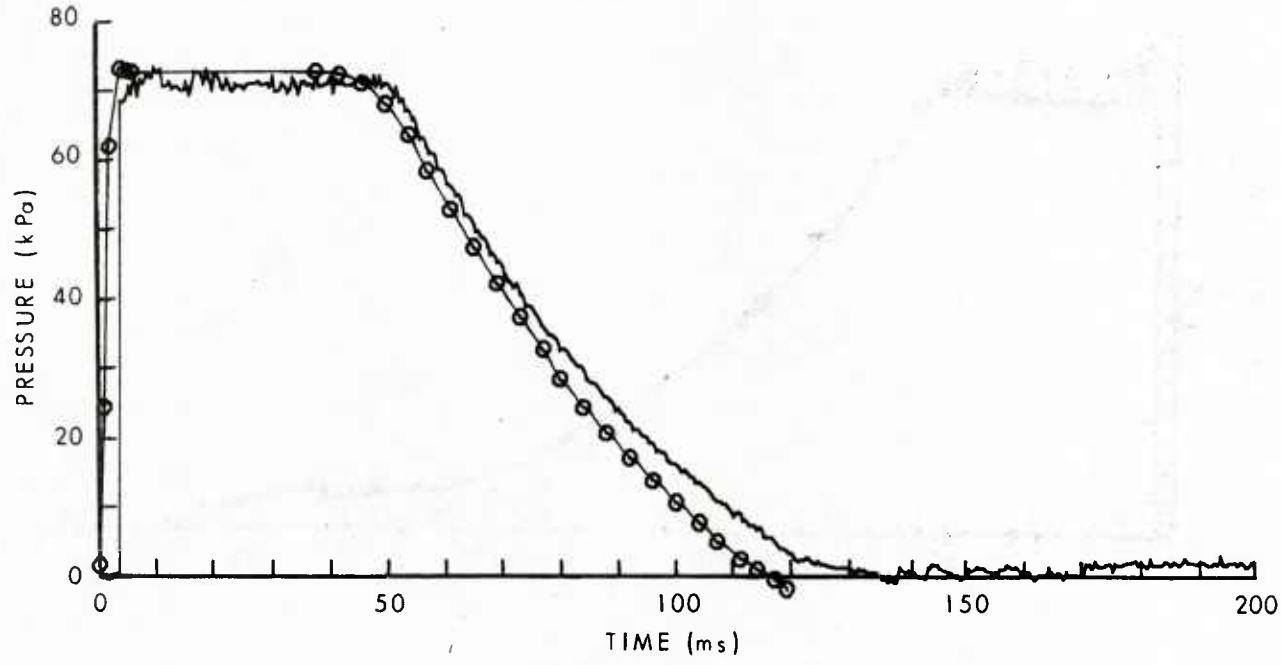

(b) Driver Pressure 3.15 atm (p_{so} = 72.2 kPa)

Figure 4. Computational and Experimental Pressure Histories for the BRL-24" Shock Tube.

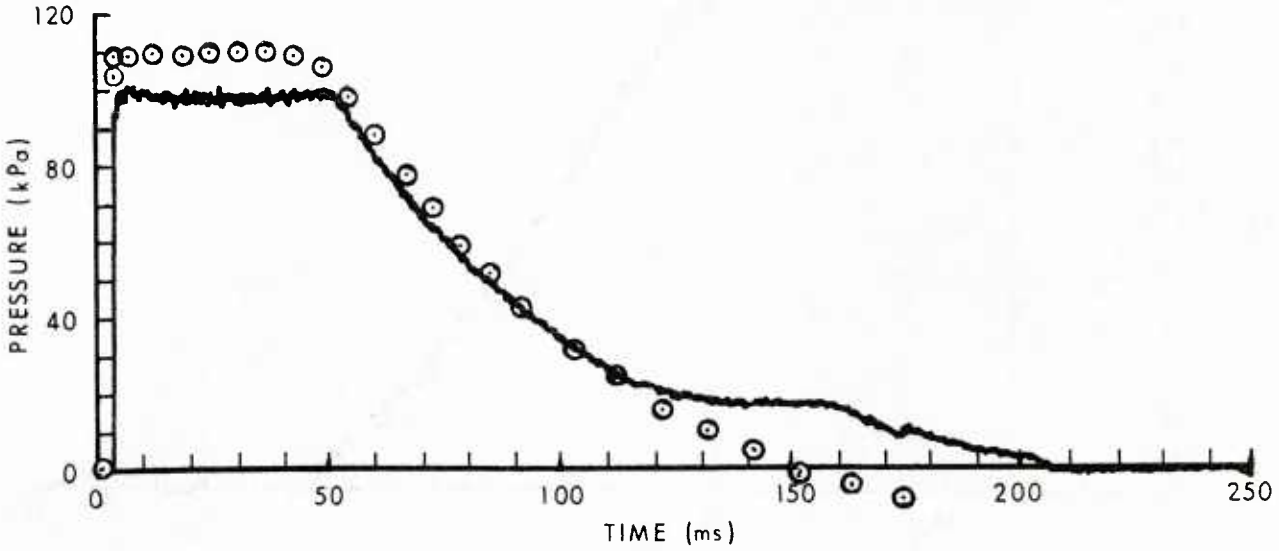

(c) Driver Pressure 4.69 atm (p_{so} = 101 kPa)

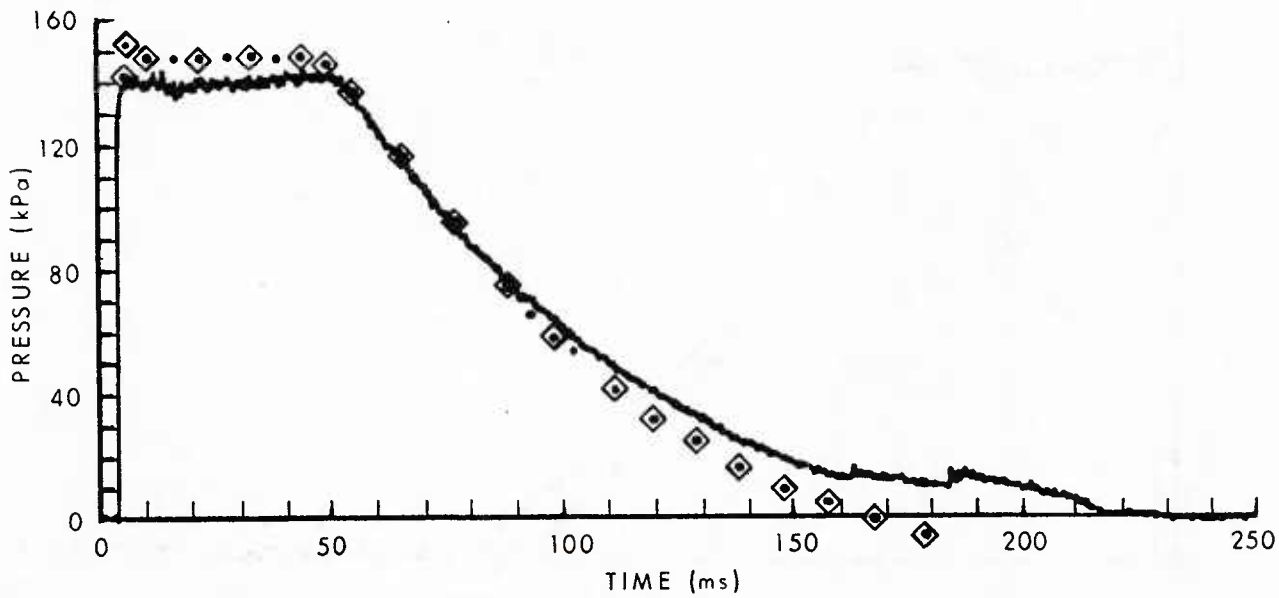

(d) Driver Pressure 6.91 atm (p_{so} = 142 kPa)

Figure 4. (concluded)

TABLE I.

TEST CONDITIONS AND RESULTS FOR BRL-24" SHOCK-TUBE EXPERIMENT

Dimensions	
Driver Length	10.85 metre
Inner Diameter of Driver Tube	0.575 metre
Center of Square Test Section	41.33 metre
Height and Width of Test Section	0.508 metre
Length of Expansion Tube	76.20 metre
Total Length of Shock Tube	87.05 metre

Test Conditions

Test Nr.		1	2	3	4
P_{amb}	kPa	102.6	102.6	102.6	102.7
T_{amb}	K	293.7	293.7	293.7	293.8
P_4/P_1	—	1.87	3.15	4.69	6.91
T_4/T_1	—	1	1	1	1

Results

$P_{so,\,exp}$	kPa	35.9	71.5	99.0	140.
$P_{so,comp}$	kPa	36.7	75.0	110.	148.
$t_{+,\,exp}$	s	.103	.131	.203	.213
$t_{+,comp}$	s	.090	.118	.142	.156
$I_{so,\,exp}$	kPa-s	2.50	5.57	9.43	13.91
$I_{so,comp}$	kPa-s	2.49	5.64	9.11	13.12

i.e. inviscid versus real, flows. As it appears, the higher shock overpressures compensate somewhat for the shorter positive-phase durations in the computation.

Figure 5 shows a comparison of the explicit MacCormack scheme with the implicit Beam-Warming method for a flow simulation in the BRL-2.44m shock tube.[13] The smoothness of the "implicit" pressure curve bears witness to the stability of the Beam-Warming scheme. The MacCormack scheme proved to be much more sensitive to area changes and prone to develop instabilities early in the computation.

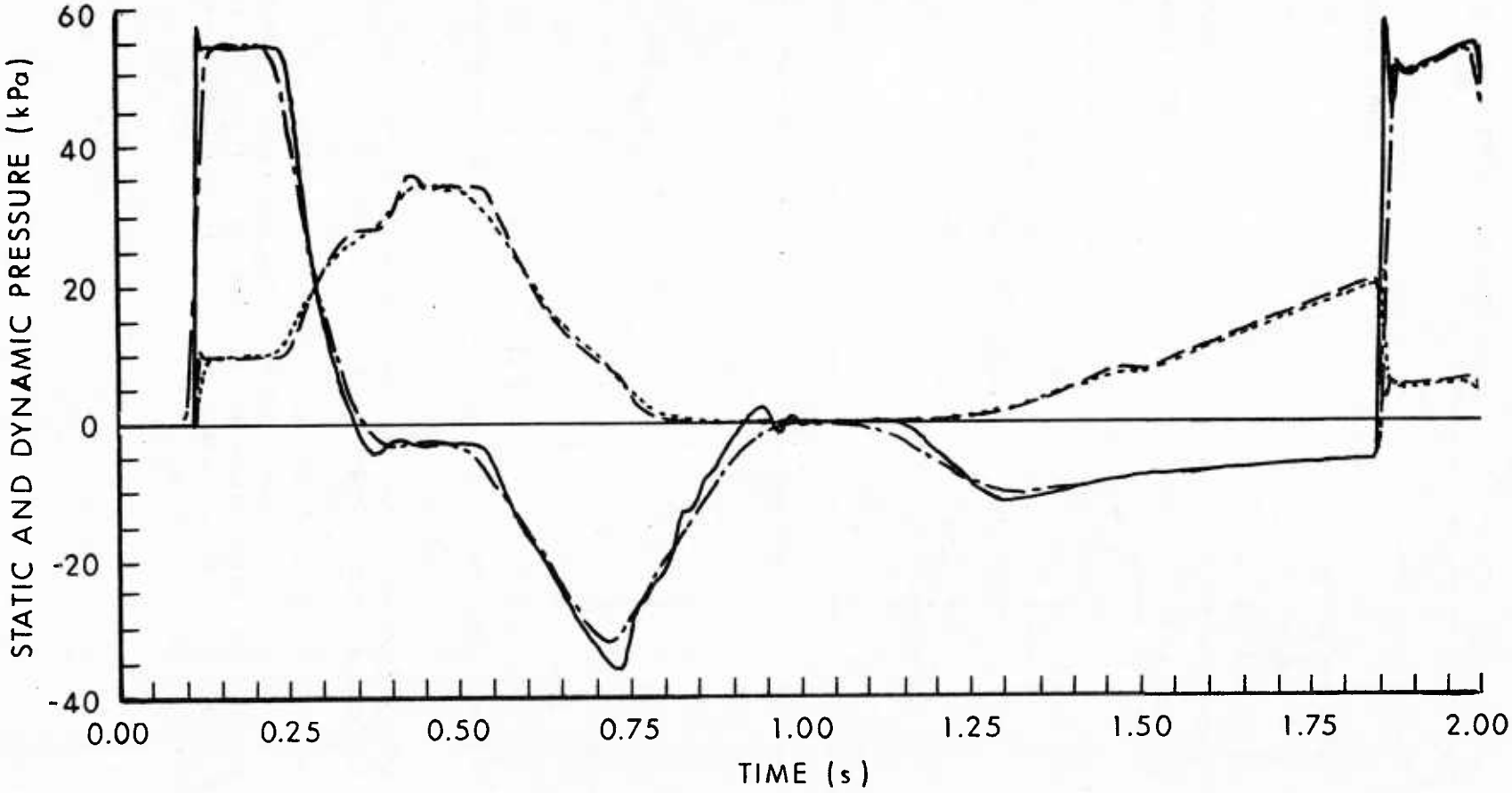

FIGURE 5: Comparison of the Explicit and Implicit Methods

4.2 SIMULATION OF THREE CEG-LBS TESTS

This section shows how a geometrically complicated blast-wave simulator can be modeled in a quasi-one-dimensional sense, and how the computational results from the BRL-Q1D code computations compare with the experimental static-, and dynamic-pressure measurements from the CEG-LBS facility.

4.2.1 Blast-Wave Simulator Model

The CEG-LBS[1] consists of seven cylindrical driver tubes of various lengths which feed compressed air through nozzles into a reinforced-concrete expansion tube (Figure 6a). The number of driver tubes was chosen such as to limit the diameter of the pressure vessels to certain material-strength and manufacturing criteria.[14] The convergent-divergent nozzles were chosen to retard the emptying of the drivers and to keep the diaphragms at a managable size.

At the open end of the expansion tube sits a rarefaction-wave eliminator (RWE) which consists basically of an array of louvers (shown removed from the exit of the expansion tube in Figure 6a). The purpose of the active RWE is to regulate the outflow of air from the expansion tube as a function of time by closing and opening the louvers. This is done in such a manner that the compression and expansion waves from the open end combine within the tube so as to generate the effect of having a much longer expansion tube behind the test section.

The combination of variable length driver tubes and active RWE produces a decaying blast wave in the expansion tube of the CEG facility. The diaphragms for all the drivers are located in the throat section of the nozzles. When they burst simultaneously, the pressure discontinuity across the diaphragms generates left-travelling rarefaction waves which reflect from the closed ends of the driver tubes at different times. After their reflection they travel forward and weaken the incident shock progressively in the early part of the pressure history. At later times, the action of the RWE governs the shape of the blast wave.

The quasi-one-dimensional computational model for this facility is shown in Figure 6b. The seven drivers of the CEG-LBS are combined into one by lumping the cross-sectional areas at any given locations into a single area and the stair-stepped driver results. The four steps indicate that the French facility uses four different driver lengths. The RWE is modeled computationally as a single lumped opening which may vary with time.

Because the lumping of the areas changes the cone angles of the convergent and divergent nozzle sections, the suggestion was made to use a 1/7 lumped-area model in the computations. In this model, the single nozzle remains unchanged, the expansion tube has 1/7 of the cross-sectional area of the CEG-LBS, and the stepped driver has 1/7 of the 7-driver volume of the French facility. This stepped 1/7 driver was shaped into a frustrum of a cone by determining the smaller end diameter from the driver volume for the given driver length and the fixed entrance diameter to the nozzle.

4.2.2 Comparison with CEG Data.

Several pressure histories from the French blast-wave simulator at CEG[15] are available for comparison with the computational results. From these, three experimental records (for peak static overpressures of 30, 47 and 67 kPa) were chosen to be simulated computationally. Initially, a considerable effort was spent to simulate the active RWE of the CEG-LBS and results of this work were reported previously.[16] However, the number of adjustments to the experimental RWE settings which was necessary to effect a matching computation and our inability to find a correlation between the experimental and computational RWE settings has convinced us that the active RWE cannot be simulated realistically by our code.

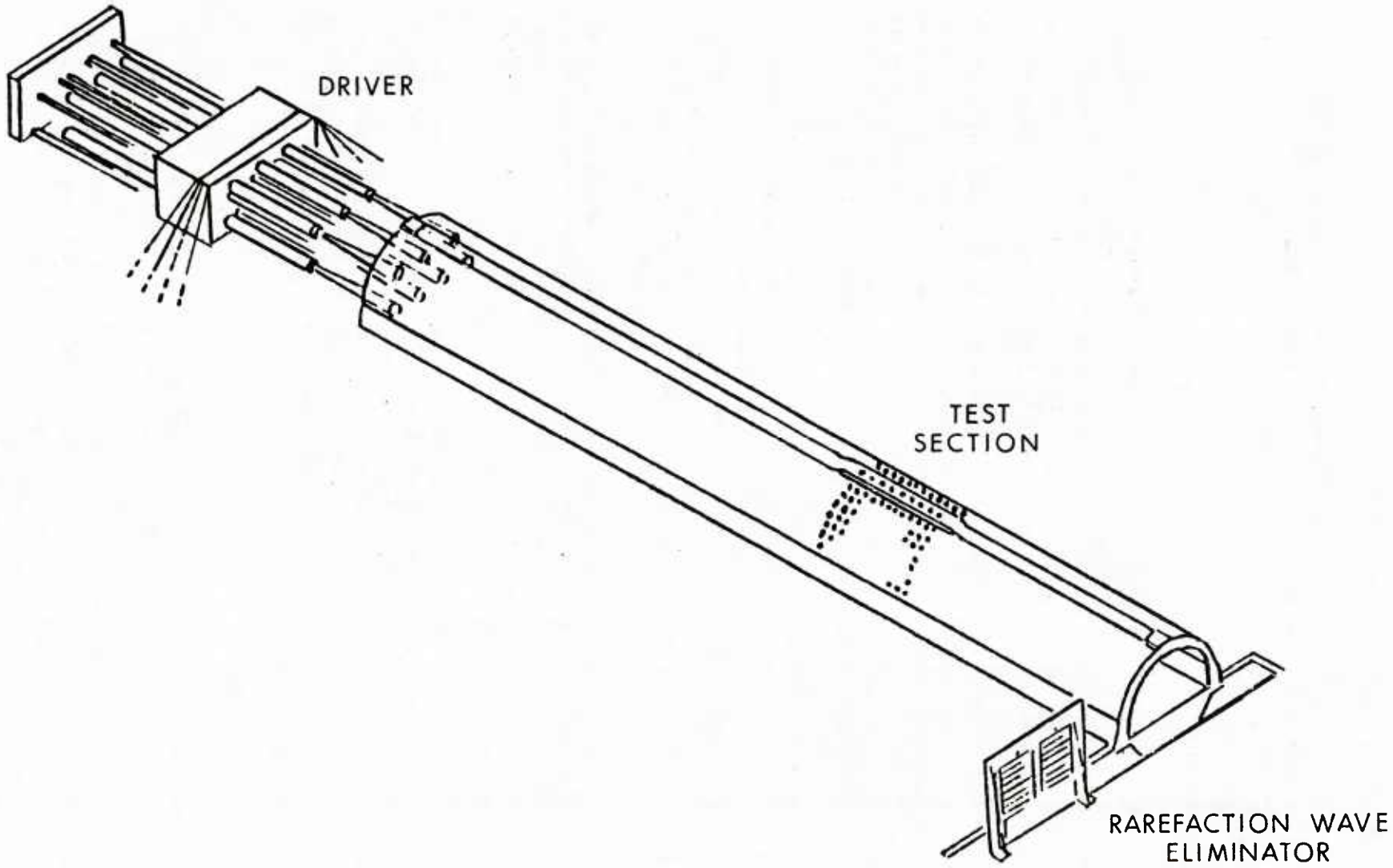

(a) The CEG-LBS at Gramat, France

Figure 6. The CEG-LBS and its Computational Equivalent

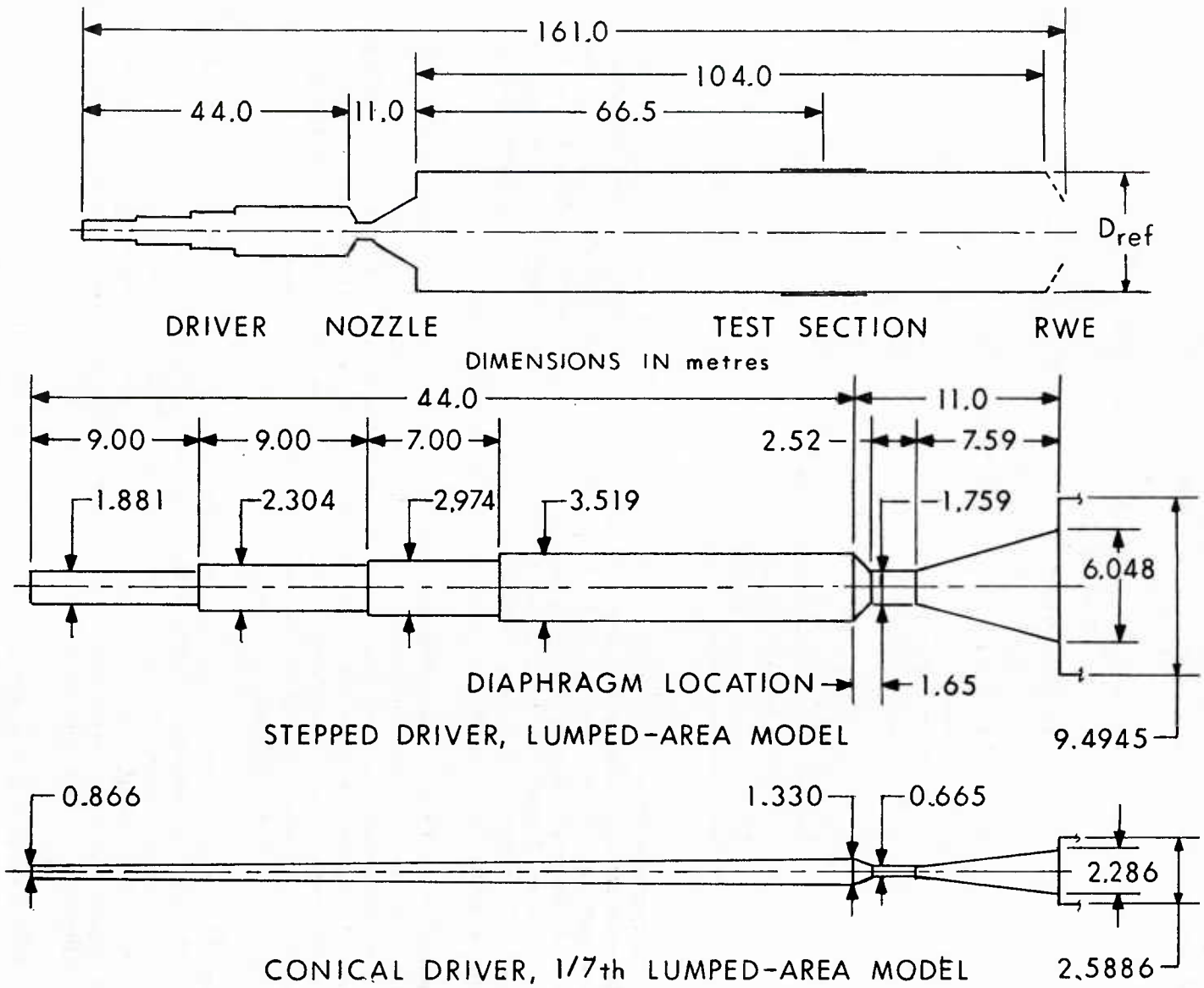

(b) The Computational Q1D Model

Figure 6. (concluded)

The computational results shown here were made for an LBS without RWE and with an extended expansion tube instead, to make up for the effect of the RWE. The initial test conditions and the substitute lengths are listed in Table II and the results are compared in Figure 7a-c. In these figures the noisy trace represents the experimental data whereas the computational results are the smooth line. The solid lines are for the static overpressure while the dashed lines indicate the computed dynamic pressure.

TABLE II.
INITIAL CONDITIONS FOR CEG TESTS

Test Nr.	P_4/P_1 —	T_4/T_1 —	P_{amb} kPa	T_{amb} $^\circ C$	ΔL_{ET}[a] m
5[b]	10.1	.982	99.0	12	200
9	15.4	.993	98.8	4	210
8	26.8	.994	99.0	7	200

[a] substitute for active RWE in computation
[b] target in test section: 25% blockage

The comparisons show that the general features (wave reflections and expansions) of the pressure histories are replicated in the computational simulations. However, distinct differences in the wave patterns can be observed also because, due to the absence of the RWE in the computation, all the wave shaping is done by the expansion waves coming out of the driver. In the first comparison (Figure 7a) the agreement between the computational and experimental data is good. The computational peak overpressure is only 10% below the experimental value and the computational curve follows the experimental trace as well as can be expected.

Further study of the pressure histories in Figures 7b and 7c reveals however that the computation fails to replicate the peak overpressure with increasing driver pressure. A comparison of the pressure histories shows that the computational history falls initially below the experimental history the more the higher the driver pressure. In the second comparison (Figure 7b) the computational peak overpressure is 25% below the experimental value at a driver pressure of 15.4 atm and in the third comparison the peak overpressure is 39% below the experimental value at 26.8 atm driver pressure.

More blast-wave characteristics are listed for comparison in Table III. From the comparison of the computational and experimental data we learn, that none of the blast-wave characteristics are truly matched by the computation, although the computations come close to the experiment. Most significantly, the computational impulses fall below the experimental values and because the peak overpressure values are lower, the weapon yields turn out relatively high. The differences can be explained, however.

It is indeed surprising that a crude quasi-one-dimensional model can at all approximate the complicated, three-dimensional flow process in the CEG-LBS. Consider, for example, the seven drivers of different lengths. As they are emptied on bursting of the diaphragms, rarefaction waves empty the tubes at different rates. Subsequent compression and expansion waves from the throats and RWE influence the flow differently in every tube. The shock waves emerging from each nozzle form a shock bubble and then coalesce forming a complicated array

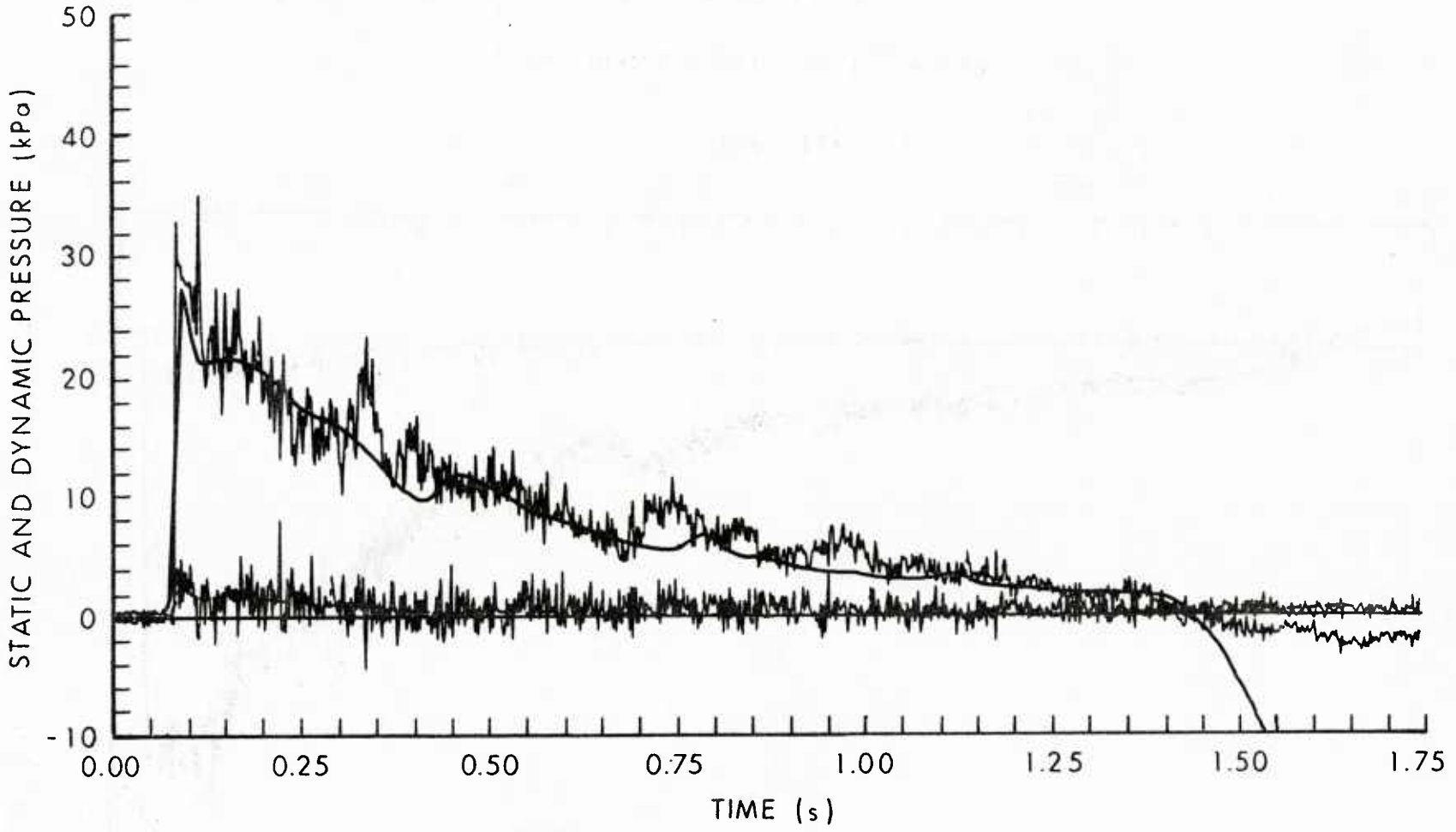

(a) Test 5: Driver Pressure 10.1 atm (p_{so} = 30 kPa)

Figure 7. Three Computations Compared with CEG-LBS Experiments

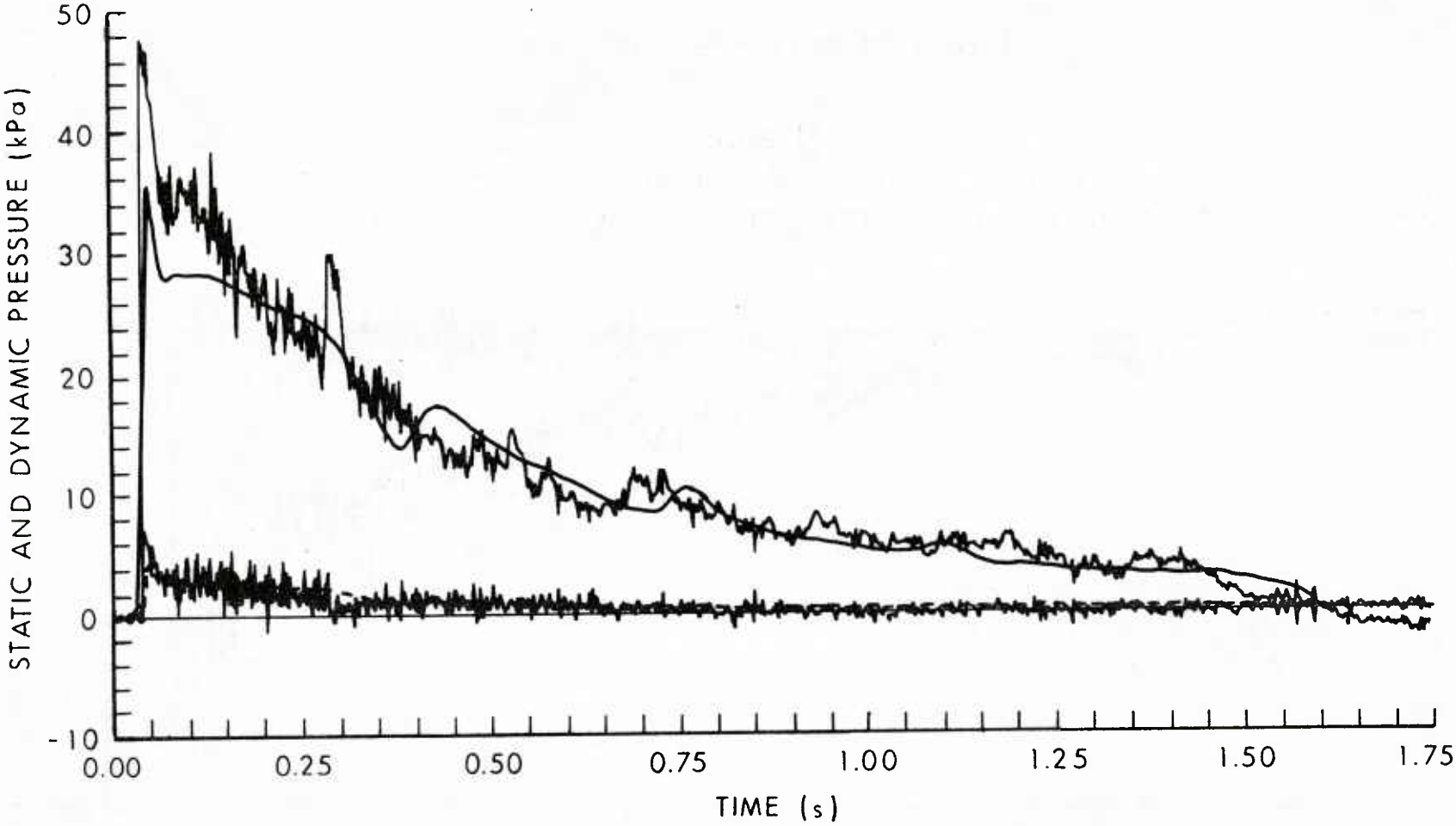

(b) Test 9: Driver Pressure 15.4 atm (p_{so} = 47 kPa)

Figure 7. (continued)

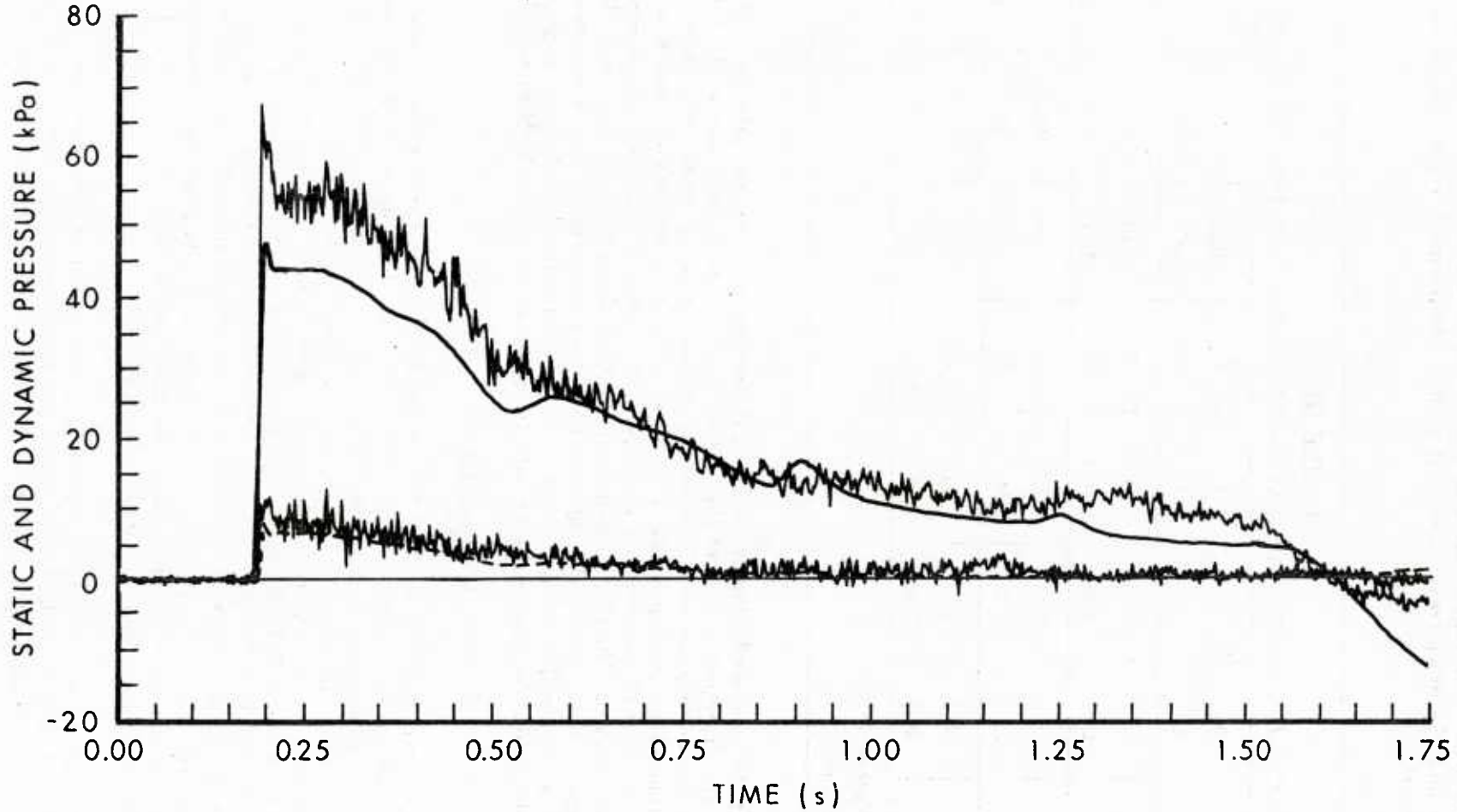

(c) Test 8: Driver Pressure 26.8 atm (p_{so} = 67 kPa)

Figure 7. (concluded)

of Mach stems and spherical shocks. The flow at the exit of the driver nozzles experiences a sudden change in area. The global nature of the flow is to form a smooth transition between the nozzle exits and the downstream flow field with a "dead-water" region in the immediate vicinity of the nozzles.

TABLE III.

COMPUTATIONAL/EXPERIMENTAL BLAST-WAVE CHARACTERISTICS FOR CEG TESTS

Test Nr.		p_{so} *kPa*	t_+ *s*	I_{so} *kPa-s*	Y_{so} *kT*	q_{so} *kPa*	I_q *kPa-s*	Y_q *kT*
5[a]	exp	30.2	1.33	11.8	28	3.10	0.79	21
	comp	28.1	1.36	10.4	22	4.01	0.90	41
9	exp	46.8	1.44	17.3	42	7.38	0.64[?]	–
	comp	35.5	1.45	16.1	50	4.33	1.02	19
8	exp	67.3	1.40	30.5	131	14.6	3.02	31
	comp	48.3	1.42	25.8	127	7.87	2.57	75

[a] test section blockage 25%.

[?] questionable value.

The computational model lumps the seven drivers and their nozzles into one. The seven 6° cone half-angle, divergent nozzles of the CEG-LBS are lumped into a single 16° cone half-angle divergent nozzle with an area discontinuity where the nozzle opens into the expansion tube. The computation cannot generate a "dead-water" region, as does the real flow at this location. The emptying of this one driver occurs with a different, single system of rarefaction and recompression waves. The three-dimensional effects of the interacting flow from the seven drivers are absent from the model. The flow in the vicinity of the nozzle exit is indeed not well represented with a one-dimensional model. It is therefore desirable to compare the computational data with the experimental results from a quasi-one-dimensional LBS model.

4.3 SIMULATION OF BRL-LBS MODEL-A EXPERIMENTS

It should be expected that the flow from a shock tube with variable area resembling the computational model more closely than the CEG-LBS will eliminate some of the ambiguity introduced into the comparison by the complexity of the mixing of the seven driver flows and associated phenomena. Therefore, an experimental, axisymmetric, 1/37-scale model of the computational blast-wave simulator was designed (Figure 8) and built at the BRL to validate the predictions from the BRL-Q1D code. The shock tube was used to produce decaying blast waves from 23 to 230 kPa (3.3 to 33.3 psi). Experiments were conducted with heated and unheated driver gas. The data were recorded at a test station located 7 hydraulic diameters downstream from the exit of the divergent nozzle. Selected results from these experiments[12,17] covering the whole shock-overpressure range are compared with the computational data in Figure 8a-f. The initial test conditions are listed in Table IV.

The experiments are listed in ascending order of shock overpressure. From this arrangement it is obvious that the heated driver gas produces stronger shocks at lower driver pressures than the unheated driver gas at even the highest driver pressure (e.g. Test 12).

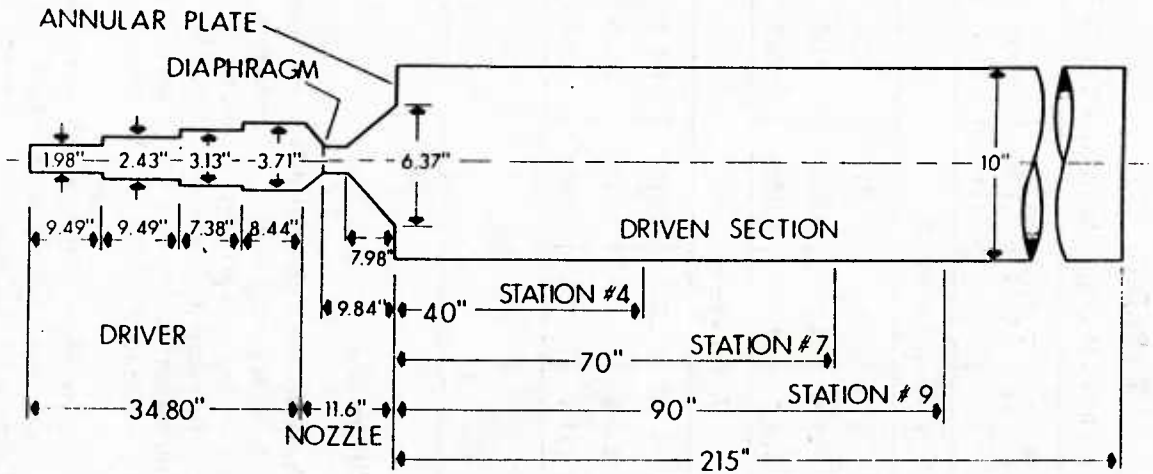

Figure 8. Experimental, Axisymmetric BRL-LBS Model-A[17]

Initially, all computations were executed with the nominal throat area implying that the rupturing diaphragm would open fully without causing a partial obstruction of the throat area. The actual throat areas were obtained from the ruptured diaphragms after the tests[12] and the equivalent diameters determined which are given in the table. It was found that the computational fit improved when the calculations were executed with the actual rather than the nominal throat area. The comparison of the computational and experimental pressure histories in Figure 8 shows satisfactory agreement.

TABLE IV.

INITIAL CONDITIONS FOR LBS-MODEL-A TESTS[12].

Test Nr.	P_{amb} *kPa*	T_{amb} *K*	P_4/P_1 —	T_4/T_1 —	D_{THR} m	$p_{so,exp}$[a] kPa	$p_{so,comp}$ kPa
Unheated Driver Gas							
20	105.7	278.5	6.75	1.0	0.0472[b]	22.9	22.0
3	101.8	313.0	28.37	1.0	0.0447	81.3	71.6
12	101.5	296.9	134.7	1.0	0.0396	175.7	180.5
Heated Driver Gas							
25	102.0	299.8	92.95	1.593	0.0463	190.3	192.7
26	101.4	299.8	107.8	1.593	0.0435	201.6	197.6
28	102.7	299.8	131.4	1.778	0.0472[b]	229.6	251.5

[a] measured at Test Station 7

[b] nominal throat diameter

4.3.1 Experiments with Unheated Driver Gas

Three examples of pressure histories for unheated driver gas were chosen from Reference 17. Test 20 (Figure 9a) represents the shock-tube test with the lowest pressure ratio across the diaphragm, $P_4/P_1 = 6.75$. The computational-experimental match is very good including the spike at the shock front even though the computation was executed for the nominal throat area. This agrees with our previous observation in Section 4.2 (Figure 7a) where we found good agreement between computation and experiment at the low driver pressure.

Test 3 presents a 81 kPa (12 psi) pressure history which was generated with a diaphragm pressure ratio of $P_4/P_1 = 28.4$. As observed previously in Section 4.2 (Figure 7c), the BRL-Q1D computation in Reference 17 underpredicts the shock overpressure at the beginning of the experimental record. It seems reasonable to assume that this discrepancy is caused by the inability of the one-dimensional computational scheme to simulate two-dimensional phenomena which occur in the experimental flow, like a "dead-water" region at the nozzle exit. Perhaps the flow would be modeled computationally closer to reality with the divergent nozzle extended to the full diameter of the expansion tube. This was done for Test 3 and the result in Figure 9b shows an improved agreement between computation and experiment.

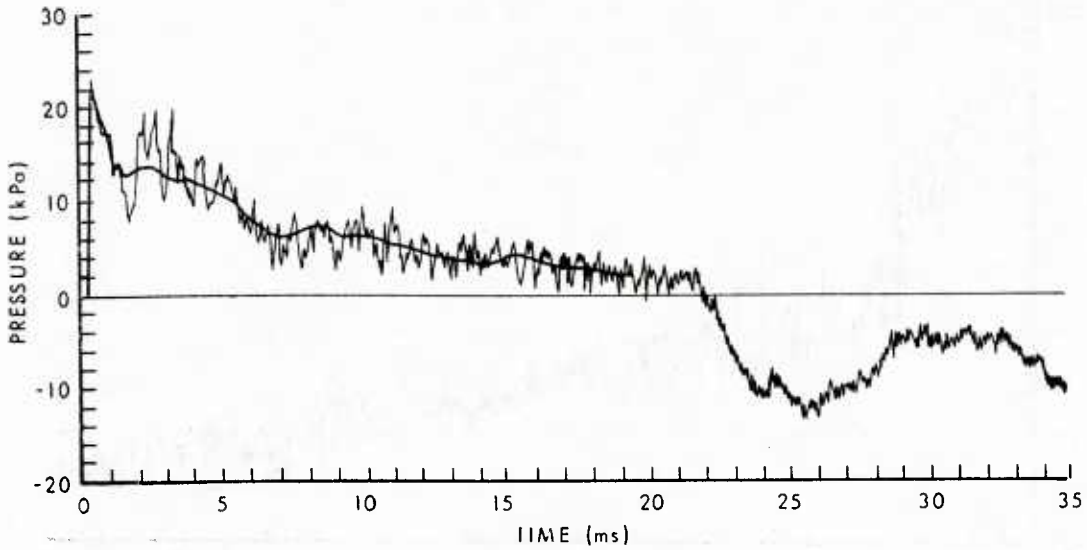

(a) Shock Overpressure 23 kPa (Test 20)[17]

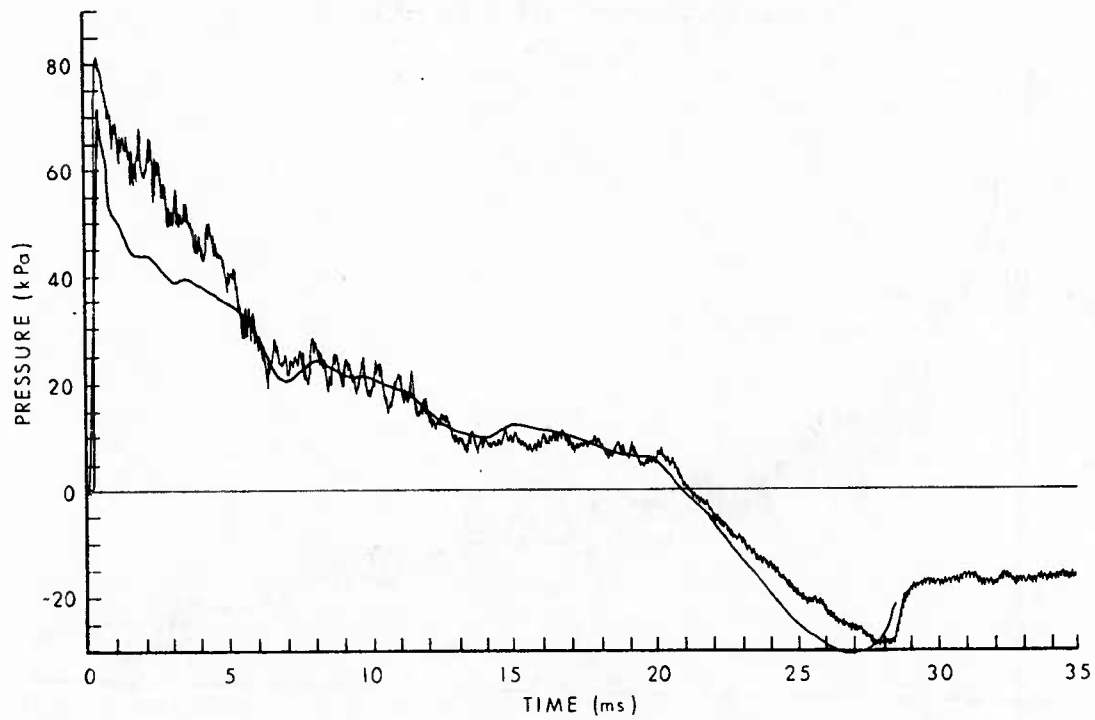

(b) Shock Overpressure 81 kPa (Test 3)

Figure 9. Computational and Experimental Pressure Histories for the BRL-LBS Model-A

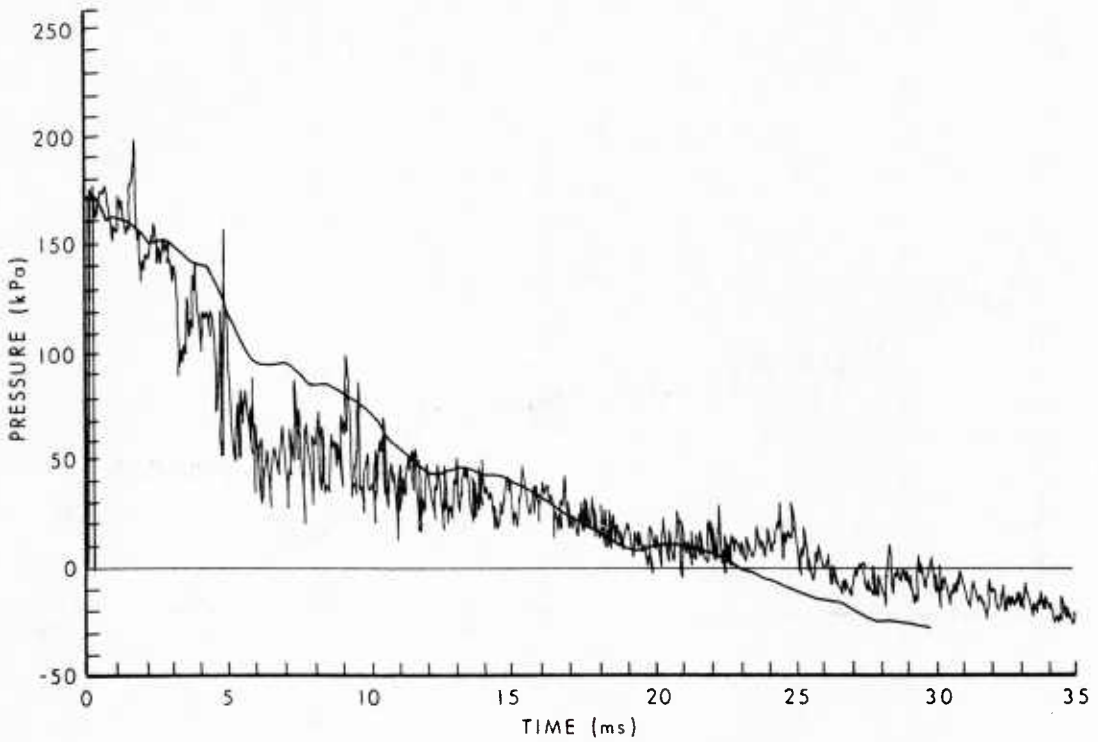

(c) Shock Overpressure 175 kPa (Test 12)

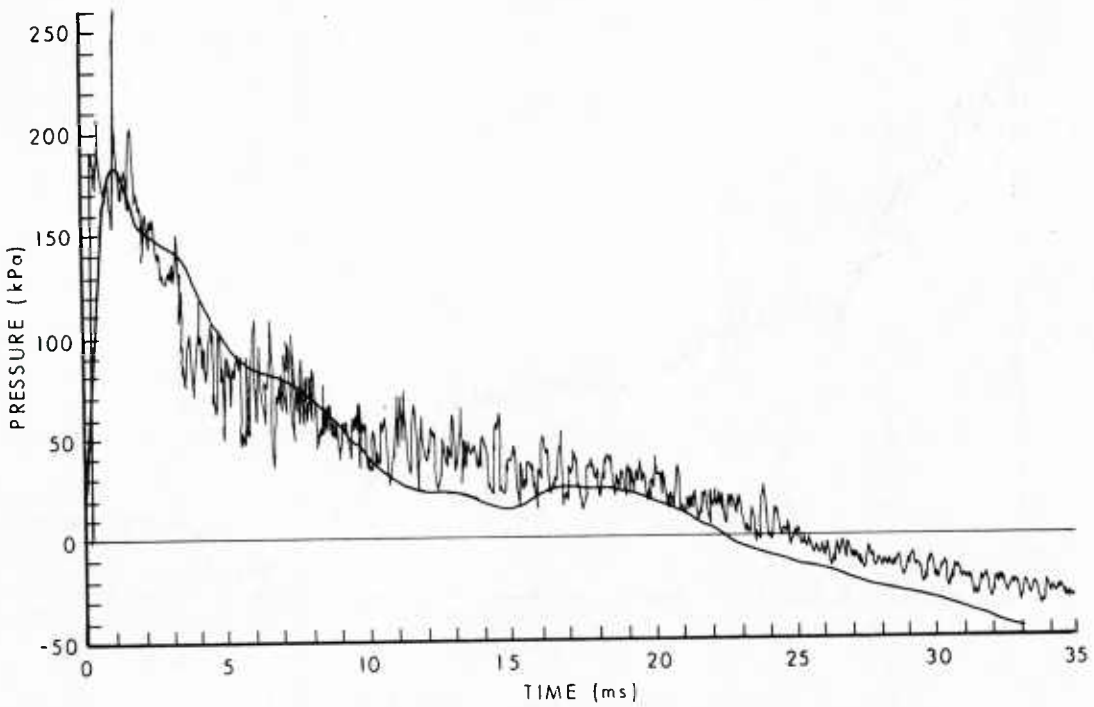

(d) Shock Overpressure 190 kPa (Test 25)

Figure 9. (continued)

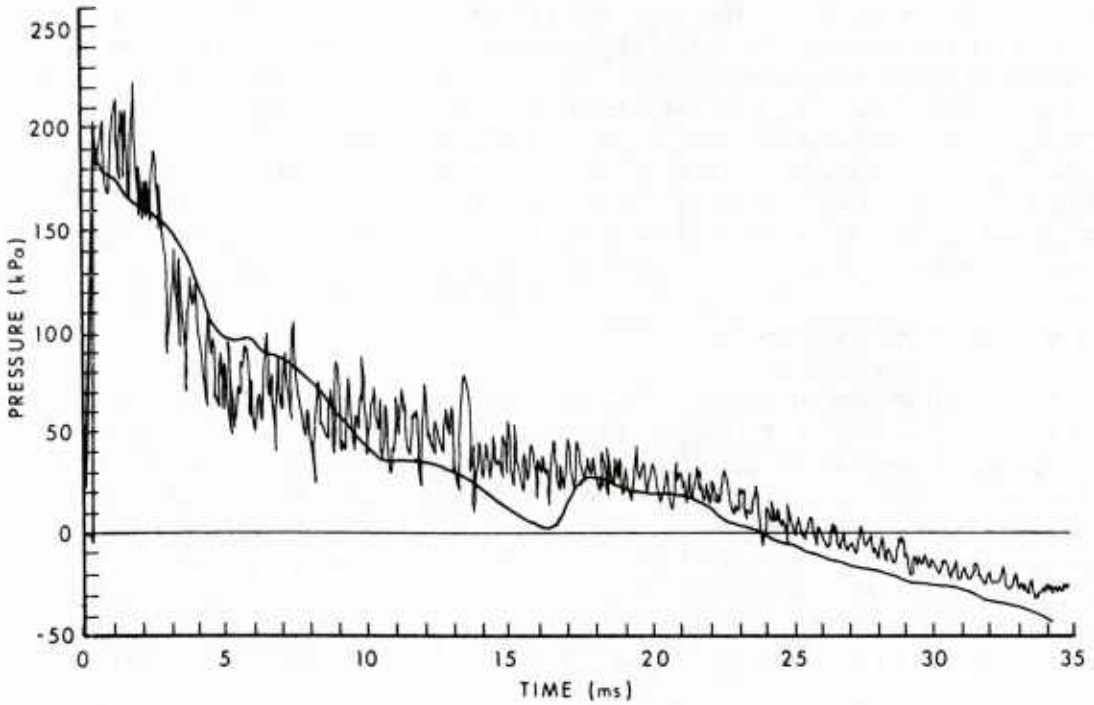

(e) Shock Overpressure 202 kPa (Test 26)

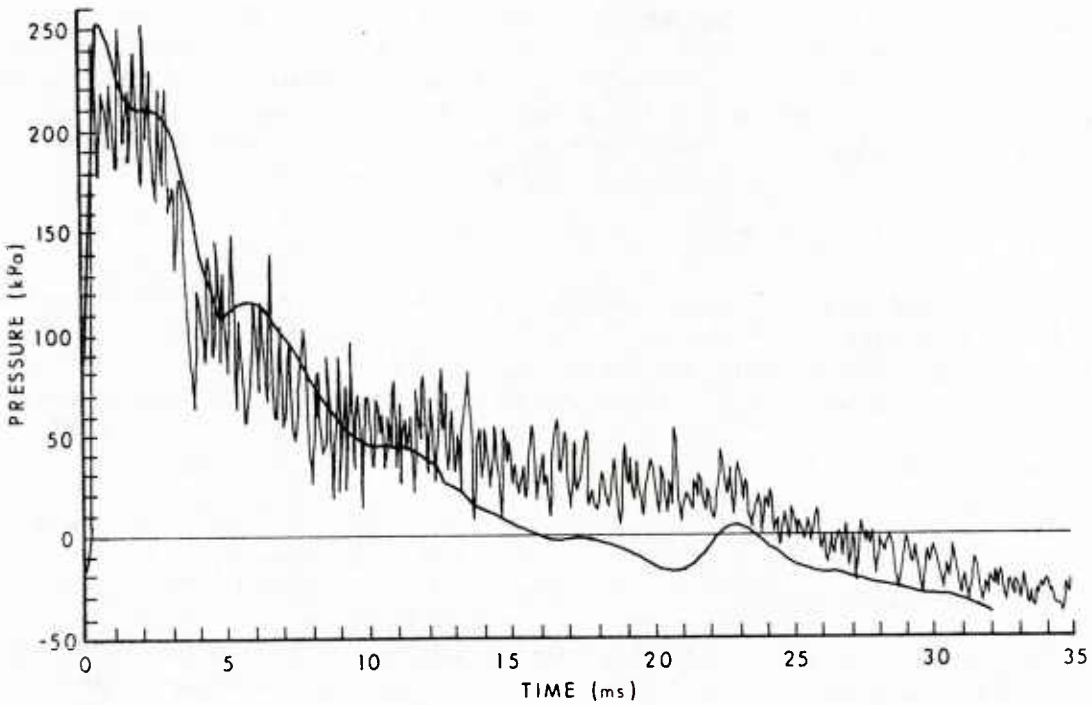

(f) Shock Overpressure 241 kPa (Test 28)

Figure 9. (concluded)

An altogether different phenomenon is observed in Test 12 which represents the highest diaphragm pressure ratio, $P_4/P_1 = 135$, used in this series of experiments. The computation presented in Reference 17 overpredicts the experimental overpressure during the first ten milliseconds of the pressure history, and thereafter the computed overpressure decays much more rapidly than the experimental curve. This computation was repeated with the throat area reduced to its actual size which was measured on the burst diaphragm after the test (Table IV). The resulting pressure history (Figure 9c) shows much better agreement with the experiment. It may be concluded therefore, that at high driver pressures (which necessitate thicker diaphragms), the blockage caused in the throat by the folded diaphragm petals has to be accounted for in the computational model. This conclusion is confirmed in the following comparisons for heated driver gas.

4.3.2 Experiments with Heated Driver Gas

Three comparisons of computational-experimental[12] pressure histories for heated driver gas are shown. Test 25 and 26 (Figures 9d and 9e) present a good match of the computational and experimental pressure histories generated with a diaphragm pressure ratio of $P_4/P_1 = 93$, and 108 resp., and a temperature ratio across the diaphragm of $T_4/T_1 = 1.59$. Both computations were made using the actual throat area given in Table IV. The computed overpressure in Figure 9e indicates the passage of a second shock through the test station at about 17 ms which compensates for the preceding rapid pressure decay. The plot of density versus distance for Test 26 (page 77 in the Appendix) reveals that this shock is the reflection of the recompression shock which is reflected downstream from the area discontinuity at the nozzle exit.

Test 28 (Figure 9f) represents the pressure history for the highest shock overpressure obtained in this series of experiments. It was generated with a diaphragm pressure ratio of $P_4/P_1 = 131$, and a diaphragm temperature ratio of $T_4/T_1 = 1.78$. The computation was done with the nominal throat area because the actual throat area was not known. Consequently, the computation predicts the shock overpressure too high and the positive-phase duration too short. These are clear indications that the throat area in the experiment was necked down by the petals of a thick diaphragm. Although the computation with the actual throat area would give better agreement, the present comparison is satisfactory in itself.

4.4 MATCHING THE CEG PRESSURE HISTORIES

In this final section we will discuss two methods of improving the computational-experimental mismatch. First, we will discuss the influence of the area discontinuity on the overpressure spike, then we will study the influence of the driver volume on the initial pressure-decay rate behind the pressure spike together with adjustments of the driver pressure.

4.4.1 Pressure-Spike Study

It is known that the flow in pipes forms a dead-water region in the vicinity of a sudden diameter change to facilitate a smooth transition. Extending the divergent nozzle to the full diameter of the expansion tube replicates such a dead-water region in the computational LBS model. The effect of doing this was studied computationally and the results are presented in Figure 10. Two curves are shown. The bottom curve represents the pressure spike for the standard nozzle with the discontinuity in the cross- sectional area, whereas the top curve is for the extended nozzle. For the same initial condition, only the cone half angle is varied. The result is a dramatic difference in the amplitude of the initial pressure spike. The extended nozzle more nearly approximates the pressure spikes found in the experimental records shown in Figures 7 and 9.

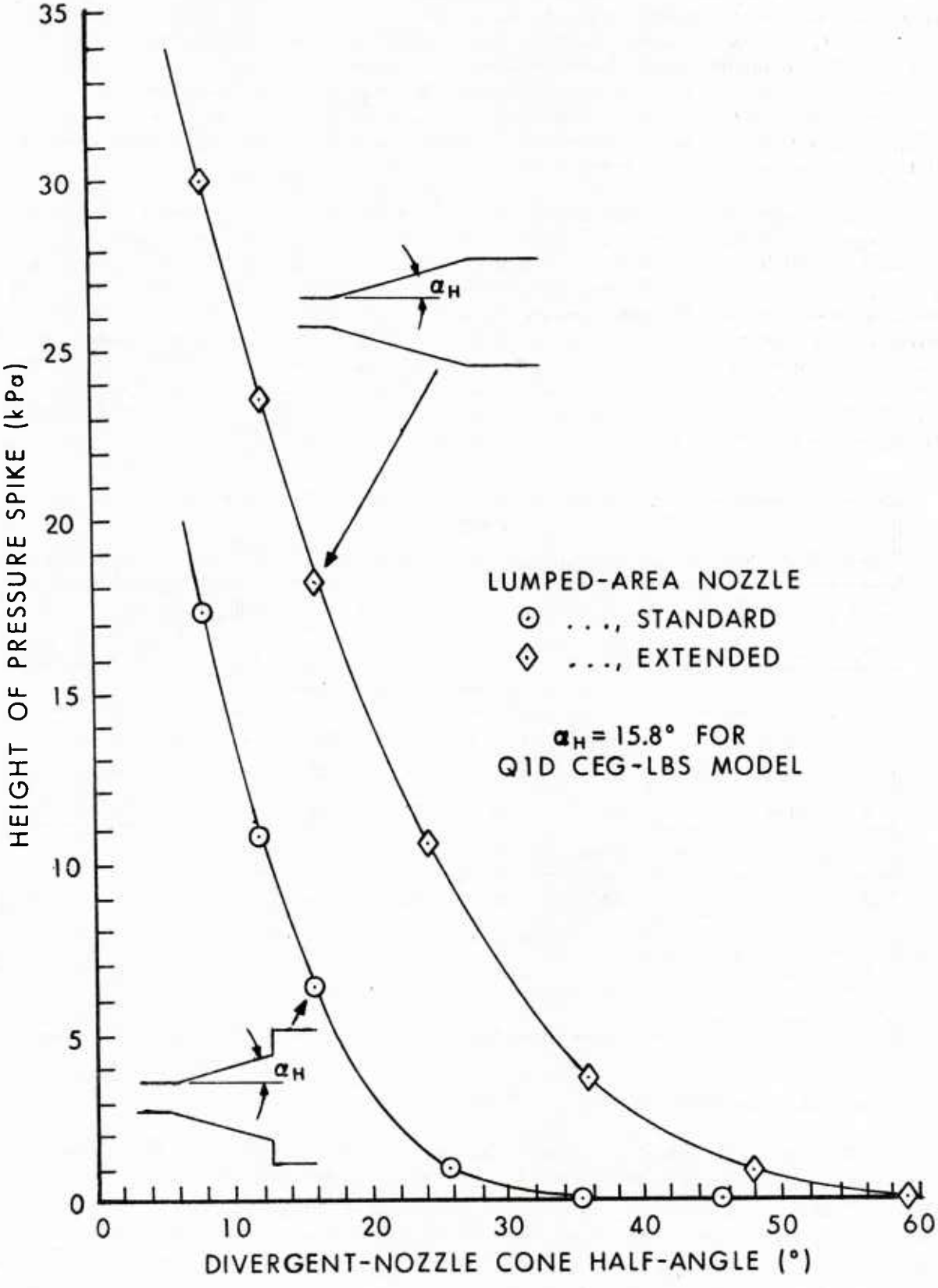

Figure 10. Computed Pressure-Spike Amplitude Versus the Cone Half-Angle of the Divergent Nozzle

This result clearly shows in the following figure. Figure 11 presents a comparison of the computational shock strength with the experimental results as a function of the diaphragm pressure ratio. A computational curve for the standard nozzle as well as for the extended nozzle is given. The extended nozzle clearly improves the prediction of the shock overpressure relative to the experimental data in the lower range of the driver pressure (10 to 100 atm). At driver pressures above 100 atm, the extension of the nozzle has no longer an effect on the pressure spike. But without doubt, real-gas effects become responsible for the trend of the experimental data below the computational curve in this pressure region.

The computational simulations of the CEG pressure histories reported in Subsection 4.2.2 were repeated for the Q1D model with extended nozzle and the results are tabulated in Table V. Those data which now match the experimental value are printed in bold type. It is evident that the extended nozzle causes the amplitude of the pressure spike to increase. This applies to the static as well as to the dynamic pressure. However, this increase is somewhat capricious. The pressure spike increase is too much at the lowest driver pressure (Test 5), and not enough at the next highest driver pressure (Test 9). The increase is right only at the highest driver pressure (Test 8). The same capriciousness is observed for the other blast-wave characteristics, and the overall impression is somewhat disappointing. Therefore, another procedure was followed in trying to match the experimental pressure histories for the CEG tests.

TABLE V.

MATCHING THE EXPERIMENTAL BLAST-WAVE CHARACTERISTICS FOR CEG TESTS

Test Nr.	P_4 *atm*	V_4 *%*	p_{so} *kPa*	t_+ *s*	I_{so} kPa-s	Y_{so} kT	q_{so} kPa	I_q kPa-s	Y_q kT
Computation with Extended Nozzle									
5[a]	**10.1**		32.5	**1.35**	10.5	17	5.16	**.902**	**21**
9	**15.4**	**100**	43.6	**1.45**	**16.4**	**37**	6.46	1.08	9
8	**26.8**		**66.7**	**1.41**	26.9	88	**14.6**	**2.98**	**28**
Computation with Increased P_4 and Reduced V_4									
5[a]	11.4	95	**30.2**	**1.35**	**11.3**	**24**	4.54	1.08	50
9	22.9	73	43.5	**1.42**	**17.4**	**45**	6.43	1.37	18
8	37.5	84	62.0	**1.42**	**30.5**	**142**	12.7	3.71	78

[a] test section blockage 25%.

4.4.2 Adjusting the Driver Pressure and Volume

The pressure histories of free-field blast waves such as are generated by HE or nuclear explosions, can be characterized ideally by a three-, or four-parameter, exponentially decaying function[9] as e.g. the modified Friedlander equation, or Ethridge's equation. These equations allow matching of three or four blast-wave characteristics, which are the peak overpressure, p_{so}, the positive-phase duration, t_+, the static-overpressure impulse, I_{so} and the initial decay rate, $dp/dt|_{ta}$, at shock arrival time. It is therefore reasonable to use experimentally determined blast-wave characteristics for comparing the computational and experimental pressure histories.

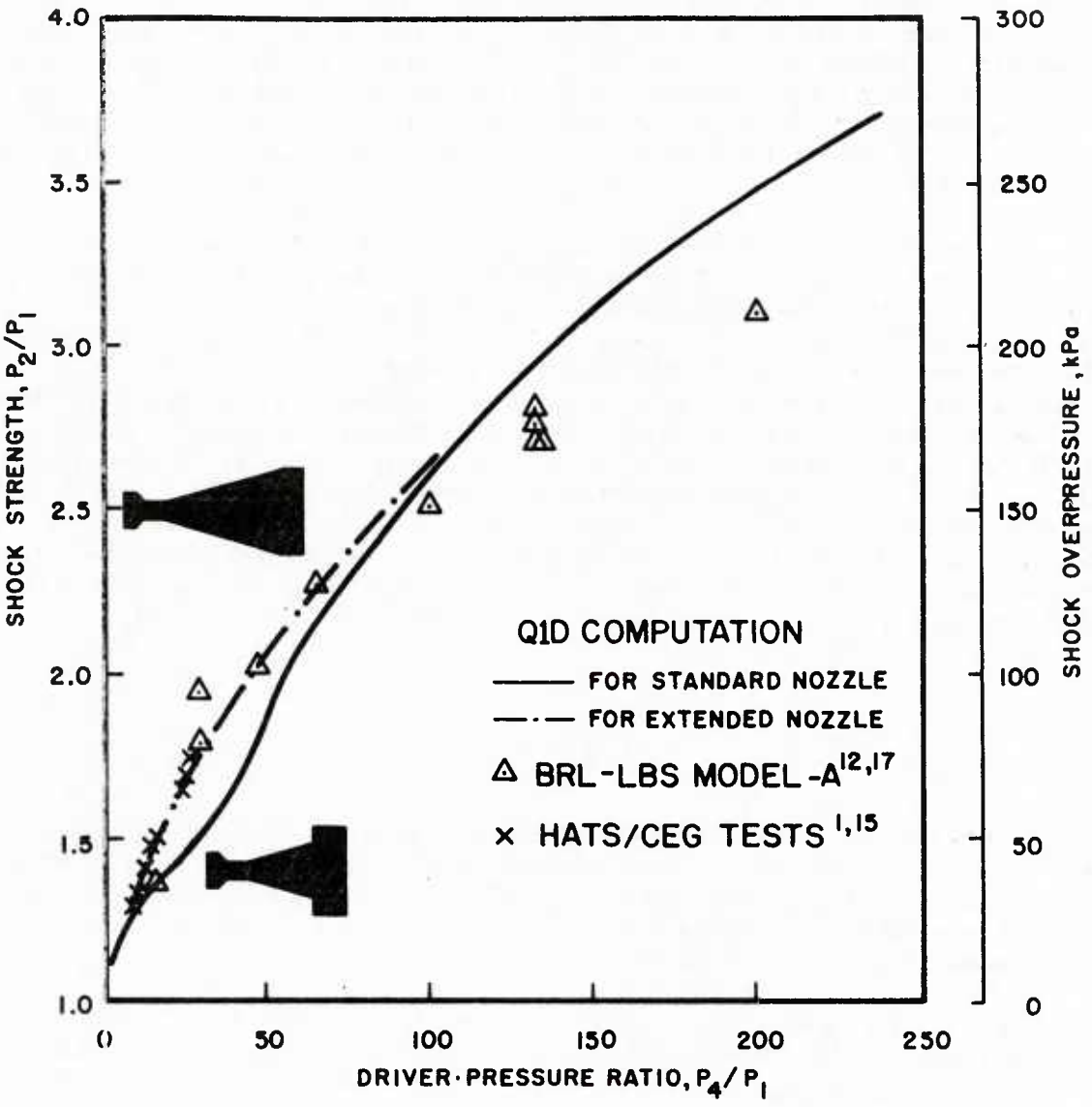

Figure 11. Shock Strength Versus Diaphragm Pressure Ratio

Consequently, we modified the input to our Q1D code and repeated the computations until the blast-wave characteristics matched. This was done for the three CEG tests under discussion and the results are listed in Table V, also.

The shock overpressure is adjusted obviously by raising and lowering the driver pressure, P_4. The positive-phase is curtailed by the arrival at the test station of the first expansion wave from the open end of the shock tube. It is not quite so obvious that the static-overpressure impulse and the initial pressure-decay rate behind the shock depend on the volume and shape of the driver. More precisely, both impulses, for the static as well as for the dynamic pressure history, are proportional to the mass of the driver gas which, for constant driver pressure and temperature, is determined by the volume of the driver. The initial pressure-decay rate is influenced by a number of parameters, among them the volume and shape of the driver and the size of the throat area. In the present study, however, the throat area and the driver length are considered given constants so that the driver volume could be adjusted only by changing the conical shape of the driver.

In our efforts to match the experimental blast-wave characteristics computationally, we gave preference to matching the static-overpressure impulse and the positive-phase duration. The initial pressure-decay rate was matched visually if possible even when it became necessary to compromise the matching of the peak static overpressure. We feel justified to do so because the overpressure spike varies somewhat with the number and location of the grid points in the computational grid, whereas the experimental overpressure spike is most likely affected by instrumental noise. (The French scientists at the CEG, for instance, related during meetings at the BRL that they ignore the spike in their data evaluation.) The resulting computational pressure histories match the experimental histories very well. They would match the experimental records even better if the actual throat areas of the burst diaphragms could have been accounted for in the computations. With only the nominal throat area known, the computational pressure histories tend to be just above the data in the initial part of the positive phase and slightly below the data toward the latter part of the positive phase.

5. CONCLUSIONS

The computational studies discussed here have shown that the BRL-Q1D code is a useful tool for predicting shock-tube flows with complicated geometries. The present quasi-one-dimensional model represents ideal (not real!) flow and one may expect that the computational predictions would be improved by the inclusion of losses due to friction and heat transfer. But even without these losses modeled, the scheme performs well.

The scheme is for instance sensitive to area changes like the necked-down diaphragm opening formed by the folded petals of the real diaphragm. It has been shown here that a knowledge of the necking effect in the diaphragm (i.e., throat) area improves the prediction markedly.

When decaying blast waves are simulated, relating the blast-wave characteristics of the computational pressure histories to those of free-field blast waves is very helpful in qualifying the predictions.

In the case of the axisymmetric LBS model it was found that the flow in the vicinity of the sudden area change at the nozzle exit can be more realistically modeled by extending the divergent nozzle to the full diameter of the expansion tube. However, a fully three-dimensional

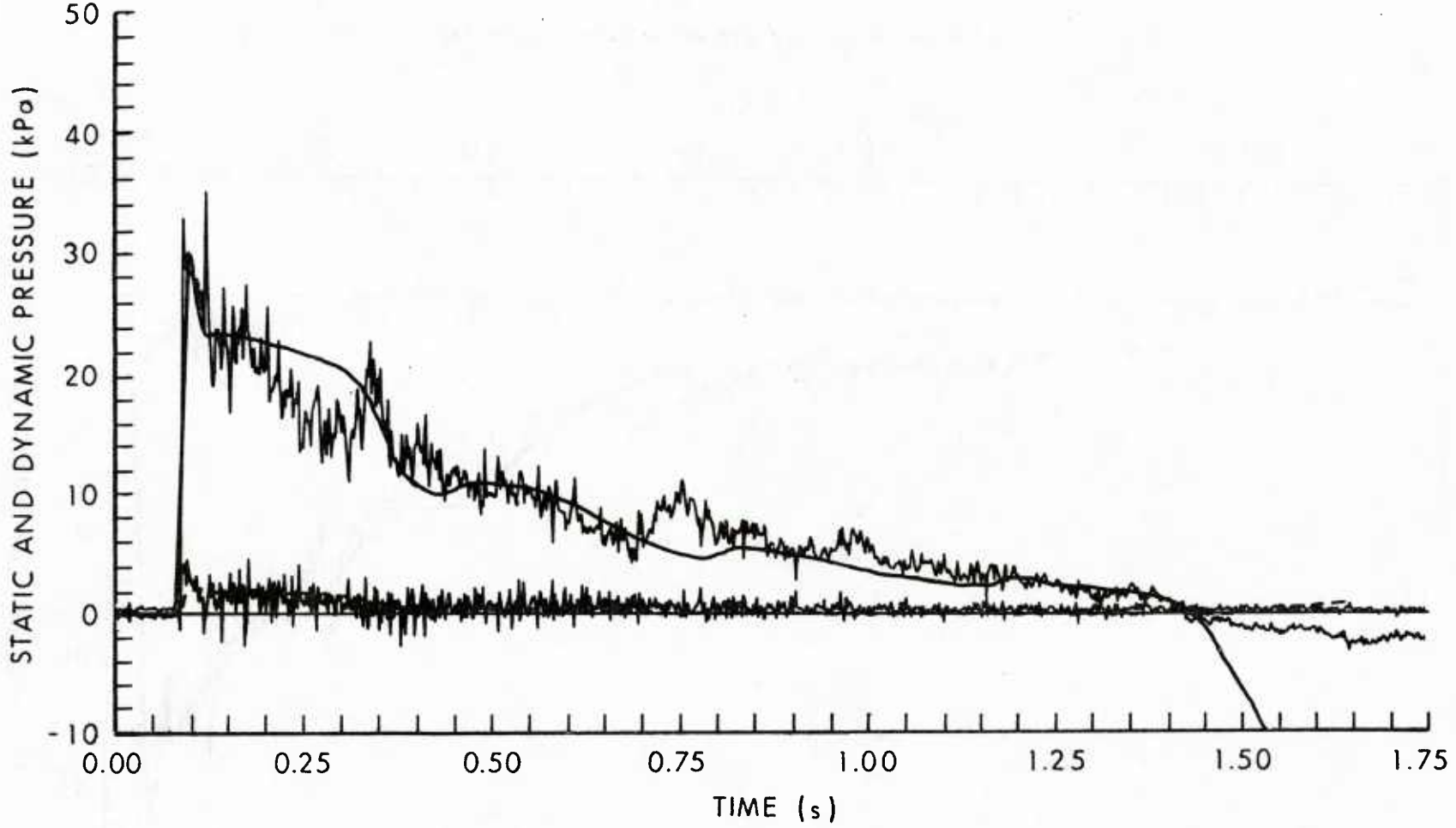

(a) Test 5: Driver Pressure 11.4 atm, Driver Volume 95%

Figure 12. Matched Computations for the CEG Experiments

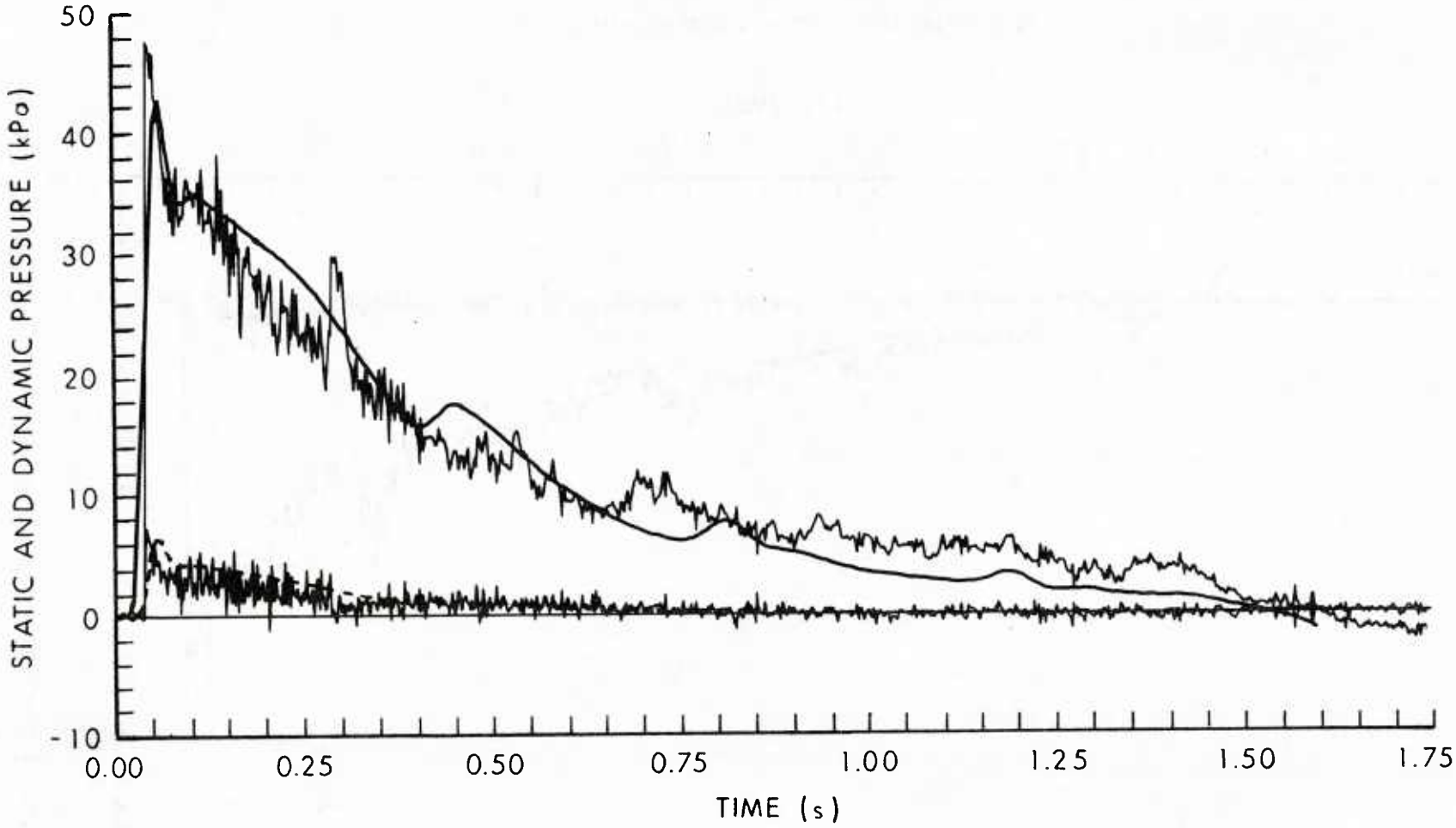

(b) Test 9: Driver Pressure 22.9 atm, Driver Volume 73%

Figure 12. (continued)

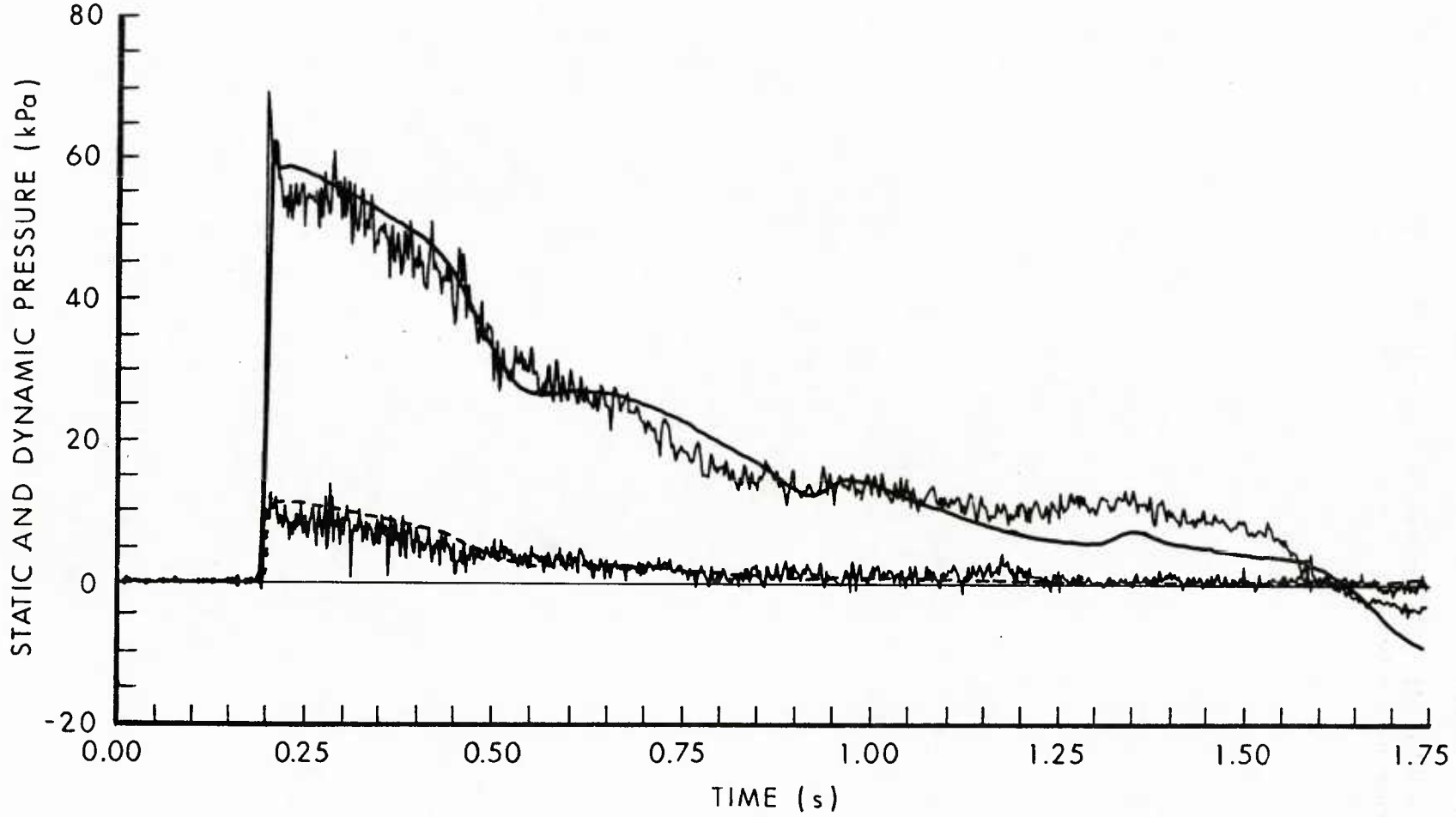

(c) Test 8: Driver Pressure 37.5 atm, Driver Volume 84%

Figure 12. (concluded)

computation is needed to more accurately treat the flow details in the mixing region behind the exits of the multiple divergent nozzles.

Overall, the BRL-Q1D code performs well in providing good predictions and correct trends with efficiency and low cost.

REFERENCES

[1] Gratias, S. and Monzac, J. B. G., "The Large-Scale Nuclear-Blast Simulator of the Gramat Research Center: (1) Concept, Research, Performance;
(2) Description and Operational Utilization."
Proceedings of the Seventh International Symposium on the Military Application of Blast Simulation, Medicine Hat, Alberta, Canada, 13-17 July 1981.

[2] Beam, R. M. and Warming, R. F., "An Implicit Factored Scheme for the Compressible Navier-Stokes Equations," AIAA Journal, Vol. 16, No. 4, April 1978, pp. 393-402.

[3] Warming, R. F., and Beam, R. M., "On the Construction and Application of Implicit Factored Schemes for Conservation Laws," SIAM-AMS Proceedings, Symposium on Computational Fluid Dynamics, New York, NY, April 1977

[4] Beam, R. M., and Warming, R. F., "An Implicit Factored Scheme for the Compressible Navier-Stokes Equations II: The Numerical ODE Connection," Paper No. 79-1446, AIAA 4th Computational Fluid Dynamics Conference, Williamsburgh, VA, 23-24 July 1979

[5] Roach, P. J., "Computational Fluid Dynamics," Hermosa Publishers, Albuquerque, NM, 1976

[6] Peyret, R., and Viviand, H., "Computations of Viscous Compressible Flow Based on the Navier-Stokes Equations," AGARD-AG-212, 1975

[7] Lomax, H., "Stable Implicit and Explicit Numerical Methods for Integrating Quasi-Linear Differential Equations with Parasitic-Stiff and Parasitic-Saddle Eigenvalues," NASA TN D-4703, 1986

[8] Briley, W. R., and McDonald, H., "Solution of the Three-Dimensional Compressible Navier-Stokes Equations by an Implicit Technique," Proceedings of the 4th International Conference on Numerical Methods in Fluid Dynamics, Lecture Notes in Physics, Vol. 35, Springer-Verlag, Berlin, 1975

[9] Baker, W. E., ed. "Explosions in Air: Engineering Design Handbook, Part One," AMC Pamphlet No. 706-181, Headquarters, U. S. Army Material Command, Alexandria, VA, July 1974

[10] "DISSPLA (Display Integrated Software System and Plotting Language)" Copyrighted 1975 by ISSCO: Integrated Software Systems Corporation, 4186 Sorrento Valley Blvd, San Diego, California 92121.

[11] Coulter, G. A. and Bertrand, B. P., "BRL Shock Tube Facility for the Simulation of Air Blast Effects," BRL-MR-1685, US Army Ballistic Research Laboratory, Aberdeen Proving Ground, Maryland 21005, August 1965.

[12] Bertrand, B. P., Private Communications, Ballistic Research Laboratory, Terminal Ballistics Division, Aberdeen Proving Ground, Maryland.

[13] Bertrand, B. P., "BRL Dual Shock-Tube Facility," BRL-MR-2001, Ballistic Research Laboratory, Aberdeen Proving Ground, Maryland 21005, August 1969.

[14] Amann, H. O., "Theoretical and Experimental Investigations for the Driving Mechanism of a Large-Diameter Shock Tube," Proceedings of the Fourth International Symposium on the Military Application of Blast Simulation, Southend-on-Sea, Great Britain, 9-12 September 1974.

[15] Teel, G, Private Communication, U. S. Army Ballistic Research Laboratory, Terminal Ballistics Division, Aberdeen Proving Ground Maryland 21005.

[16] Mark, A., Opalka, K. O., et al., "Simulation of Nuclear Blasts with Large-Scale Shock Tubes," Proceedings of the Eighth International Symposium on Military Applications of Blast Simulation, Spiez, Switzerland, 20-24 June 1983.

[17] Hisley, D. M., Gion, E. J. and Bertrand, B. P., "Performance and Predictions for a Large Blast Simulator Model," BRL-TR-2647, U. S. Army Ballistic Research Laboratory, Aberdeen Proving Ground, Maryland, April 1985

APPENDIX

CONTENTS

```
C  **   **   **   **   **   **   **   **   **   **   **   **   **   **
C
C                  QUASI 1-D EULER IMPLICIT/EXPLICIT CODE
C                  ======================================
C
C  **   **   **   **   **   **   **   **   **   **   **   **   **   **
C
C     THIS CODE COMPUTES THE FLOW IN SHOCK TUBES WITH VARIABLE CROSS-
C     SECTIONAL AREA BY SOLVING THE QUASI-ONE-DIMENSIONAL EULER EQUATIONS
C     EMPLOYING ONE OF THE FOLLOWING FINITE-DIFFERENCE SCHEMES.
C       (A) BEAM & WARMING'S IMPLICIT, BLOCK-SIMULTANEOUS SOLUTION,
C       (B) MACCORMACK'S EXPLICIT, PREDICTOR/CORRECTOR TECHNIQUE.
C
C     ALL INPUT VARIABLES ARE NONDIMENSIONALIZED IN THE CODE:
C     DIMENSIONLESS  =     DIMENSIONAL        VARIABLE
C     ------------------------------------------------------------
C       TAU          =     AAMB*TIME/REFL     TIME
C       X            =     X/REFL             PHYS. LENGTH
C       XI           =     XI/REFL            COMPUT. LENGTH
C       A            =     A/REFL**2          AREA
C       RHO          =     RHO/RHO4           DENSITY
C       U            =     U/AAMB             VELOCITY
C       P            =     P/(RHO4*AAMB**2)   PRESSURE
C       E            =     E/(RHO4*AAMB**2)   ENERGY
C
C
C**    ***   ***   ***   ***   O U T P U T   ***   ***   ***   ***   ***
C
C    THIS CODE WRITES TO FILE OUTPUT (=TAPE6) AND TO TAPE15 AND TAPE16.
C
C    (1) OUTPUT (=TAPE6) IS WRITTEN IN SEVERAL SUBROUTINES:
C        READIN AND AREA ECHO THE INPUT DATA.
C        WRIT WRITES THE PHYSICAL SHOCK-TUBE AND GAS PARAMETERS AT
C        A GIVEN TIME STEP.
C        OUTPOT WRITES THE PRESSURE VS TIME RECORD, AND RECORDS
C        THE BLAST-WAVE PARAMETERS (PSO,TA,PPD,ISO,IQ).
C
C    (2) TAPE15 IS WRITTEN IN SUBROUTINE PLOTX.  IT CONTAINS PRESSURE &
C        DENSITY VS DISTANCE RECORDS FOR PLOTTING WITH PROGRAM PX1DPLT.
C        DATA ARE WRITTEN TO TAPE15 IN BINARY FORMAT FOR EACH TIME STEP
C        FOR WHICH N/NPLOX IS A WHOLE NUMBER.  TAPE15 HAS TO BE READ
C        EXACTLY THE WAY IT WAS WRITTEN IN SUBROUTINE PLOTX, NAMELY
C
C          READ(15) JM1,KCS,KTUBE,LS,MTRX,NPL,NSTA,PRAT,TIME,DREF,REFL,
C         +         TEST,VOLD,XCLST,XSTA
C                            (NOTE THAT XSTA IS AN ARRAY OF DIMENSION(6)!)
C          READ(15) (X(J),J=1,JM1)
C          READ(15) (FP(J),J=1,JM1)
C          READ(15) (Q1(J),J=1,JM1)
C          READ(15) (FU(J),J=1,JM1)
C          READ(15) (ARA(J),J=1,JM1)
C
C    (3) TAPE16 IS WRITTEN IN SUBROUTINE OUTPOT.  IT CONTAINS PRESSURE
C        & DENSITY VS TIME RECORDS FOR PLOTTING WITH PROGRAM PT1DPLT.
C        DATA ARE WRITTEN TO TAPE16 IN BINARY FORMAT FOR EVERY IOUT-TH
C        TIME STEP.  TAPE16 HAS TO BE READ EXACTLY THE WAY IT WAS WRITTEN
C        IN SUBROUTINE OUTPOT, NAMELY
C
```

```
C        READ(16) DVNL,DRVL,PRAT,TRAT,TSTA,JMAX,NMAX,KTUBE,REFL,VOLD,
C       + PAMB,TAMB,RWEL,PPD,PSO,QIM,QS,SIM,TAR,WYS,WYQ,PPF,NXK,TEST,VALV
C        DO NN M=1,NMAX
C     NN   READ(16) TIME(M),VFLO(M),OPS(M),PDYN(M),ARJX(M)
C
C
C**   ***   ***   I N P U T   R E Q U I R E M E N T S   ***   ***   ***
C
C     ALL DIMENSIONS MUST ACCORD WITH THE INTERNATIONAL SYSTEM OF UNITS,
C     I. E. METRE (M) FOR LENGTH, KILOGRAM (KG) FOR MASS (WEIGHT),
C     DEGREES CELSIUS (C) FOR TEMPERATURE, KILOPASCAL (KPA) FOR PRESSURE,
C     MILLISECONDS (MS) FOR TIME, METRE/SECOND (M/S) FOR VELOCITY,
C     CUBIC METRE (M**3) FOR VOLUME, AND KG/M**3 FOR DENSITY.
C
C
C     TO CONVERT FROM          TO                        MULTIPLY BY
C     ------------------------------------------------------------------
C      FAHRENHEIT (TF)         CELSIUS (TC)              TC=(5/9)*(TF-32)
C      FOOT(/SECOND)           METRE(/SECOND)            .3048    E+00
C      INCH(/SECOND)           METRE(/SECOND)            .0254    E+00
C      KILOMETRE/HOUR          METRE/SECOND              .27778   E+00
C      KNOT (NAUT. MILE/HOUR)  METRE/SECOND              .51444   E+00
C      LBM (POUND MASS)        KILOGRAM                  .45359   E+00
C      LBM/FT**3 (DENSITY)     KILOGRAM/METRE**3         .16018   E+02
C      LBM/IN**3 (DENSITY)     KILOGRAM/METRE**3         .27680   E+05
C      MILE, NAUTICAL          METRE                     .1852    E+04
C      MILE, STATUTE           METRE                     .16093   E+04
C      MILE/HOUR               METRE/SECOND              .44704   E+00
C      POUND MASS (LBM)        KILOGRAM                  .45359   E+00
C      PSI (POUND/INCH**2)     KILOPASCAL                .68948   E+01
C      RANKINE (TR)            CELSIUS (TC)              TC=(5/9)*TR-273.15
C      SLUG                    KILOGRAM                  .14594   E+02
C      SLUG/FOOT**3            KILOGRAM/METRE**3         .51538   E+03
C      YARD                    METRE                     .9144    E+00
C     ------------------------------------------------------------------
C
C
C  ***   ***   ***   I N P U T   D A T A   F O R M A T   ***   ***   ***
C
C     ALL INPUT IS LIST DIRECTED.  DATA ARE STORED ON CARD IMAGES EACH
C     CONSISTING OF A STRING OF VALUES WHICH ARE DESCRIBED BELOW.
C     THE VALUES ARE SEPARATED BY ONE OR MORE BLANKS, OR BY A COMMA OR
C     SLASH, EITHER OF WHICH CAN BE PRECEEDED OR FOLLOWED BY ANY NUMBER
C     OF BLANKS.  ALSO, A LINE BOUNDARY SERVES AS A SEPARATOR.
C
C     EMBEDDED BLANKS ARE NOT ALLOWED IN INPUT VALUES EXCEPT CHARACTER
C     VALUES AND COMPLEX NUMBERS.  WHEN THE VALUE SEPARATOR IS A SLASH,
C     REMAINING LIST ELEMENTS ARE TREATED AS NULLS AND THE REMAINDER
C     OF THE CURRENT RECORD IS DISREGARDED.
C     INPUT VALUES MUST CORRESPOND IN TYPE TO VARIABLES IN THE I/O LIST.
C     HOWEVER, REAL NUMBERS MAY LOOK LIKE INTEGERS.  THE FORMAT OF VALUES
C     IN THE INPUT RECORD IS AS FOLLOWS.
C
C        INTEGERS             FORMAT IS SAME AS FOR INTEGER CONSTANTS.
C
C        REAL NUMBERS         ANY VALID FORTRAN FORMAT.  THE DECIMAL POINT
C                             MAY BE OMITTED  IT IS ASSUMED TO BE TO THE
C                             RIGHT OF THE MANTISSA.
C
```

```
C        CHARACTER VALUES  A STRING OF CHARACTERS ENCLOSED BY
C                          APOSTROPHES  ... CAN ONLY BE READ INTO
C                          CHARACTER ARRAYS, VARIABLES AND SUBSTRINGS.
C
C        LOGICAL VALUES    T OR F FOLLOWED BY OPTIONAL CHARACTERS
C                          EXCLUSIVE OF SEPARATORS (, AND /) OPTIONALLY
C                          PRECEEDED OR ENCLOSED BY PERIODS.
C
C
C  ***   ***   ***    I N P U T   D A T A   C A R D S    ***   ***   ***
C
C
C**  CARD 1:  PROGRAM I/O CONTROL PARAMETERS (7 VALUES)
C    ------------------------------------------------
C
C    1. TEST  - PROBLEM IDENTIFICATION CODE (USE FORMAT A10)
C               *** N O T E :  THE CHARACTER STRING HAS TO BE ENCLOSED
C                 BY DELIMITERS, E. G. 'A NEW TEST'.
C
C    2. METH  - CHOICE OF COMPUTATIONAL SCHEME
C               = 1, BEAM-WARMING IMPLICIT TECHNIQUE
C               = 2, MACCORMACK'S EXPLICIT TECHNIQUE
C
C    3. IOUT  - FLAG FOR PRINTED OUTPUT OF FLOW PARAMETERS VS TIME
C                 AT A PREDEFINED X-STATION (XSTA).
C                 FOR IOUT > 0, EVERY IOUT-TH TIME STEP WILL BE PRINTED
C                 FOR IOUT <=0, NO PRINTED OUTPUT(!)
C
C    4. IPLOT - LOGICAL FLAG FOR STORING THE PRESSURE-TIME RECORD
C                 ON TAPE16 FOR LATER PLOTTING: T(RUE) OR F(ALSE).
C
C    5. NWRIT - FLAG FOR PRINTED OUTPUT OF PHYSICAL AND FLOW PARAMETERS
C                 AT ALL GRID POINTS, AFTER EVERY NWRIT-TH TIME STEP.
C                 USE SPARINGLY, E.G. SET NWRIT = NMAX, NMAX/2, OR
C                 NMAX/3, ETC.  SET NWRIT <= 0, IF NO OUTPUT WANTED.
C
C    6. NSTA  - NUMBER OF FIXED STATIONS AT WHICH PARTIAL OUTPUT
C                 IS WANTED, FROM 1 TO 6.
C
C    7. NPLOX - FLAG FOR PLOTTING P-X DATA EVERY NPLOX-TH ITERATION
C    .           <=0, FOR NO PLOTS.
C
C
C**  CARD 2:  OUTPUT STATIONS ("NSTA" VALUES, MAX. 6)
C    ------------------------------------------------
C
C     XSTA(J)  -  DISTANCE OF THE J-TH OUTPUT STATION FROM THE
C                 UPSTREAM END OF THE DRIVEN TUBE, METRE.
C
C
C**  CARD 3:  COMPUTATIONAL-GRID PARAMETERS (4 VALUES)
C    ------------------------------------------------
C
C    1. JMAX  - TOTAL NUMBER OF GRID POINTS (MAXIMUM 1,002)
C                 (1) FOR A SIMPLE, LINEAR GRID WITH CONSTANT CELL SIZE
C                       JMAX = REF.-LENGTH/CELL-SIZE + 2
C                 (2) FOR A LINEAR GRID WITH FINE-GRID OVERLAY ABOUT
C                     REGIONS OF AREA CONSTRICTIONS (BAFFLES OR NOZZLE)
C                       JMAX = REF.-LENGTH/CELL-SIZE + BET*NXK
```

```
C                (3) FOR NON-LINEAR CLUSTERING OF GRID POINTS ABOUT A
C                    SINGLE POINT USING SINH FUNCTION, CONSULT
C                    CLUSTERING GRAPH FOR CHOICE OF CELL SIZE AND BET.
C              FOR FURTHER INFO, SEE MTRX.
C
C     2. MTRX  - FLAG FOR CHOICE OF GRIDDING FUNCTION.
C              = 1, LINEAR GRID-DISTRIBUTION FUNCTION USED,
C                   CELL WIDTH EQUALS REFL/(JMAX-2).
C              = 2, LINEAR MULTIPLE-GRID FUNCTION USED FOR DEFINING
C                   FINE GRID ABOUT PARABOLIC AREA CONSTRICTIONS,
C                   SHORT DRIVER, NOZZLE, AND RWE.
C              = 3, ARCSINH FUNCTION USED FOR CLUSTERING ABOUT XCLST
C                   NOTE:  ONLY ONE CLUSTER REGION IN GRID POSSIBLE.
C
C     3. BET   - FACTOR USED FOR GRID CLUSTERING (E.G. BET=20).
C              FOR MTRX=2: EQUALS NO. OF POINTS IN PARABOLIC
C                          AREA CONSTRICTIONS.
C              FOR MTRX=3: AUGMENTS CLUSTER EFFECT ABOUT XCLST.
C
C     4. XCLST - CLUSTER ABOUT PHYSICAL X-LOCATION, IN METRE,
C              MEASURED FROM DRIVER END OF SHOCK TUBE.
C              USED ONLY WHEN MTRX = 3.
C
C
C**   CARD 4:  COMPUTATIONAL-SCHEME PARAMETERS (5 VALUES)
C     ---------------------------------------------------
C
C     1. NMAX  - NUMBER OF TIME STEPS IN COMPUTATION
C              NOTE: ONLY 6000 TIME STEPS WILL BE STORED
C                    FOR OUTPUT AND LATER PLOTTING.
C
C     2. NUST  - NEW TIME STEP COMPUTED AFTER EVERY NUST-TH ITERATION.
C              <=0, FOR CONSTANT TIME STEP.
C
C     3. CN    - COURANT NUMBER
C              = 1.0, FOR IMPLICIT SCHEME (METH=1)
C              = 0.9, FOR EXPLICIT SCHEME (METH=2)
C
C     4. SMU   - SMOOTHING COEFFICIENT FOR DISSIPATIVE TERM
C              = 0.04, FOR IMPLICIT SCHEME (METH=1)
C              = 0.02, FOR EXPLICIT SCHEME (METH=2)
C
C     5. LS    - NUMBER OF CELLS OVER WHICH THE SHOCK IS STRETCHED
C              ON EITHER SIDE OF THE DISCONTINUITY,
C              = 0 FOR STEP SHOCK,  >0 FOR STRETCHING.
C
C
C**   CARD 5:  INITIAL (TEST) CONDITIONS (8 VALUES)
C     ---------------------------------------------
C
C     1. PAMB  - AMBIENT PRESSURE [KPA]
C
C     2. TAMB  - AMBIENT TEMPERATURE [KELVIN]
C
C     3. PRAT  - RATIO OF DRIVER/DRIVEN-TUBE PRESSURES
C
C     4. TRAT  - RATIO OF DRIVER/DRIVEN-TUBE TEMPERATURE
C
C     5. P51   - PRESSURE RATIO IN THERMAL REGION 5
```

```
C
C     6. T51    - TEMPERATURE RATIO IN THERMAL REGION 5
C
C     7. XTH1   - START OF THERMAL REGION (MIN X-COORDINATE), METRE,
C                 MEASURED FROM THE EXIT OF THE DIVERGENT NOZZLE.
C
C     8. XTH2   - END OF THERMAL REGION (MAX X-COORDINATE), METRE,
C                 MEASURED FROM THE EXIT OF THE DIVERGENT NOZZLE.
C
C
C**   CARD 6:   SHOCK-TUBE CONFIGURATION (10 VALUES)
C     ----------------------------------------------
C
C     1. KTUBE  - TYPE OF SHOCK TUBE
C               = 1, CYLINDRICAL SHOCK TUBE WITH, OR WITHOUT PARABOLIC
C                    AREA CONSTRICTIONS (BAFFLES) IN DRIVER, DIAPHRAGM
C                    LOCATION, OR DRIVEN TUBE (I.E. TEST TUBE).
C                    NOTE THAT A DRIVER DIAMETER OTHER THAN THAT OF THE
C                    DRIVEN TUBE IS PERMITTED WITH THIS CONFIGURATION.
C               = 2, SHOCK TUBE AS DESCRIBED ABOVE WITH A CONVERGENT
C                    -DIVERGENT NOZZLE.
C               = 3, SHOCK TUBE WITH STEPPED DRIVER WITH/WITHOUT
C                    CONVERGENT-DIVERGENT NOZZLE AND/OR PARABOLIC AREA
C                    CONSTRICTIONS (BAFFLES).
C               = 4, SHOCK TUBE WITH CONICAL DRIVER AND WITH/WITHOUT
C                    CONVERGENT-DIVERGENT NOZZLE AND/OR PARABOLIC AREA
C                    CONSTRICTIONS (BAFFLES).
C                 ALL OTHER VALUES DEFAULT TO 1
C
C     2. VALV   - LOGICAL FLAG FOR BLAST VALVE IN DIAPHRAGM LOCATION
C                 (TRUE OR FALSE)
C
C     3. NXK    - NUMBER OF PARABOLIC AREA CONSTRICTIONS (FROM 0 TO 11).
C                 N O T E :   UP TO 11 CONSTRICTIONS MAY BE PLACED
C                 ANYWHERE IN THE SHOCK TUBE EXCEPT IN THE DIVERGING
C                 OR CONVERGING SECTIONS OF THE NOZZLE.
C
C     4. IRWE   - FLAG FOR RAREFACTION-WAVE ELIMINATOR (RWE).
C               < 0, NO RWE (ANY NEGATIVE VALUE)
C               = 0, STATIC RWE (ZERO ONLY)
C               > 0, MOVING RWE (ANY NON-ZERO, POSITIVE VALUE)
C
C     5. REFL   - OVERALL REFERENCE LENGTH OF SHOCK TUBE [METRE]
C
C     6. ERRL   - PERMISSIBLE ERROR IN CHECK OF TOTAL LENGTH [METRE]
C
C     7. DREF   - REFERENCE DIAMETER OF SHOCK TUBE, I.E.
C                  DIAMETER OF DRIVEN TUBE, METRE.
C
C     8. DVNL   - LENGTH OF DRIVEN TUBE [METRE]
C
C     9. DRVL   - TOTAL LENGTH OF DRIVER (DIAPHRAGM LOCATION), METRE
C
C    10. DTHR   - DRIVER DIAMETER AT THE DIAPHRAGM LOCATION, METRE,
C                 USED WHEN KTUBE = 1.
C
C
```

```
C**   CARD 7:  BLAST VALVE (9 VALUES)
C     ------------------------------
C     N O T E :   THIS CARD ONLY IF   VALV= .TRUE.   ON CARD 6!
C
C     1. XBEG  - X-COORDINATE AT WHICH THE BLAST VALVE (PARABOLIC
C                CONTRACTION) STARTS, MEASURED FROM THE UPSTREAM END
C                OF THE SHOCK TUBE, METRE.
C
C     2. XEND  - X-COORDINATE AT WHICH THE BLAST VALVE (PARABOLIC
C                CONTRACTION) ENDS, MEASURED FROM THE UPSTREAM END
C                OF THE SHOCK TUBE, METRE.
C
C     3. DBEG  - DIAMETER OF INITIAL BLAST VALVE OPENING, METRE.
C
C     4. DMID  - DIAMETER OF FULLY OPEN BLAST VALVE, METRE.
C
C     5. DEND  - DIAMETER OF FINAL BLAST VALVE OPENING, METRE.
C
C     6. TV1   - TIME AT WHICH BLAST VALVE BEGINS TO OPEN, SECONDS,
C                MEASURED FROM START OF THE COMPUTATION (ZERO TIME).
C
C     7. TV2   - OPENING TIME OF BLAST VALVE, STARTING AT TV1, SECONDS.
C
C     8. TV3   - TIME PERIOD DURING WHICH BLAST VALVE STAYS FULLY OPEN,
C
C     9. TV4   - CLOSING TIME OF BLAST VALVE TO DEND, FOLLOWING TV3,
C                SECONDS.
C
C
C**   CARD 8:  AREA CONSTRICTIONS ("NXK" CARDS, 4 VALUES EACH), METRE.
C     ------------------------------------------------------------------
C               N O T E :   THIS CARD ONLY IF  NXK > 0  ON CARD 6.
C                           MAXIMUM OF 11 CARDS PERMITTED.
C
C     1. DK(J) - THROAT DIAMETER OF THE J-TH AREA CONSTRICTION.
C
C     2. X1(J) - X-COORDINATE (MIN) AT WHICH THE CONSTRICTION STARTS
C                MEASURED FROM THE UPSTREAM END OF THE SHOCK TUBE.
C
C     3. X0(J) - CENTER POINT (THROAT) X-COORDINATE OF CONSTRICTION
C                MEASURED FROM THE UPSTREAM END OF THE SHOCK TUBE.
C
C     4. X2(J) - X-COORDINATE (MAX) AT WHICH THE CONSTRICTION ENDS
C                MEASURED FROM THE UPSTREAM END OF THE SHOCK TUBE
C
C
C**   CARD 9:  COMPONENT DRIVER DIMENSIONS (8 VALUES), METRE.
C     ------------------------------------------------------
C               N O T E :   THIS CARD ONLY IF  KTUBE > 1  ON CARD 6!
C
C     1. XDR1  - LENGTH    \
C                           > DRIVER SECTION 1
C     2. DDR1  - DIAMETER  /
C
C     3. XDR2  - LENGTH    \
C                           > DRIVER SECTION 2
C     4. DDR2  - DIAMETER  /
C
```

```
C     5. XDR3   - LENGTH    \
C                            > DRIVER SECTION 3
C     6. DDR3   - DIAMETER  /
C
C     7. XDR4   - LENGTH    \
C                            > DRIVER SECTION 4
C     8. DDR4   - DIAMETER  /
C
C     NOTE:  FOR LESS THAN 4 SECTIONS USE ANY 2 OR 3 SECTIONS,
C            AND SET REMAINDER EQUAL TO ZERO.
C
C
C**   CARD 10:  COMPONENT NOZZLE DIMENSIONS (6 VALUES), METRE.
C     ------------------------------------------------------
C               N O T E :   THIS CARD ONLY IF  KTUBE > 1  ON CARD 6!
C
C     1. XCON   - LENGTH OF THE CONVERGING-NOZZLE SECTION.
C
C     2. XTHR   - LENGTH OF THE CYLINDRICAL THROAT SECTION.
C
C     3. DTHR   - DIAMETER OF THE THROAT SECTION.
C
C     4. XDIV   - LENGTH OF THE DIVERGENT-NOZZLE SECTION.
C
C     5. DDIV   - DIAMETER OF THE DIVERGENT-NOZZLE EXIT.
C
C     6. XDPH   - LOCATION OF DIAPHRAGM MEASURED FROM END OF DRIVER,
C                 (I.E. BEGINNING OF NOZZLE) WHEN CARD 9 IS SPECIFIED
C                 N O T E :   IF (KTUBE.LT.3) THEN XDPH = 0 !!!
C
C
C**   CARD 11:  RAREFACTION WAVE ELIMINATOR - RWE (7 VALUES).
C     ------------------------------------------------------
C               N O T E :   THIS CARD ONLY IF  IRWE >= 0  ON CARD 6!
C
C     1. RWEL   - LENGTH OF THE RAREFACTION WAVE ELIMINATOR (RWE).
C
C     2. AFIR   - RATIO OF INITIALLY OPEN RWE-AREA RELATIVE TO
C                 THE TOTAL CROSSECTIONAL AREA OF THE DRIVEN TUBE.
C
C     3. TAU1   - TIME PERIOD DURING WHICH AFIR IS CONSTANT, SECONDS,
C                 MEASURED FROM START OF COMPUTATION (ZERO-TIME).
C
C     4. TAU2   - CLOSING TIME OF RWE, STARTING AT TAU1, SECONDS.
C
C     5. AMIN   - RATIO OF THE MINIMUM OPEN RWE-AREA AT TAU2 RELATIVE TO
C                 THE TOTAL CROSSECTIONAL AREA OF THE DRIVEN TUBE.
C
C     6. TAU3   - TIME PERIOD DURING WHICH RWE STAYS CLOSED, SECONDS.
C
C     7. TAU4   - OPENING TIME OF RWE TO AMAX FOLLOWING TAU3, SECONDS.
C
C     8. AMAX   - RATIO OF THE FINAL, FULLY-OPEN RWE-AREA RELATIVE TO
C                 THE TOTAL CROSSECTIONAL AREA OF THE DRIVEN TUBE.
C
C
C  **    **    **    **    **    **    **    **    **    **    **    **    **    **
```

INPUT JOB STREAM USING THE CALCOMP UTILITY FOR PLOTTING:

```
KOPALKA,STMFZ,T400,P3.        PF=HATS8
ACCOUNT,*****.
DISPOSE(OUTPUT,ST=MFA,*PR)
COMMENT.   ***********************************************
COMMENT.   *              HATS TEST AT CEG                 *
COMMENT.   *          FRENCH LBS - 1/7TH MODEL:            *
COMMENT.   *      SHOT #8 (27 NOV 81) - PSO= 67 KPA        *
COMMENT.   *    ------------------------------------       *
COMMENT.   *    (1) STEPPED DRIVER-    V= 43.22 M**3       *
COMMENT.   *        'HATS8/CEG'  L= 44 M,  P41= 26.8        *
COMMENT.   *    (2) CONICAL DRIVER-    V= 36.49 M**3       *
COMMENT.   *        'HATS8/Q1D'  L= 44 M,  P41= 37.5        *
COMMENT.   *    ------------------------------------       *
COMMENT.   *    DRIVEN-  L= 310.0 METRE,    NO RWE!         *
COMMENT.   *    OUTPUT STATION #7: XSTA= 121.5 METRE        *
COMMENT.   ***********************************************
ATTACH(Q1DUB,ID=OPALKA)
MAP(OFF)
Q1DUB.
RETURN,Q1DUB.
REWIND(TAPE15,TAPE16)
ATTACH(CALCMP,ID=DISSPLA)
ATTACH(DISSPLA,ID=DISSPLA)
LIBRARY(DISSPLA,CALCMP)
REWIND(TAPE15,TAPE16)
ATTACH(PXPLT,ID=OPALKA)
PXPLT.
RETURN(TAPE15,PXPLT)
ATTACH(PTPLT,ID=OPALKA)
PTPLT.
BEGIN,PLOT,CALCOMP,TAPE7.
*EOR
  'HATS8/CEG'    1   30    T    -9999    1    60
   66.5
  502    0   2700    1   1   0   3   .04
    5    45.65    0    0
   99.0    280.15    26.8     1    1    1    0    0
    3   F   0   -1    365.0   .01    3.5886   310.0    45.65   0.665
    9   .711     9   .871     7   1.124     19   1.33
    0.89    2.52    0.665    7.59    2.286    1.65
  'HATS8/Q1D'    1   30    T    -9999    1    60
   66.5
  502    0   2700    1   1   0   3   .04
    5    45.65    0    0
   99.0    280.15    37.5     1    1    1    0    0
    4   F   0   -1    365.0   .01    3.5886   310.0    45.65   0.665
    0   0    0   0    0   0.66    44   1.33
    0.89    2.52    0.665    7.59    2.286    1.65
*EOR
   8.5   11.   4   47   0.01   5   'CALCMP'
   0.    1.    .1    5
  .00    .5    .05   5
*EOR
   11.   8.5   2.1   1.1   7   4.5
    0   1.75   .25   5
  -20    100   20    5
    0    6.4   2.2   .19   2   'CALCMP'
```

INPUT JOB STREAM USING THE DISSPOP UTILITY FOR PLOTTING:

```
OPALKA,STMFZ,T400,P3.
ACCOUNT,*****.
DISPOSE(OUTPUT,ST=MFA,*PR)
COMMENT.
COMMENT.   ****************************************
COMMENT.   *   MATCHING BERTRAND'S EXPERIMENTS     *
COMMENT.   *     LBS-MODEL A2 - SCALE 1:37.4       *
COMMENT.   *           TEST # 24-84-26             *
COMMENT.   *   ---------------------------------   *
COMMENT.   *   STEPPED DRIVER-     P41= 107.8      *
COMMENT.   *       L= 0.884 M      T41= 1.593      *
COMMENT.   *   ---------------------------------   *
COMMENT.   *   EXPANSION TUNNEL-  L= 5.461 M;      *
COMMENT.   *    TEST-STA # 7 (X= 1.778 METRE)      *
COMMENT.   *   ---------------------------------   *
COMMENT.   *       JMAX= 502 WITH MTRX= 3          *
COMMENT.   ****************************************
COMMENT.
ATTACH,Q1DUB,ID=OPALKA.
MAP(OFF)
Q1DUB.
RETURN,Q1DUB.
REQUEST,PLFILE,*PF.
ATTACH,DISSPLA,ID=DISSPLA.
ATTACH,COMPRS,ID=DISSPLA.
LIBRARY,DISSPLA,COMPRS.
REWIND(TAPE15,TAPE16)
ATTACH,PTPLT,ID=OPALKA.
PTPLT.
SAVEPF(PLFILE,PTA26,UN=OPALKA,UP=*****,ST=MFA,CH=*****,PN=**,TY=SAVE)
RETURN(TAPE16,PTPLT)
REWIND,PLFILE.
ATTACH,PXPLT,ID=OPALKA.
PXPLT.
SAVEPF(PLFILE,RXA26,UN=OPALKA,UP=*****,ST=MFA,CH=*****,PN=**,TY=SAVE)
*EOR
   'MOD.A2-26'   1    45    T    2100    1    90
   1.778
   502    0    4320    1    1.0    0    3    .04
    5    .928    0    0
   101.4    299.8    107.8    1.593   1   1   0   0
     3    F   0   -1    6.64    .001    .254    5.461    .928    .0435
   .241   .0503    .241   .0617    .187   .0795    .215   .0942
   .024    .068   .0435    .202   .1618    .044
*EOR
   11    8.5    2.1   1.1    7.0   4.5
    0   .035   .005   5
  -50    250    50    5
    0    6.4    2.2   .19    2   'COMPRS'
*EOR
    8.5   11    4    49   .01   5   'COMPRS'
    0.    1.    .1    5
    0.   .55   .05    5
```

INPUT PARAMETERS FOR CASE NO. 1

```
$CARD1
TEST    = 'MOD.A2-26 ',
METH    = 1,
IOUT    = 45,
IPLOT   = T,
NWRIT   = 2100,
NSTA    = 1,
NPLOX   = 90,
$END
$CARD2:  OUTPUT (TEST) STATIONS
   XSTA(I) =  .17780E+01

$CARD3
JMAX    = 502,
JAGD    = 0,
NMAX    = 4320,
NUST    = 1,
CN      = .1E+01,
LS      = 0,
MTRX    = 3,
SMU     = .4E-01,
$END

$CARD4
BET     = .5E+01,
XCLST   = .928E+00,
US      = 0.0,
SLPE    = 0.0,
$END
```

*** N O T E : STRETCHING FUNCTION USED IS
XI = ALPHA*ARCSINH(BET*(X-X0))

```
$CARD5
PAMB    = .1014E+03,
TAMB    = .2998E+03,
PRAT    = .1078E+03,
TRAT    = .1593E+01,
P51     = .1E+01,
T51     = .1E+01,
XTH1    = 0.0,
XTH2    = 0.0,
$END
   ***  NO THERMAL LAYER SPECIFIED!  ***

$CARD6
KTUBE   = 3,
VALV    = F,
NXK     = 0,
IRVE    = -1,
REFL    = .664E+01,
ERRL    = .1E-02,
DREF    = .254E+00,
DVNL    = .5461E+01,
DRVL    = .928E+00,
DTHR    = .435E-01,
$END
$CARD7
   **  NO BLAST VALVE SPECIFIED!  **
$CARD8
   ** NO AREA CONSTRICTIONS SPECIFIED, NXK.LE.0! **

$CARD9
XDR1    = .241E+00,
```

```
DDR1    = .503E-01,
XDR2    = .241E+00,
DDR2    = .617E-01,
XDR3    = .187E+00,
DDR3    = .795E-01,
XDR4    = .215E+00,
DDR4    = .942E-01,
$END

$CARD10
XCON    = .24E-01,
XTHR    = .68E-01,
DTHR    = .435E-01,
XDIV    = .202E+00,
DDIV    = .1618E+00,
XDPH    = .44E-01,
$END
$CARD11:
   ***  NO RWE SPECIFIED!  ***
   NORMALIZED DIMENSIONS:
   ----------------------

   XDR1=      XDR2=      XDR3=      XDR4=      XCON=      XDPH=      XTHR=      XDIV=      XRWE=
    .03630     .07259     .10075     .13313     .13675     .13976     .14699     .17741     .99985

   NORMALIZED DIAMETERS:
   ---------------------

    DDR1=         (DDR2=)      (DDR3=)      DDR4=         DTHR=         DDIV=
     .7575E-02     .9292E-02    .1197E-01    .1419E-01     .6551E-02     .2437E-01

   OUTPUT GAS PARAMETERS AT STATION(S):     .44518

   **  GRID CLUSTERING ABOUT XCLST= .13976  **

   THE REFERENCE AREA (COMPUTED FROM DREF) IS .5067E-01 SQUAREMETRES.

   THE DRIVER VOLUME WAS COMPUTED FROM AREA(J) TO .3739E-02 CUBICMETRES.

  ============================  END OF INPUT DATA - RESULTS FOLLOW  ============================
```

** N = 0 AND TIME(SEC) = .00000E+00

"X"

1	10	-.13724E-02	.00000E+00	.13724E-02	.27405E-02	.41042E-02	.54635E-02	.68187E-02	.81696E-02	.95163E-02	.10859E-01
11	20	.12197E-01	.13532E-01	.14862E-01	.16189E-01	.17511E-01	.18830E-01	.20145E-01	.21456E-01	.22763E-01	.24067E-01
21	30	.25367E-01	.26663E-01	.27956E-01	.29245E-01	.30530E-01	.31812E-01	.33091E-01	.34367E-01	.35639E-01	.36907E-01
31	40	.38173E-01	.39435E-01	.40694E-01	.41950E-01	.43203E-01	.44452E-01	.45699E-01	.46943E-01	.48183E-01	.49421E-01
41	50	.50656E-01	.51888E-01	.53118E-01	.54344E-01	.55568E-01	.56789E-01	.58008E-01	.59224E-01	.60437E-01	.61648E-01
51	60	.62857E-01	.64063E-01	.65266E-01	.66468E-01	.67667E-01	.68863E-01	.70058E-01	.71250E-01	.72440E-01	.73627E-01
61	70	.74813E-01	.75997E-01	.77179E-01	.78358E-01	.79536E-01	.80712E-01	.81886E-01	.83058E-01	.84228E-01	.85397E-01
71	80	.86563E-01	.87729E-01	.88892E-01	.90054E-01	.91214E-01	.92373E-01	.93530E-01	.94686E-01	.95840E-01	.96993E-01
81	90	.98145E-01	.99295E-01	.10044E+00	.10159E+00	.10274E+00	.10388E+00	.10503E+00	.10617E+00	.10731E+00	.10845E+00
91	100	.10959E+00	.11073E+00	.11187E+00	.11301E+00	.11414E+00	.11528E+00	.11642E+00	.11755E+00	.11868E+00	.11982E+00
101	110	.12095E+00	.12208E+00	.12321E+00	.12434E+00	.12547E+00	.12660E+00	.12773E+00	.12886E+00	.12999E+00	.13111E+00
111	120	.13224E+00	.13337E+00	.13450E+00	.13562E+00	.13675E+00	.13788E+00	.13900E+00	.14013E+00	.14126E+00	.14238E+00
121	130	.14351E+00	.14464E+00	.14577E+00	.14689E+00	.14802E+00	.14915E+00	.15028E+00	.15140E+00	.15253E+00	.15366E+00
131	140	.15479E+00	.15592E+00	.15705E+00	.15819E+00	.15932E+00	.16045E+00	.16158E+00	.16272E+00	.16385E+00	.16499E+00
141	150	.16612E+00	.16726E+00	.16840E+00	.16954E+00	.17068E+00	.17182E+00	.17296E+00	.17410E+00	.17524E+00	.17639E+00
151	160	.17754E+00	.17868E+00	.17983E+00	.18098E+00	.18213E+00	.18328E+00	.18444E+00	.18559E+00	.18675E+00	.18791E+00
161	170	.18907E+00	.19023E+00	.19139E+00	.19256E+00	.19372E+00	.19489E+00	.19606E+00	.19723E+00	.19841E+00	.19958E+00
171	180	.20076E+00	.20194E+00	.20312E+00	.20430E+00	.20549E+00	.20667E+00	.20786E+00	.20905E+00	.21025E+00	.21144E+00
181	190	.21264E+00	.21384E+00	.21505E+00	.21625E+00	.21746E+00	.21867E+00	.21988E+00	.22110E+00	.22231E+00	.22353E+00
191	200	.22476E+00	.22598E+00	.22721E+00	.22844E+00	.22968E+00	.23091E+00	.23215E+00	.23340E+00	.23464E+00	.23589E+00
201	210	.23714E+00	.23840E+00	.23965E+00	.24092E+00	.24218E+00	.24345E+00	.24472E+00	.24599E+00	.24727E+00	.24855E+00
211	220	.24984E+00	.25112E+00	.25241E+00	.25371E+00	.25501E+00	.25631E+00	.25762E+00	.25893E+00	.26024E+00	.26156E+00
221	230	.26288E+00	.26420E+00	.26553E+00	.26687E+00	.26820E+00	.26954E+00	.27089E+00	.27224E+00	.27359E+00	.27495E+00
231	240	.27631E+00	.27768E+00	.27905E+00	.28043E+00	.28181E+00	.28319E+00	.28458E+00	.28597E+00	.28737E+00	.28877E+00
241	250	.29018E+00	.29159E+00	.29301E+00	.29443E+00	.29586E+00	.29729E+00	.29873E+00	.30017E+00	.30162E+00	.30307E+00
251	260	.30453E+00	.30599E+00	.30746E+00	.30893E+00	.31041E+00	.31189E+00	.31338E+00	.31488E+00	.31638E+00	.31788E+00
261	270	.31939E+00	.32091E+00	.32243E+00	.32396E+00	.32550E+00	.32704E+00	.32859E+00	.33014E+00	.33170E+00	.33326E+00
271	280	.33483E+00	.33641E+00	.33799E+00	.33958E+00	.34118E+00	.34278E+00	.34439E+00	.34601E+00	.34763E+00	.34926E+00
281	290	.35089E+00	.35253E+00	.35418E+00	.35584E+00	.35750E+00	.35917E+00	.36084E+00	.36253E+00	.36422E+00	.36592E+00
291	300	.36762E+00	.36933E+00	.37105E+00	.37278E+00	.37451E+00	.37625E+00	.37800E+00	.37976E+00	.38152E+00	.38329E+00
301	310	.38507E+00	.38686E+00	.38865E+00	.39046E+00	.39227E+00	.39409E+00	.39591E+00	.39775E+00	.39959E+00	.40144E+00
311	320	.40330E+00	.40517E+00	.40705E+00	.40893E+00	.41083E+00	.41273E+00	.41464E+00	.41656E+00	.41849E+00	.42042E+00
321	330	.42237E+00	.42433E+00	.42629E+00	.42826E+00	.43024E+00	.43224E+00	.43424E+00	.43625E+00	.43827E+00	.44030E+00
331	340	.44233E+00	.44438E+00	.44644E+00	.44851E+00	.45059E+00	.45267E+00	.45477E+00	.45688E+00	.45900E+00	.46112E+00
341	350	.46326E+00	.46541E+00	.46757E+00	.46974E+00	.47191E+00	.47410E+00	.47630E+00	.47852E+00	.48074E+00	.48297E+00
351	360	.48521E+00	.48747E+00	.48973E+00	.49201E+00	.49430E+00	.49660E+00	.49891E+00	.50123E+00	.50356E+00	.50591E+00
361	370	.50826E+00	.51063E+00	.51301E+00	.51540E+00	.51781E+00	.52022E+00	.52265E+00	.52509E+00	.52754E+00	.53001E+00
371	380	.53248E+00	.53497E+00	.53747E+00	.53999E+00	.54251E+00	.54505E+00	.54761E+00	.55017E+00	.55275E+00	.55534E+00
381	390	.55795E+00	.56057E+00	.56320E+00	.56584E+00	.56850E+00	.57117E+00	.57386E+00	.57656E+00	.57927E+00	.58200E+00
391	400	.58474E+00	.58750E+00	.59027E+00	.59305E+00	.59585E+00	.59866E+00	.60149E+00	.60433E+00	.60719E+00	.61006E+00
401	410	.61295E+00	.61585E+00	.61877E+00	.62170E+00	.62465E+00	.62761E+00	.63059E+00	.63358E+00	.63659E+00	.63962E+00
411	420	.64266E+00	.64572E+00	.64879E+00	.65188E+00	.65498E+00	.65811E+00	.66124E+00	.66440E+00	.66757E+00	.67076E+00
421	430	.67396E+00	.67719E+00	.68043E+00	.68368E+00	.68696E+00	.69025E+00	.69356E+00	.69688E+00	.70022E+00	.70359E+00
431	440	.70697E+00	.71036E+00	.71378E+00	.71721E+00	.72066E+00	.72414E+00	.72762E+00	.73113E+00	.73466E+00	.73820E+00
441	450	.74177E+00	.74535E+00	.74896E+00	.75258E+00	.75622E+00	.75988E+00	.76356E+00	.76726E+00	.77098E+00	.77472E+00
451	460	.77848E+00	.78226E+00	.78607E+00	.78989E+00	.79373E+00	.79759E+00	.80148E+00	.80538E+00	.80931E+00	.81326E+00
461	470	.81723E+00	.82122E+00	.82523E+00	.82926E+00	.83332E+00	.83739E+00	.84149E+00	.84562E+00	.84976E+00	.85393E+00
471	480	.85812E+00	.86233E+00	.86657E+00	.87082E+00	.87511E+00	.87941E+00	.88374E+00	.88809E+00	.89247E+00	.89687E+00
481	490	.90129E+00	.90574E+00	.91021E+00	.91471E+00	.91923E+00	.92378E+00	.92835E+00	.93294E+00	.93756E+00	.94221E+00
491	500	.94688E+00	.95158E+00	.95630E+00	.96105E+00	.96583E+00	.97063E+00	.97546E+00	.98031E+00	.98519E+00	.99010E+00
501	502	.99504E+00	.10000E+01								

"XIX"

1	10	.72980E+03	.72863E+03	.72980E+03	.73214E+03	.73446E+03	.73678E+03	.73909E+03	.74139E+03	.74368E+03	.74597E+03
11	20	.74824E+03	.75050E+03	.75275E+03	.75499E+03	.75722E+03	.75944E+03	.76165E+03	.76385E+03	.76603E+03	.76821E+03
21	30	.77037E+03	.77251E+03	.77465E+03	.77677E+03	.77888E+03	.78098E+03	.78306E+03	.78513E+03	.78719E+03	.78923E+03
31	40	.79125E+03	.79327E+03	.79526E+03	.79724E+03	.79921E+03	.80116E+03	.80309E+03	.80501E+03	.80691E+03	.80879E+03
41	50	.81066E+03	.81251E+03	.81434E+03	.81616E+03	.81796E+03	.81974E+03	.82150E+03	.82324E+03	.82496E+03	.82666E+03
51	60	.82835E+03	.83001E+03	.83166E+03	.83328E+03	.83489E+03	.83647E+03	.83804E+03	.83958E+03	.84110E+03	.84261E+03

61	70	.84409E+03	.84554E+03	.84698E+03	.84839E+03	.84978E+03	.85115E+03	.85250E+03	.85382E+03	.85512E+03	.85640E+03
71	80	.85766E+03	.85889E+03	.86009E+03	.86127E+03	.86243E+03	.86357E+03	.86468E+03	.86576E+03	.86682E+03	.86786E+03
81	90	.86887E+03	.86985E+03	.87081E+03	.87174E+03	.87265E+03	.87353E+03	.87439E+03	.87522E+03	.87602E+03	.87680E+03
91	100	.87755E+03	.87827E+03	.87897E+03	.87964E+03	.88028E+03	.88090E+03	.88149E+03	.88205E+03	.88259E+03	.88309E+03
101	110	.88357E+03	.88403E+03	.88445E+03	.88485E+03	.88522E+03	.88556E+03	.88587E+03	.88616E+03	.88642E+03	.88665E+03
111	120	.88685E+03	.88702E+03	.88717E+03	.88728E+03	.88737E+03	.88743E+03	.88747E+03	.88747E+03	.88745E+03	.88740E+03
121	130	.88732E+03	.88721E+03	.88707E+03	.88691E+03	.88672E+03	.88650E+03	.88625E+03	.88597E+03	.88567E+03	.88534E+03
131	140	.88498E+03	.88459E+03	.88417E+03	.88373E+03	.88326E+03	.88276E+03	.88224E+03	.88168E+03	.88110E+03	.88050E+03
141	150	.87986E+03	.87920E+03	.87851E+03	.87780E+03	.87706E+03	.87629E+03	.87549E+03	.87467E+03	.87383E+03	.87295E+03
151	160	.87205E+03	.87113E+03	.87018E+03	.86920E+03	.86820E+03	.86718E+03	.86612E+03	.86505E+03	.86395E+03	.86282E+03
161	170	.86167E+03	.86050E+03	.85930E+03	.85808E+03	.85683E+03	.85556E+03	.85427E+03	.85295E+03	.85161E+03	.85025E+03
171	180	.84887E+03	.84746E+03	.84603E+03	.84458E+03	.84311E+03	.84162E+03	.84010E+03	.83857E+03	.83701E+03	.83543E+03
181	190	.83383E+03	.83222E+03	.83058E+03	.82892E+03	.82724E+03	.82554E+03	.82383E+03	.82209E+03	.82034E+03	.81856E+03
191	200	.81677E+03	.81496E+03	.81314E+03	.81129E+03	.80943E+03	.80755E+03	.80566E+03	.80375E+03	.80182E+03	.79987E+03
201	210	.79791E+03	.79594E+03	.79395E+03	.79194E+03	.78992E+03	.78788E+03	.78583E+03	.78377E+03	.78169E+03	.77960E+03
211	220	.77749E+03	.77538E+03	.77324E+03	.77110E+03	.76894E+03	.76677E+03	.76459E+03	.76240E+03	.76020E+03	.75798E+03
221	230	.75575E+03	.75352E+03	.75127E+03	.74901E+03	.74674E+03	.74446E+03	.74217E+03	.73988E+03	.73757E+03	.73526E+03
231	240	.73293E+03	.73060E+03	.72826E+03	.72591E+03	.72355E+03	.72119E+03	.71882E+03	.71644E+03	.71405E+03	.71166E+03
241	250	.70926E+03	.70686E+03	.70445E+03	.70203E+03	.69961E+03	.69718E+03	.69475E+03	.69231E+03	.68986E+03	.68742E+03
251	260	.68497E+03	.68251E+03	.68005E+03	.67759E+03	.67512E+03	.67265E+03	.67018E+03	.66770E+03	.66522E+03	.66274E+03
261	270	.66025E+03	.65777E+03	.65528E+03	.65279E+03	.65029E+03	.64780E+03	.64531E+03	.64281E+03	.64031E+03	.63781E+03
271	280	.63531E+03	.63281E+03	.63031E+03	.62781E+03	.62531E+03	.62282E+03	.62032E+03	.61782E+03	.61532E+03	.61282E+03
281	290	.61032E+03	.60783E+03	.60533E+03	.60284E+03	.60035E+03	.59786E+03	.59537E+03	.59288E+03	.59040E+03	.58792E+03
291	300	.58544E+03	.58296E+03	.58048E+03	.57801E+03	.57554E+03	.57307E+03	.57061E+03	.56815E+03	.56569E+03	.56324E+03
301	310	.56079E+03	.55834E+03	.55590E+03	.55346E+03	.55102E+03	.54859E+03	.54616E+03	.54374E+03	.54132E+03	.53891E+03
311	320	.53650E+03	.53409E+03	.53169E+03	.52930E+03	.52690E+03	.52452E+03	.52214E+03	.51976E+03	.51739E+03	.51502E+03
321	330	.51266E+03	.51031E+03	.50796E+03	.50562E+03	.50328E+03	.50094E+03	.49862E+03	.49630E+03	.49398E+03	.49167E+03
331	340	.48937E+03	.48707E+03	.48478E+03	.48250E+03	.48022E+03	.47795E+03	.47568E+03	.47342E+03	.47117E+03	.46892E+03
341	350	.46668E+03	.46445E+03	.46222E+03	.46000E+03	.45779E+03	.45558E+03	.45339E+03	.45119E+03	.44901E+03	.44683E+03
351	360	.44466E+03	.44249E+03	.44034E+03	.43818E+03	.43604E+03	.43391E+03	.43178E+03	.42965E+03	.42754E+03	.42543E+03
361	370	.42333E+03	.42124E+03	.41916E+03	.41708E+03	.41501E+03	.41294E+03	.41089E+03	.40884E+03	.40680E+03	.40477E+03
371	380	.40274E+03	.40072E+03	.39871E+03	.39671E+03	.39471E+03	.39273E+03	.39075E+03	.38877E+03	.38681E+03	.38485E+03
381	390	.38290E+03	.38096E+03	.37902E+03	.37710E+03	.37518E+03	.37327E+03	.37136E+03	.36946E+03	.36758E+03	.36569E+03
391	400	.36382E+03	.36196E+03	.36010E+03	.35825E+03	.35640E+03	.35457E+03	.35274E+03	.35092E+03	.34911E+03	.34731E+03
401	410	.34551E+03	.34372E+03	.34194E+03	.34016E+03	.33840E+03	.33664E+03	.33489E+03	.33314E+03	.33141E+03	.32968E+03
411	420	.32796E+03	.32625E+03	.32454E+03	.32284E+03	.32115E+03	.31947E+03	.31779E+03	.31613E+03	.31447E+03	.31281E+03
421	430	.31117E+03	.30953E+03	.30790E+03	.30628E+03	.30466E+03	.30305E+03	.30145E+03	.29986E+03	.29827E+03	.29669E+03
431	440	.29512E+03	.29355E+03	.29200E+03	.29045E+03	.28890E+03	.28737E+03	.28584E+03	.28432E+03	.28281E+03	.28130E+03
441	450	.27980E+03	.27831E+03	.27682E+03	.27534E+03	.27387E+03	.27241E+03	.27095E+03	.26950E+03	.26806E+03	.26662E+03
451	460	.26519E+03	.26377E+03	.26236E+03	.26095E+03	.25954E+03	.25815E+03	.25676E+03	.25538E+03	.25401E+03	.25264E+03
461	470	.25128E+03	.24992E+03	.24857E+03	.24723E+03	.24590E+03	.24457E+03	.24325E+03	.24194E+03	.24063E+03	.23933E+03
471	480	.23803E+03	.23674E+03	.23546E+03	.23418E+03	.23291E+03	.23165E+03	.23039E+03	.22914E+03	.22790E+03	.22666E+03
481	490	.22543E+03	.22421E+03	.22299E+03	.22177E+03	.22057E+03	.21937E+03	.21817E+03	.21698E+03	.21580E+03	.21462E+03
491	500	.21345E+03	.21229E+03	.21113E+03	.20998E+03	.20883E+03	.20769E+03	.20656E+03	.20543E+03	.20431E+03	.20319E+03
501	502	.20208E+03	.20097E+03								

"TUBE AREA"

VALUES FROM J = 1 THROUGH 20 ARE .4507033E-04

21	30	.45070E-04	.45070E-04	.45070E-04	.45070E-04	.45070E-04	.45070E-04	.45070E-04	.45070E-04	.45070E-04	.67815E-04

VALUES FROM J = 31 THROUGH 50 ARE .6781489E-04

51	60	.67815E-04	.67815E-04	.67815E-04	.67815E-04	.67815E-04	.67815E-04	.67815E-04	.67815E-04	.67815E-04	.11259E-03

VALUES FROM J = 61 THROUGH 80 ARE .1125872E-03

81	90	.11259E-03	.11259E-03	.11259E-03	.15807E-03	.15807E-03	.15807E-03	.15807E-03	.15807E-03	.15807E-03	.15807E-03

VALUES FROM J = 91 THROUGH 110 ARE .1580726E-03

111	120	.15807E-03	.14715E-03	.10040E-03	.62568E-04	.33708E-04	.33708E-04	.33708E-04	.33708E-04	.33708E-04	.33708E-04
121	130	.33708E-04	.33708E-04	.33708E-04	.33708E-04	.40217E-04	.47985E-04	.56440E-04	.65583E-04	.75417E-04	.85940E-04
131	140	.97155E-04	.10906E-03	.12167E-03	.13496E-03	.14896E-03	.16365E-03	.17904E-03	.19514E-03	.21194E-03	.22944E-03
141	150	.24765E-03	.26657E-03	.28620E-03	.30655E-03	.32761E-03	.34940E-03	.37190E-03	.39513E-03	.41908E-03	.44376E-03

VALUES FROM J = 151 THROUGH 502 ARE .1149270E-02

"ARY = DA/DX"

VALUES FROM J = 1 THROUGH 20 ARE .0000000E+00

21	30	.00000E+00	.00000E+00	.00000E+00	.00000E+00	.00000E+00	.00000E+00	.00000E+00	.00000E+00	.11372E-04	.11372E-04

VALUES FROM J = 31 THROUGH 50 ARE .0000000E+00

```
  51   60  .00000E+00  .00000E+00  .00000E+00  .00000E+00  .00000E+00  .00000E+00  .00000E+00  .00000E+00  .22386E-04  .22386E-04
VALUES FROM J =   61 THROUGH   80 ARE  .0000000E+00
  81   90  .00000E+00  .00000E+00  .22743E-04  .22743E-04  .00000E+00  .00000E+00  .00000E+00  .00000E+00  .00000E+00  .00000E+00
VALUES FROM J =   91 THROUGH  110 ARE  .0000000E+00
 111  120 -.54619E-05 -.28835E-04 -.42291E-04 -.33347E-04 -.14430E-04  .00000E+00  .00000E+00  .00000E+00  .00000E+00  .00000E+00
 121  130  .00000E+00  .00000E+00  .00000E+00  .32547E-05  .71384E-05  .81113E-05  .87994E-05  .94883E-05  .10178E-04  .10869E-04
 131  140  .11562E-04  .12255E-04  .12950E-04  .13646E-04  .14344E-04  .15043E-04  .15744E-04  .16446E-04  .17151E-04  .17857E-04
 141  150  .18566E-04  .19277E-04  .19990E-04  .20705E-04  .21422E-04  .22142E-04  .22865E-04  .23590E-04  .24319E-04  .36510E-03
 151  160  .35275E-03  .00000E+00  .00000E+00  .00000E+00  .00000E+00  .00000E+00  .00000E+00  .00000E+00  .00000E+00  .00000E+00
VALUES FROM J =  161 THROUGH  500 ARE  .0000000E+00
 501  502  .00000E+00  .69389E-17

 AREA TILDE = TUBE AREA/XIX
   1   10  .61757E-07  .61856E-07  .61757E-07  .61560E-07  .61365E-07  .61172E-07  .60981E-07  .60791E-07  .60604E-07  .60419E-07
  11   20  .60235E-07  .60054E-07  .59874E-07  .59696E-07  .59521E-07  .59347E-07  .59175E-07  .59004E-07  .58836E-07  .58670E-07
  21   30  .58505E-07  .58342E-07  .58181E-07  .58022E-07  .57865E-07  .57710E-07  .57556E-07  .57405E-07  .57255E-07  .85926E-07
  31   40  .85706E-07  .85488E-07  .85274E-07  .85062E-07  .84853E-07  .84646E-07  .84442E-07  .84241E-07  .84043E-07  .83847E-07
  41   50  .83654E-07  .83463E-07  .83275E-07  .83090E-07  .82908E-07  .82728E-07  .82551E-07  .82376E-07  .82204E-07  .82034E-07
  51   60  .81868E-07  .81703E-07  .81542E-07  .81383E-07  .81226E-07  .81072E-07  .80921E-07  .80772E-07  .80626E-07  .13362E-06
  61   70  .13338E-06  .13315E-06  .13293E-06  .13271E-06  .13249E-06  .13228E-06  .13207E-06  .13186E-06  .13166E-06  .13147E-06
  71   80  .13127E-06  .13109E-06  .13090E-06  .13072E-06  .13055E-06  .13037E-06  .13021E-06  .13004E-06  .12989E-06  .12973E-06
  81   90  .12958E-06  .12943E-06  .12929E-06  .18133E-06  .18114E-06  .18096E-06  .18078E-06  .18061E-06  .18044E-06  .18028E-06
  91  100  .18013E-06  .17998E-06  .17984E-06  .17970E-06  .17957E-06  .17944E-06  .17932E-06  .17921E-06  .17910E-06  .17900E-06
 101  110  .17890E-06  .17881E-06  .17872E-06  .17864E-06  .17857E-06  .17850E-06  .17844E-06  .17838E-06  .17833E-06  .17828E-06
 111  120  .17824E-06  .16589E-06  .11317E-06  .70516E-07  .37986E-07  .37984E-07  .37982E-07  .37982E-07  .37983E-07  .37985E-07
 121  130  .37989E-07  .37993E-07  .37999E-07  .38006E-07  .45355E-07  .54128E-07  .63684E-07  .74024E-07  .85152E-07  .97070E-07
 131  140  .10978E-06  .12329E-06  .13760E-06  .15272E-06  .16864E-06  .18538E-06  .20294E-06  .22132E-06  .24053E-06  .26058E-06
 141  150  .28146E-06  .30320E-06  .32578E-06  .34923E-06  .37354E-06  .39872E-06  .42479E-06  .45174E-06  .47959E-06  .50835E-06
 151  160  .13179E-05  .13193E-05  .13207E-05  .13222E-05  .13237E-05  .13253E-05  .13269E-05  .13286E-05  .13303E-05  .13320E-05
 161  170  .13338E-05  .13356E-05  .13375E-05  .13394E-05  .13413E-05  .13433E-05  .13453E-05  .13474E-05  .13495E-05  .13517E-05
 171  180  .13539E-05  .13561E-05  .13584E-05  .13608E-05  .13631E-05  .13655E-05  .13680E-05  .13705E-05  .13731E-05  .13757E-05
 181  190  .13783E-05  .13810E-05  .13837E-05  .13865E-05  .13893E-05  .13921E-05  .13950E-05  .13980E-05  .14010E-05  .14040E-05
 191  200  .14071E-05  .14102E-05  .14134E-05  .14166E-05  .14198E-05  .14231E-05  .14265E-05  .14299E-05  .14333E-05  .14368E-05
 201  210  .14403E-05  .14439E-05  .14475E-05  .14512E-05  .14549E-05  .14587E-05  .14625E-05  .14663E-05  .14702E-05  .14742E-05
 211  220  .14782E-05  .14822E-05  .14863E-05  .14904E-05  .14946E-05  .14988E-05  .15031E-05  .15074E-05  .15118E-05  .15162E-05
 221  230  .15207E-05  .15252E-05  .15298E-05  .15344E-05  .15390E-05  .15438E-05  .15485E-05  .15533E-05  .15582E-05  .15631E-05
 231  240  .15680E-05  .15731E-05  .15781E-05  .15832E-05  .15884E-05  .15936E-05  .15988E-05  .16041E-05  .16095E-05  .16149E-05
 241  250  .16204E-05  .16259E-05  .16315E-05  .16371E-05  .16427E-05  .16485E-05  .16542E-05  .16601E-05  .16659E-05  .16719E-05
 251  260  .16779E-05  .16839E-05  .16900E-05  .16961E-05  .17023E-05  .17086E-05  .17149E-05  .17212E-05  .17277E-05  .17341E-05
 261  270  .17407E-05  .17472E-05  .17539E-05  .17606E-05  .17673E-05  .17741E-05  .17810E-05  .17879E-05  .17949E-05  .18019E-05
 271  280  .18090E-05  .18161E-05  .18233E-05  .18306E-05  .18379E-05  .18453E-05  .18527E-05  .18602E-05  .18678E-05  .18754E-05
 281  290  .18831E-05  .18908E-05  .18986E-05  .19064E-05  .19143E-05  .19223E-05  .19303E-05  .19384E-05  .19466E-05  .19548E-05
 291  300  .19631E-05  .19714E-05  .19799E-05  .19883E-05  .19969E-05  .20054E-05  .20141E-05  .20228E-05  .20316E-05  .20405E-05
 301  310  .20494E-05  .20584E-05  .20674E-05  .20765E-05  .20857E-05  .20949E-05  .21043E-05  .21136E-05  .21231E-05  .21326E-05
 311  320  .21422E-05  .21518E-05  .21615E-05  .21713E-05  .21812E-05  .21911E-05  .22011E-05  .22112E-05  .22213E-05  .22315E-05
 321  330  .22418E-05  .22521E-05  .22625E-05  .22730E-05  .22836E-05  .22942E-05  .23049E-05  .23157E-05  .23265E-05  .23375E-05
 331  340  .23485E-05  .23595E-05  .23707E-05  .23819E-05  .23932E-05  .24046E-05  .24161E-05  .24276E-05  .24392E-05  .24509E-05
 341  350  .24626E-05  .24745E-05  .24864E-05  .24984E-05  .25105E-05  .25226E-05  .25349E-05  .25472E-05  .25596E-05  .25721E-05
 351  360  .25846E-05  .25973E-05  .26100E-05  .26228E-05  .26357E-05  .26487E-05  .26617E-05  .26749E-05  .26881E-05  .27014E-05
 361  370  .27148E-05  .27283E-05  .27419E-05  .27555E-05  .27693E-05  .27831E-05  .27970E-05  .28110E-05  .28251E-05  .28393E-05
 371  380  .28536E-05  .28680E-05  .28825E-05  .28970E-05  .29117E-05  .29264E-05  .29412E-05  .29561E-05  .29712E-05  .29863E-05
 381  390  .30015E-05  .30168E-05  .30322E-05  .30477E-05  .30633E-05  .30790E-05  .30948E-05  .31106E-05  .31266E-05  .31427E-05
 391  400  .31589E-05  .31752E-05  .31916E-05  .32080E-05  .32246E-05  .32413E-05  .32581E-05  .32750E-05  .32920E-05  .33091E-05
 401  410  .33263E-05  .33436E-05  .33611E-05  .33786E-05  .33962E-05  .34140E-05  .34318E-05  .34498E-05  .34678E-05  .34860E-05
 411  420  .35043E-05  .35227E-05  .35412E-05  .35598E-05  .35786E-05  .35974E-05  .36164E-05  .36355E-05  .36547E-05  .36740E-05
 421  430  .36934E-05  .37130E-05  .37326E-05  .37524E-05  .37723E-05  .37923E-05  .38125E-05  .38327E-05  .38531E-05  .38736E-05
 431  440  .38943E-05  .39150E-05  .39359E-05  .39569E-05  .39780E-05  .39993E-05  .40207E-05  .40422E-05  .40638E-05  .40856E-05
 441  450  .41075E-05  .41295E-05  .41517E-05  .41739E-05  .41964E-05  .42189E-05  .42416E-05  .42644E-05  .42874E-05  .43105E-05
 451  460  .43337E-05  .43571E-05  .43806E-05  .44042E-05  .44280E-05  .44519E-05  .44760E-05  .45002E-05  .45246E-05  .45491E-05
 461  470  .45737E-05  .45985E-05  .46234E-05  .46485E-05  .46737E-05  .46991E-05  .47246E-05  .47503E-05  .47761E-05  .48021E-05
 471  480  .48282E-05  .48545E-05  .48810E-05  .49076E-05  .49343E-05  .49612E-05  .49883E-05  .50155E-05  .50429E-05  .50704E-05
 481  490  .50981E-05  .51260E-05  .51540E-05  .51822E-05  .52105E-05  .52390E-05  .52677E-05  .52966E-05  .53256E-05  .53548E-05
 491  500  .53841E-05  .54137E-05  .54434E-05  .54733E-05  .55033E-05  .55335E-05  .55639E-05  .55945E-05  .56252E-05  .56562E-05
 501  502  .56873E-05  .57185E-05
```

```
 DENSITY
VALUES FROM J =    1 THROUGH  110 ARE  .1000000E+01
 111  120  .10000E+01  .10000E+01  .10000E+01  .10000E+01  .10000E+01  .10000E+01  .10000E+01  .10000E+01  .14777E-01  .14777E-01
VALUES FROM J =  121 THROUGH  502 ARE  .1477737E-01

 VELOCITY
VALUES FROM J =    1 THROUGH  502 ARE  .0000000E+00

 PRESSURE
VALUES FROM J =    1 THROUGH  110 ARE  .1137613E+01
 111  120  .11376E+01  .11376E+01  .11376E+01  .11376E+01  .11376E+01  .11376E+01  .11376E+01  .11376E+01  .10553E-01  .10553E-01
VALUES FROM J =  121 THROUGH  502 ARE  .1055300E-01

 SOUND SPEED
VALUES FROM J =    1 THROUGH  110 ARE  .1262141E+01
 111  120  .12621E+01  .12621E+01  .12621E+01  .12621E+01  .12621E+01  .12621E+01  .12621E+01  .12621E+01  .10000E+01  .10000E+01
VALUES FROM J =  121 THROUGH  502 ARE  .1000000E+01
```

** N = 4200 AND TIME(SEC) = .36513E-01

DENSITY

1	10	.57873E-01	.57867E-01	.57873E-01	.57872E-01	.57875E-01	.57879E-01	.57884E-01	.57891E-01	.57901E-01	.57913E-01
11	20	.57929E-01	.57950E-01	.57976E-01	.58010E-01	.58051E-01	.58103E-01	.58165E-01	.58240E-01	.58328E-01	.58430E-01
21	30	.58546E-01	.58675E-01	.58816E-01	.58973E-01	.59143E-01	.59291E-01	.59486E-01	.59849E-01	.59645E-01	.59938E-01
31	40	.60413E-01	.60357E-01	.60450E-01	.60600E-01	.60719E-01	.60834E-01	.60956E-01	.61078E-01	.61201E-01	.61327E-01
41	50	.61456E-01	.61586E-01	.61719E-01	.61854E-01	.61991E-01	.62133E-01	.62280E-01	.62435E-01	.62601E-01	.62781E-01
51	60	.62977E-01	.63192E-01	.63429E-01	.63695E-01	.63996E-01	.64290E-01	.64630E-01	.65195E-01	.65071E-01	.65400E-01
61	70	.65984E-01	.65972E-01	.66135E-01	.66328E-01	.66467E-01	.66589E-01	.66695E-01	.66781E-01	.66848E-01	.66898E-01
71	80	.66933E-01	.66955E-01	.66966E-01	.66968E-01	.66963E-01	.66954E-01	.66942E-01	.66931E-01	.66922E-01	.66898E-01
81	90	.66884E-01	.66972E-01	.66759E-01	.66819E-01	.66977E-01	.66866E-01	.66856E-01	.66864E-01	.66858E-01	.66855E-01
91	100	.66854E-01	.66852E-01	.66851E-01	.66850E-01	.66849E-01	.66849E-01	.66849E-01	.66848E-01	.66846E-01	.66842E-01
101	110	.66833E-01	.66822E-01	.66811E-01	.66803E-01	.66799E-01	.66788E-01	.66747E-01	.66660E-01	.66572E-01	.66554E-01
111	120	.66639E-01	.66885E-01	.66390E-01	.64700E-01	.57107E-01	.44108E-01	.38465E-01	.36656E-01	.36140E-01	.36253E-01
121	130	.37153E-01	.38201E-01	.38116E-01	.33350E-01	.25635E-01	.19807E-01	.15830E-01	.13031E-01	.10956E-01	.93750E-02
131	140	.81071E-02	.71036E-02	.63172E-02	.54124E-02	.53992E-02	.40886E-02	.32100E-02	.88672E-02	.15305E-01	.16670E-01
141	150	.16304E-01	.16479E-01	.16830E-01	.17051E-01	.17222E-01	.17408E-01	.17572E-01	.17715E-01	.18092E-01	.17683E-01
151	160	.17945E-01	.18267E-01	.18053E-01	.17999E-01	.17967E-01	.17898E-01	.17828E-01	.17755E-01	.17671E-01	.17574E-01
161	170	.17462E-01	.17341E-01	.17217E-01	.17100E-01	.17001E-01	.16923E-01	.16868E-01	.16832E-01	.16808E-01	.16785E-01
171	180	.16756E-01	.16712E-01	.16650E-01	.16568E-01	.16468E-01	.16352E-01	.16225E-01	.16092E-01	.15957E-01	.15822E-01
181	190	.15690E-01	.15563E-01	.15441E-01	.15324E-01	.15212E-01	.15107E-01	.15007E-01	.14913E-01	.14827E-01	.14749E-01
191	200	.14680E-01	.14620E-01	.14568E-01	.14526E-01	.14492E-01	.14464E-01	.14443E-01	.14427E-01	.14414E-01	.14403E-01
201	210	.14392E-01	.14382E-01	.14370E-01	.14357E-01	.14342E-01	.14326E-01	.14309E-01	.14291E-01	.14271E-01	.14251E-01
211	220	.14231E-01	.14210E-01	.14188E-01	.14165E-01	.14140E-01	.14114E-01	.14084E-01	.14052E-01	.14016E-01	.13976E-01
221	230	.13932E-01	.13883E-01	.13830E-01	.13772E-01	.13711E-01	.13646E-01	.13578E-01	.13509E-01	.13440E-01	.13372E-01
231	240	.13307E-01	.13245E-01	.13190E-01	.13142E-01	.13101E-01	.13068E-01	.13044E-01	.13026E-01	.13013E-01	.13002E-01
241	250	.12991E-01	.12974E-01	.12948E-01	.12909E-01	.12851E-01	.12770E-01	.12664E-01	.12530E-01	.12367E-01	.12174E-01
251	260	.11953E-01	.11707E-01	.11441E-01	.11158E-01	.10866E-01	.10569E-01	.10276E-01	.99917E-02	.97221E-02	.94723E-02
261	270	.92462E-02	.90466E-02	.88751E-02	.87323E-02	.86175E-02	.85293E-02	.84655E-02	.84231E-02	.83992E-02	.83906E-02
271	280	.83940E-02	.84065E-02	.84255E-02	.84488E-02	.84744E-02	.85011E-02	.85277E-02	.85537E-02	.85787E-02	.86024E-02
281	290	.86251E-02	.86467E-02	.86676E-02	.86880E-02	.87081E-02	.87280E-02	.87481E-02	.87684E-02	.87890E-02	.88100E-02
291	300	.88314E-02	.88532E-02	.88755E-02	.88981E-02	.89212E-02	.89445E-02	.89681E-02	.89920E-02	.90159E-02	.90400E-02
301	310	.90641E-02	.90882E-02	.91121E-02	.91359E-02	.91594E-02	.91827E-02	.92056E-02	.92282E-02	.92504E-02	.92721E-02
311	320	.92933E-02	.93141E-02	.93344E-02	.93541E-02	.93733E-02	.93919E-02	.94098E-02	.94270E-02	.94435E-02	.94591E-02
321	330	.94738E-02	.94875E-02	.95002E-02	.95118E-02	.95224E-02	.95320E-02	.95405E-02	.95482E-02	.95551E-02	.95613E-02
331	340	.95671E-02	.95726E-02	.95780E-02	.95834E-02	.95889E-02	.95947E-02	.96007E-02	.96069E-02	.96133E-02	.96196E-02
341	350	.96257E-02	.96315E-02	.96366E-02	.96408E-02	.96440E-02	.96461E-02	.96470E-02	.96467E-02	.96453E-02	.96430E-02
351	360	.96401E-02	.96369E-02	.96338E-02	.96312E-02	.96294E-02	.96289E-02	.96299E-02	.96329E-02	.96378E-02	.96449E-02
361	370	.96541E-02	.96654E-02	.96786E-02	.96935E-02	.97098E-02	.97274E-02	.97458E-02	.97648E-02	.97842E-02	.98038E-02
371	380	.98234E-02	.98429E-02	.98624E-02	.98817E-02	.99009E-02	.99201E-02	.99394E-02	.99589E-02	.99786E-02	.99986E-02
381	390	.10019E-01	.10038E-01	.10054E-01	.10064E-01	.10065E-01	.10055E-01	.10045E-01	.10078E-01	.10241E-01	.10640E-01
391	400	.11302E-01	.12109E-01	.12851E-01	.13369E-01	.13642E-01	.13756E-01	.13818E-01	.13902E-01	.14029E-01	.14188E-01
401	410	.14352E-01	.14503E-01	.14632E-01	.14741E-01	.14836E-01	.14924E-01	.15009E-01	.15092E-01	.15175E-01	.15256E-01
411	420	.15335E-01	.15412E-01	.15488E-01	.15562E-01	.15634E-01	.15703E-01	.15768E-01	.15826E-01	.15877E-01	.15919E-01
421	430	.15952E-01	.15976E-01	.15990E-01	.15995E-01	.15993E-01	.15986E-01	.15974E-01	.15960E-01	.15945E-01	.15931E-01
431	440	.15917E-01	.15906E-01	.15896E-01	.15888E-01	.15881E-01	.15875E-01	.15868E-01	.15859E-01	.15847E-01	.15831E-01
441	450	.15811E-01	.15785E-01	.15755E-01	.15718E-01	.15678E-01	.15634E-01	.15587E-01	.15539E-01	.15493E-01	.15449E-01
451	460	.15410E-01	.15379E-01	.15356E-01	.15345E-01	.15347E-01	.15362E-01	.15391E-01	.15431E-01	.15481E-01	.15538E-01
461	470	.15600E-01	.15663E-01	.15726E-01	.15786E-01	.15845E-01	.15902E-01	.15958E-01	.16015E-01	.16075E-01	.16137E-01
471	480	.16202E-01	.16272E-01	.16345E-01	.16421E-01	.16500E-01	.16581E-01	.16664E-01	.16746E-01	.16828E-01	.16906E-01
481	490	.16979E-01	.17044E-01	.17097E-01	.17135E-01	.17155E-01	.17152E-01	.17125E-01	.17069E-01	.16984E-01	.16869E-01
491	500	.16725E-01	.16554E-01	.16361E-01	.16150E-01	.15931E-01	.15715E-01	.15513E-01	.15340E-01	.15196E-01	.15065E-01
501	502	.14910E-01	.14715E-01								

VELOCITY

1	10	-.30512E-02	.00000E+00	.30512E-02	.61341E-02	.91558E-02	.12167E-01	.15178E-01	.18176E-01	.21156E-01	.24113E-01
11	20	.27037E-01	.29917E-01	.32742E-01	.35496E-01	.38166E-01	.40738E-01	.43200E-01	.45540E-01	.47754E-01	.49839E-01
21	30	.51804E-01	.53654E-01	.55394E-01	.57100E-01	.58775E-01	.60035E-01	.61787E-01	.65363E-01	.60358E-01	.48248E-01
31	40	.44410E-01	.48232E-01	.50445E-01	.51984E-01	.53878E-01	.55779E-01	.57589E-01	.59361E-01	.61084E-01	.62738E-01
41	50	.64313E-01	.65798E-01	.67178E-01	.68437E-01	.69557E-01	.70516E-01	.71290E-01	.71852E-01	.72172E-01	.72215E-01
51	60	.71953E-01	.71356E-01	.70381E-01	.69066E-01	.67460E-01	.65106E-01	.62801E-01	.62642E-01	.53189E-01	.36593E-01

61	70	.28545E-01	.28546E-01	.26804E-01	.24858E-01	.23618E-01	.22689E-01	.22054E-01	.21759E-01	.21767E-01	.22043E-01
71	80	.22554E-01	.23265E-01	.24143E-01	.25160E-01	.26293E-01	.27523E-01	.28831E-01	.30226E-01	.31721E-01	.33111E-01
81	90	.34692E-01	.37381E-01	.35927E-01	.30312E-01	.29426E-01	.32245E-01	.34104E-01	.35827E-01	.37749E-01	.39682E-01
91	100	.41629E-01	.43614E-01	.45625E-01	.47656E-01	.49701E-01	.51755E-01	.53814E-01	.55880E-01	.57957E-01	.60053E-01
101	110	.62172E-01	.64315E-01	.66481E-01	.68663E-01	.70854E-01	.73055E-01	.75245E-01	.77401E-01	.79707E-01	.81917E-01
111	120	.83852E-01	.94409E-01	.13745E+00	.25189E+00	.46017E+00	.65069E+00	.74917E+00	.78357E+00	.79436E+00	.79329E+00
121	130	.77965E+00	.75875E+00	.77204E+00	.85018E+00	.95132E+00	.10393E+01	.11063E+01	.11574E+01	.11974E+01	.12308E+01
131	140	.12577E+01	.12835E+01	.12985E+01	.13338E+01	.13186E+01	.13377E+01	.16918E+01	.68527E+00	.28378E+00	.22822E+00
141	150	.23906E+00	.22433E+00	.20329E+00	.18892E+00	.17719E+00	.16659E+00	.15611E+00	.14619E+00	.14764E+00	.11430E+00
151	160	.62019E-01	.45425E-01	.53813E-01	.55517E-01	.55882E-01	.57479E-01	.58993E-01	.60372E-01	.61795E-01	.63227E-01
161	170	.64653E-01	.66081E-01	.67515E-01	.68957E-01	.70407E-01	.71868E-01	.73340E-01	.74822E-01	.76314E-01	.77815E-01
171	180	.79324E-01	.80839E-01	.82356E-01	.83874E-01	.85386E-01	.86889E-01	.88376E-01	.89841E-01	.91277E-01	.92676E-01
181	190	.94030E-01	.95332E-01	.96576E-01	.97754E-01	.98862E-01	.99897E-01	.10086E+00	.10174E+00	.10255E+00	.10330E+00
191	200	.10398E+00	.10461E+00	.10521E+00	.10576E+00	.10631E+00	.10684E+00	.10737E+00	.10792E+00	.10849E+00	.10909E+00
201	210	.10973E+00	.11041E+00	.11113E+00	.11189E+00	.11271E+00	.11356E+00	.11446E+00	.11540E+00	.11638E+00	.11739E+00
211	220	.11844E+00	.11951E+00	.12062E+00	.12174E+00	.12289E+00	.12406E+00	.12525E+00	.12645E+00	.12767E+00	.12890E+00
221	230	.13014E+00	.13140E+00	.13266E+00	.13394E+00	.13523E+00	.13652E+00	.13783E+00	.13915E+00	.14047E+00	.14181E+00
231	240	.14315E+00	.14450E+00	.14586E+00	.14723E+00	.14860E+00	.14999E+00	.15137E+00	.15276E+00	.15416E+00	.15556E+00
241	250	.15696E+00	.15836E+00	.15977E+00	.16117E+00	.16257E+00	.16397E+00	.16537E+00	.16677E+00	.16816E+00	.16955E+00
251	260	.17093E+00	.17232E+00	.17370E+00	.17509E+00	.17647E+00	.17786E+00	.17924E+00	.18063E+00	.18203E+00	.18342E+00
261	270	.18483E+00	.18624E+00	.18765E+00	.18908E+00	.19051E+00	.19195E+00	.19340E+00	.19486E+00	.19633E+00	.19781E+00
271	280	.19930E+00	.20080E+00	.20231E+00	.20384E+00	.20538E+00	.20693E+00	.20849E+00	.21007E+00	.21166E+00	.21326E+00
281	290	.21488E+00	.21651E+00	.21816E+00	.21981E+00	.22149E+00	.22318E+00	.22488E+00	.22660E+00	.22833E+00	.23008E+00
291	300	.23184E+00	.23362E+00	.23542E+00	.23723E+00	.23906E+00	.24090E+00	.24277E+00	.24465E+00	.24654E+00	.24845E+00
301	310	.25038E+00	.25233E+00	.25429E+00	.25627E+00	.25827E+00	.26028E+00	.26231E+00	.26435E+00	.26641E+00	.26848E+00
311	320	.27057E+00	.27267E+00	.27479E+00	.27691E+00	.27905E+00	.28119E+00	.28335E+00	.28551E+00	.28768E+00	.28986E+00
321	330	.29204E+00	.29422E+00	.29641E+00	.29860E+00	.30079E+00	.30297E+00	.30516E+00	.30734E+00	.30952E+00	.31169E+00
331	340	.31386E+00	.31603E+00	.31818E+00	.32034E+00	.32249E+00	.32463E+00	.32677E+00	.32891E+00	.33104E+00	.33317E+00
341	350	.33530E+00	.33743E+00	.33956E+00	.34169E+00	.34383E+00	.34597E+00	.34811E+00	.35026E+00	.35241E+00	.35457E+00
351	360	.35674E+00	.35891E+00	.36109E+00	.36327E+00	.36547E+00	.36767E+00	.36987E+00	.37209E+00	.37431E+00	.37653E+00
361	370	.37876E+00	.38100E+00	.38324E+00	.38548E+00	.38772E+00	.38997E+00	.39222E+00	.39446E+00	.39670E+00	.39894E+00
371	380	.40118E+00	.40341E+00	.40563E+00	.40784E+00	.41004E+00	.41223E+00	.41439E+00	.41652E+00	.41863E+00	.42071E+00
381	390	.42278E+00	.42493E+00	.42731E+00	.43020E+00	.43396E+00	.43866E+00	.44325E+00	.44389E+00	.43258E+00	.40011E+00
391	400	.34562E+00	.28232E+00	.22841E+00	.19412E+00	.17860E+00	.17457E+00	.17411E+00	.17208E+00	.16697E+00	.15970E+00
401	410	.15204E+00	.14534E+00	.14010E+00	.13612E+00	.13293E+00	.13008E+00	.12730E+00	.12452E+00	.12177E+00	.11908E+00
411	420	.11648E+00	.11396E+00	.11148E+00	.10900E+00	.10650E+00	.10397E+00	.10142E+00	.98895E-01	.96460E-01	.94187E-01
421	430	.92162E-01	.90470E-01	.89196E-01	.88413E-01	.88179E-01	.88533E-01	.89496E-01	.91067E-01	.93231E-01	.95958E-01
431	440	.99211E-01	.10294E+00	.10711E+00	.11166E+00	.11654E+00	.12170E+00	.12711E+00	.13271E+00	.13848E+00	.14435E+00
441	450	.15031E+00	.15632E+00	.16233E+00	.16831E+00	.17423E+00	.18003E+00	.18567E+00	.19109E+00	.19623E+00	.20101E+00
451	460	.20534E+00	.20913E+00	.21230E+00	.21476E+00	.21646E+00	.21738E+00	.21755E+00	.21706E+00	.21605E+00	.21469E+00
461	470	.21318E+00	.21167E+00	.21029E+00	.20912E+00	.20815E+00	.20735E+00	.20665E+00	.20599E+00	.20527E+00	.20447E+00
471	480	.20356E+00	.20252E+00	.20139E+00	.20017E+00	.19891E+00	.19761E+00	.19628E+00	.19494E+00	.19358E+00	.19220E+00
481	490	.19079E+00	.18936E+00	.18792E+00	.18649E+00	.18511E+00	.18384E+00	.18277E+00	.18198E+00	.18157E+00	.18166E+00
491	500	.18231E+00	.18358E+00	.18545E+00	.18782E+00	.19055E+00	.19338E+00	.19608E+00	.19839E+00	.20007E+00	.20085E+00
501	502	.20076E+00	.20063E+00								

PRESSURE

1	10	.21098E-01	.21095E-01	.21098E-01	.21098E-01	.21099E-01	.21102E-01	.21104E-01	.21108E-01	.21113E-01	.21120E-01
11	20	.21128E-01	.21138E-01	.21152E-01	.21169E-01	.21190E-01	.21217E-01	.21249E-01	.21287E-01	.21332E-01	.21384E-01
21	30	.21444E-01	.21511E-01	.21583E-01	.21664E-01	.21750E-01	.21824E-01	.21924E-01	.22115E-01	.22017E-01	.22173E-01
31	40	.22419E-01	.22390E-01	.22439E-01	.22518E-01	.22581E-01	.22643E-01	.22709E-01	.22774E-01	.22839E-01	.22905E-01
41	50	.22972E-01	.23039E-01	.23107E-01	.23176E-01	.23247E-01	.23321E-01	.23398E-01	.23480E-01	.23568E-01	.23663E-01
51	60	.23768E-01	.23883E-01	.24010E-01	.24151E-01	.24309E-01	.24460E-01	.24640E-01	.24950E-01	.24903E-01	.25093E-01
61	70	.25409E-01	.25404E-01	.25494E-01	.25600E-01	.25675E-01	.25739E-01	.25794E-01	.25837E-01	.25870E-01	.25894E-01
71	80	.25910E-01	.25921E-01	.25927E-01	.25929E-01	.25929E-01	.25927E-01	.25923E-01	.25919E-01	.25915E-01	.25903E-01
81	90	.25896E-01	.25947E-01	.25835E-01	.25871E-01	.25959E-01	.25899E-01	.25893E-01	.25895E-01	.25890E-01	.25886E-01
91	100	.25883E-01	.25880E-01	.25878E-01	.25876E-01	.25875E-01	.25874E-01	.25875E-01	.25875E-01	.25875E-01	.25874E-01
101	110	.25872E-01	.25868E-01	.25862E-01	.25855E-01	.25846E-01	.25837E-01	.25826E-01	.25814E-01	.25808E-01	.25790E-01
111	120	.25699E-01	.25566E-01	.25111E-01	.24381E-01	.20640E-01	.14370E-01	.11751E-01	.10947E-01	.10725E-01	.10769E-01
121	130	.11152E-01	.11595E-01	.11530E-01	.95435E-02	.66283E-02	.46186E-02	.33697E-02	.25635E-02	.20099E-02	.16155E-02
131	140	.13173E-02	.10986E-02	.91883E-03	.77773E-03	.66513E-03	.69436E-03	.00000E+00	.27900E-02	.60037E-02	.65772E-02
141	150	.63020E-02	.63389E-02	.64718E-02	.65383E-02	.65817E-02	.66323E-02	.66661E-02	.66868E-02	.68506E-02	.66414E-02
151	160	.67822E-02	.69562E-02	.68584E-02	.68565E-02	.68731E-02	.68739E-02	.68760E-02	.68799E-02	.68831E-02	.68863E-02
161	170	.68895E-02	.68927E-02	.68959E-02	.68991E-02	.69025E-02	.69059E-02	.69095E-02	.69132E-02	.69170E-02	.69209E-02

171	180	.69249E-02	.69289E-02	.69330E-02	.69371E-02	.69410E-02	.69448E-02	.69484E-02	.69517E-02	.69545E-02	.69569E-02
181	190	.69587E-02	.69598E-02	.69602E-02	.69598E-02	.69585E-02	.69563E-02	.69531E-02	.69491E-02	.69442E-02	.69385E-02
191	200	.69321E-02	.69251E-02	.69175E-02	.69096E-02	.69014E-02	.68931E-02	.68849E-02	.68767E-02	.68688E-02	.68612E-02
201	210	.68540E-02	.68473E-02	.68409E-02	.68351E-02	.68298E-02	.68249E-02	.68205E-02	.68165E-02	.68129E-02	.68097E-02
211	220	.68068E-02	.68041E-02	.68017E-02	.67996E-02	.67976E-02	.67958E-02	.67941E-02	.67926E-02	.67911E-02	.67898E-02
221	230	.67885E-02	.67873E-02	.67861E-02	.67850E-02	.67839E-02	.67829E-02	.67819E-02	.67809E-02	.67800E-02	.67791E-02
231	240	.67782E-02	.67774E-02	.67765E-02	.67757E-02	.67749E-02	.67740E-02	.67732E-02	.67723E-02	.67714E-02	.67705E-02
241	250	.67695E-02	.67684E-02	.67673E-02	.67661E-02	.67648E-02	.67634E-02	.67619E-02	.67603E-02	.67587E-02	.67569E-02
251	260	.67551E-02	.67533E-02	.67513E-02	.67494E-02	.67474E-02	.67454E-02	.67435E-02	.67415E-02	.67395E-02	.67376E-02
261	270	.67357E-02	.67339E-02	.67320E-02	.67303E-02	.67285E-02	.67268E-02	.67251E-02	.67234E-02	.67218E-02	.67202E-02
271	280	.67186E-02	.67171E-02	.67156E-02	.67141E-02	.67127E-02	.67113E-02	.67099E-02	.67086E-02	.67073E-02	.67061E-02
281	290	.67049E-02	.67038E-02	.67026E-02	.67016E-02	.67006E-02	.66996E-02	.66987E-02	.66978E-02	.66970E-02	.66962E-02
291	300	.66955E-02	.66949E-02	.66943E-02	.66938E-02	.66933E-02	.66929E-02	.66925E-02	.66922E-02	.66920E-02	.66918E-02
301	310	.66917E-02	.66916E-02	.66916E-02	.66917E-02	.66918E-02	.66920E-02	.66922E-02	.66924E-02	.66927E-02	.66930E-02
311	320	.66933E-02	.66937E-02	.66940E-02	.66944E-02	.66947E-02	.66951E-02	.66954E-02	.66957E-02	.66959E-02	.66960E-02
321	330	.66961E-02	.66961E-02	.66960E-02	.66958E-02	.66955E-02	.66950E-02	.66944E-02	.66937E-02	.66928E-02	.66917E-02
331	340	.66904E-02	.66890E-02	.66873E-02	.66855E-02	.66836E-02	.66814E-02	.66791E-02	.66765E-02	.66739E-02	.66710E-02
341	350	.66681E-02	.66649E-02	.66617E-02	.66583E-02	.66548E-02	.66512E-02	.66474E-02	.66436E-02	.66397E-02	.66357E-02
351	360	.66316E-02	.66274E-02	.66231E-02	.66187E-02	.66143E-02	.66097E-02	.66051E-02	.66003E-02	.65955E-02	.65905E-02
361	370	.65854E-02	.65802E-02	.65749E-02	.65694E-02	.65637E-02	.65579E-02	.65519E-02	.65456E-02	.65392E-02	.65326E-02
371	380	.65257E-02	.65187E-02	.65114E-02	.65039E-02	.64963E-02	.64884E-02	.64805E-02	.64725E-02	.64645E-02	.64564E-02
381	390	.64481E-02	.64388E-02	.64271E-02	.64102E-02	.63850E-02	.63506E-02	.63172E-02	.63212E-02	.64395E-02	.67690E-02
391	400	.73463E-02	.80689E-02	.87372E-02	.91956E-02	.94216E-02	.94962E-02	.95234E-02	.95725E-02	.96651E-02	.97892E-02
401	410	.99212E-02	.10042E-01	.10144E-01	.10229E-01	.10304E-01	.10374E-01	.10444E-01	.10514E-01	.10582E-01	.10649E-01
411	420	.10713E-01	.10772E-01	.10828E-01	.10879E-01	.10925E-01	.10966E-01	.11002E-01	.11031E-01	.11054E-01	.11071E-01
421	430	.11080E-01	.11083E-01	.11078E-01	.11067E-01	.11050E-01	.11026E-01	.10997E-01	.10962E-01	.10922E-01	.10876E-01
431	440	.10826E-01	.10772E-01	.10713E-01	.10650E-01	.10583E-01	.10513E-01	.10440E-01	.10364E-01	.10285E-01	.10205E-01
441	450	.10122E-01	.10039E-01	.99542E-02	.98697E-02	.97858E-02	.97034E-02	.96232E-02	.95464E-02	.94740E-02	.94075E-02
451	460	.93481E-02	.92974E-02	.92566E-02	.92270E-02	.92096E-02	.92046E-02	.92117E-02	.92297E-02	.92566E-02	.92902E-02
461	470	.93276E-02	.93664E-02	.94047E-02	.94411E-02	.94755E-02	.95079E-02	.95391E-02	.95701E-02	.96016E-02	.96343E-02
471	480	.96685E-02	.97043E-02	.97415E-02	.97799E-02	.98192E-02	.98592E-02	.98998E-02	.99409E-02	.99826E-02	.10025E-01
481	490	.10068E-01	.10111E-01	.10154E-01	.10197E-01	.10240E-01	.10281E-01	.10319E-01	.10354E-01	.10384E-01	.10408E-01
491	500	.10425E-01	.10434E-01	.10436E-01	.10433E-01	.10426E-01	.10420E-01	.10418E-01	.10426E-01	.10443E-01	.10471E-01
501	502	.10505E-01	.10553E-01								

SOUND SPEED

1	10	.71449E+00	.71447E+00	.71449E+00	.71449E+00	.71450E+00	.71451E+00	.71453E+00	.71454E+00	.71457E+00	.71460E+00
11	20	.71464E+00	.71470E+00	.71476E+00	.71484E+00	.71495E+00	.71507E+00	.71523E+00	.71541E+00	.71563E+00	.71588E+00
21	30	.71617E+00	.71649E+00	.71684E+00	.71722E+00	.71760E+00	.71793E+00	.71840E+00	.71933E+00	.71896E+00	.71974E+00
31	40	.72088E+00	.72074E+00	.72096E+00	.72133E+00	.72164E+00	.72195E+00	.72227E+00	.72258E+00	.72289E+00	.72319E+00
41	50	.72348E+00	.72376E+00	.72405E+00	.72435E+00	.72465E+00	.72497E+00	.72531E+00	.72568E+00	.72607E+00	.72650E+00
51	60	.72696E+00	.72748E+00	.72805E+00	.72866E+00	.72931E+00	.72991E+00	.73065E+00	.73204E+00	.73205E+00	.73298E+00
61	70	.73432E+00	.73432E+00	.73471E+00	.73516E+00	.73546E+00	.73571E+00	.73591E+00	.73605E+00	.73615E+00	.73621E+00
71	80	.73625E+00	.73628E+00	.73630E+00	.73633E+00	.73635E+00	.73637E+00	.73638E+00	.73639E+00	.73638E+00	.73634E+00
81	90	.73633E+00	.73656E+00	.73614E+00	.73632E+00	.73670E+00	.73646E+00	.73642E+00	.73642E+00	.73637E+00	.73633E+00
91	100	.73630E+00	.73627E+00	.73624E+00	.73622E+00	.73621E+00	.73620E+00	.73621E+00	.73622E+00	.73623E+00	.73624E+00
101	110	.73626E+00	.73626E+00	.73624E+00	.73618E+00	.73608E+00	.73601E+00	.73608E+00	.73638E+00	.73679E+00	.73663E+00
111	120	.73486E+00	.73161E+00	.72777E+00	.72642E+00	.71141E+00	.67543E+00	.65405E+00	.64668E+00	.64464E+00	.64494E+00
121	130	.64833E+00	.65194E+00	.65083E+00	.63302E+00	.60173E+00	.57142E+00	.54597E+00	.52485E+00	.50685E+00	.49122E+00
131	140	.47700E+00	.46536E+00	.45130E+00	.44857E+00	.41534E+00	.48766E+00	.00000E+00	.66377E+00	.74115E+00	.74331E+00
141	150	.73570E+00	.73393E+00	.73382E+00	.73277E+00	.73153E+00	.73041E+00	.72884E+00	.72702E+00	.72817E+00	.72522E+00
151	160	.72750E+00	.73023E+00	.72938E+00	.73037E+00	.73190E+00	.73334E+00	.73491E+00	.73662E+00	.73854E+00	.74075E+00
161	170	.74328E+00	.74606E+00	.74891E+00	.75163E+00	.75402E+00	.75593E+00	.75735E+00	.75836E+00	.75912E+00	.75985E+00
171	180	.76073E+00	.76194E+00	.76359E+00	.76570E+00	.76825E+00	.77118E+00	.77438E+00	.77776E+00	.78122E+00	.78467E+00
181	190	.78806E+00	.79134E+00	.79449E+00	.79749E+00	.80033E+00	.80300E+00	.80549E+00	.80777E+00	.80982E+00	.81163E+00
191	200	.81317E+00	.81443E+00	.81542E+00	.81614E+00	.81663E+00	.81690E+00	.81700E+00	.81698E+00	.81688E+00	.81675E+00
201	210	.81662E+00	.81652E+00	.81647E+00	.81649E+00	.81659E+00	.81675E+00	.81698E+00	.81727E+00	.81761E+00	.81798E+00
211	220	.81839E+00	.81884E+00	.81933E+00	.81987E+00	.82046E+00	.82113E+00	.82188E+00	.82274E+00	.82370E+00	.82480E+00
221	230	.82603E+00	.82740E+00	.82892E+00	.83059E+00	.83238E+00	.83430E+00	.83630E+00	.83838E+00	.84048E+00	.84256E+00
231	240	.84457E+00	.84646E+00	.84818E+00	.84969E+00	.85096E+00	.85197E+00	.85272E+00	.85325E+00	.85362E+00	.85391E+00
241	250	.85423E+00	.85470E+00	.85548E+00	.85672E+00	.85857E+00	.86118E+00	.86468E+00	.86920E+00	.87482E+00	.88160E+00
251	260	.88959E+00	.89875E+00	.90903E+00	.92034E+00	.93251E+00	.94534E+00	.95860E+00	.97201E+00	.98525E+00	.99801E+00
261	270	.10100E+01	.10209E+01	.10306E+01	.10389E+01	.10456E+01	.10509E+01	.10547E+01	.10572E+01	.10586E+01	.10590E+01
271	280	.10587E+01	.10578E+01	.10565E+01	.10549E+01	.10532E+01	.10514E+01	.10497E+01	.10480E+01	.10463E+01	.10448E+01

281	290	.10433E+01	.10419E+01	.10406E+01	.10393E+01	.10380E+01	.10368E+01	.10355E+01	.10342E+01	.10330E+01	.10317E+01
291	300	.10304E+01	.10290E+01	.10277E+01	.10264E+01	.10250E+01	.10236E+01	.10222E+01	.10209E+01	.10195E+01	.10181E+01
301	310	.10168E+01	.10154E+01	.10141E+01	.10128E+01	.10115E+01	.10102E+01	.10089E+01	.10077E+01	.10065E+01	.10054E+01
311	320	.10043E+01	.10032E+01	.10021E+01	.10011E+01	.10001E+01	.99911E+00	.99818E+00	.99729E+00	.99643E+00	.99562E+00
321	330	.99486E+00	.99414E+00	.99347E+00	.99284E+00	.99227E+00	.99173E+00	.99124E+00	.99079E+00	.99037E+00	.98996E+00
331	340	.98957E+00	.98918E+00	.98878E+00	.98837E+00	.98794E+00	.98748E+00	.98700E+00	.98649E+00	.98597E+00	.98544E+00
341	350	.98490E+00	.98438E+00	.98388E+00	.98341E+00	.98299E+00	.98261E+00	.98229E+00	.98203E+00	.98181E+00	.98163E+00
351	360	.98147E+00	.98132E+00	.98116E+00	.98098E+00	.98074E+00	.98042E+00	.98003E+00	.97953E+00	.97891E+00	.97819E+00
361	370	.97734E+00	.97639E+00	.97532E+00	.97416E+00	.97292E+00	.97162E+00	.97025E+00	.96885E+00	.96741E+00	.96595E+00
371	380	.96448E+00	.96300E+00	.96152E+00	.96003E+00	.95853E+00	.95702E+00	.95551E+00	.95398E+00	.95245E+00	.95090E+00
381	390	.94935E+00	.94776E+00	.94613E+00	.94439E+00	.94250E+00	.94043E+00	.93843E+00	.93721E+00	.93834E+00	.94384E+00
391	400	.95402E+00	.96595E+00	.97572E+00	.98142E+00	.98341E+00	.98321E+00	.98238E+00	.98194E+00	.98219E+00	.98295E+00
401	410	.98386E+00	.98467E+00	.98528E+00	.98575E+00	.98617E+00	.98662E+00	.98712E+00	.98766E+00	.98819E+00	.98867E+00
411	420	.98905E+00	.98930E+00	.98941E+00	.98937E+00	.98919E+00	.98888E+00	.98846E+00	.98796E+00	.98740E+00	.98682E+00
421	430	.98622E+00	.98561E+00	.98498E+00	.98432E+00	.98360E+00	.98278E+00	.98182E+00	.98069E+00	.97935E+00	.97777E+00
431	440	.97593E+00	.97382E+00	.97145E+00	.96883E+00	.96600E+00	.96299E+00	.95984E+00	.95661E+00	.95333E+00	.95006E+00
441	450	.94682E+00	.94366E+00	.94061E+00	.93769E+00	.93490E+00	.93227E+00	.92980E+00	.92750E+00	.92537E+00	.92342E+00
451	460	.92166E+00	.92010E+00	.91874E+00	.91760E+00	.91668E+00	.91598E+00	.91549E+00	.91518E+00	.91503E+00	.91499E+00
461	470	.91502E+00	.91507E+00	.91512E+00	.91513E+00	.91510E+00	.91502E+00	.91490E+00	.91474E+00	.91456E+00	.91435E+00
471	480	.91412E+00	.91385E+00	.91356E+00	.91323E+00	.91287E+00	.91248E+00	.91209E+00	.91172E+00	.91142E+00	.91122E+00
481	490	.91120E+00	.91142E+00	.91195E+00	.91286E+00	.91424E+00	.91613E+00	.91859E+00	.92164E+00	.92528E+00	.92950E+00
491	500	.93425E+00	.93947E+00	.94511E+00	.95108E+00	.95729E+00	.96359E+00	.96975E+00	.97555E+00	.98098E+00	.98654E+00
501	502	.99327E+00	.10021E+01								

* PRESSURE HISTORY AT TEST STATION NO. 007: 1.78 METERS FR DIV'T-NOZZLE EXIT *

TIME OF SHOCK ARRIVAL, ... TA = .3556E-02 SEC
SHOCK OVERPRESSURE, ... PSO = .1976E+03 KPA (28.7 PSI)
SIDE-ON OVERPRESSURE IMPULSE, ISO = .1272E+01 KPA-S
(EQUIVALENT WEAPON YIELD, .. WSO = .2746E-02 KT)
POSITIVE-PHASE DURATION, ... PPD = .1651E-01 SEC
(EQUIV. FREE-FIELD VALUE, .. PPF = .2301E-01 SEC)

SHOCK DYNAMIC PRESSURE, ... QS = .1076E+03 KPA (15.6 PSI)
(EQUIV. FREE-FIELD VALUE, ... QF = .1078E+03 KPA)
DYNAMIC-PRESSURE IMPULSE, ... IQ = .4805E+00 KPA-S
(EQUIVALENT WEAPON YIELD, ... WQ = .1816E-02 KT)
DYNAMIC-PHASE DURATION, ... QPD = .1652E-01 SEC
(EQUIV. FREE-FIELD VALUE, .. QPF = .1728E+00 SEC)

TIME(S)	PSO(KPA)	ISO(KPA-S)	PDYN(KPA)	IDYN(KPA-S)	VFLO(M/S)	RHO(KG/M**3)
.0000E+00	.0000E+00	.0000E+00	.0000E+00	.0000E+00	.0000E+00	.1178E+01
.3280E-03	.0000E+00	.0000E+00	.0000E+00	.0000E+00	.0000E+00	.1178E+01
.6123E-03	.0000E+00	.0000E+00	.0000E+00	.0000E+00	.0000E+00	.1178E+01
.8749E-03	.0000E+00	.0000E+00	.0000E+00	.0000E+00	.0000E+00	.1178E+01
.1151E-02	.0000E+00	.0000E+00	.0000E+00	.0000E+00	.0000E+00	.1178E+01
.1429E-02	.0000E+00	.0000E+00	.0000E+00	.0000E+00	.0000E+00	.1178E+01
.1711E-02	.0000E+00	.0000E+00	.0000E+00	.0000E+00	.0000E+00	.1178E+01
.1994E-02	.0000E+00	.0000E+00	.0000E+00	.0000E+00	.0000E+00	.1178E+01
.2281E-02	.0000E+00	.0000E+00	.0000E+00	.0000E+00	.0000E+00	.1178E+01
.2570E-02	.0000E+00	.0000E+00	.0000E+00	.0000E+00	.0000E+00	.1178E+01
.2862E-02	.0000E+00	.0000E+00	.0000E+00	.0000E+00	.0000E+00	.1178E+01
.3158E-02	.0000E+00	.0000E+00	.0000E+00	.0000E+00	.0000E+00	.1178E+01
.3455E-02	-.8504E+00	.0000E+00	.2500E-02	.0000E+00	-.2066E+01	.1171E+01
.3754E-02	.1824E+03	.3581E-01	.9324E+02	.1802E-01	.2798E+03	.2381E+01
.4061E-02	.1798E+03	.9168E-01	.9085E+02	.4655E-01	.2771E+03	.2366E+01
.4367E-02	.1768E+03	.1461E+00	.8817E+02	.7380E-01	.2740E+03	.2348E+01
.4680E-02	.1737E+03	.2011E+00	.8546E+02	.1011E+00	.2708E+03	.2331E+01
.4996E-02	.1670E+03	.2549E+00	.7960E+02	.1272E+00	.2636E+03	.2291E+01
.5318E-02	.1633E+03	.3080E+00	.7646E+02	.1522E+00	.2596E+03	.2269E+01
.5649E-02	.1619E+03	.3618E+00	.7529E+02	.1773E+00	.2581E+03	.2260E+01
.5978E-02	.1572E+03	.4145E+00	.7135E+02	.2016E+00	.2529E+03	.2231E+01
.6318E-02	.1519E+03	.4669E+00	.6705E+02	.2250E+00	.2469E+03	.2200E+01
.6658E-02	.1480E+03	.5180E+00	.6468E+02	.2474E+00	.2425E+03	.2200E+01
.7000E-02	.1388E+03	.5672E+00	.6034E+02	.2689E+00	.2319E+03	.2243E+01
.7341E-02	.1258E+03	.6123E+00	.5452E+02	.2885E+00	.2167E+03	.2323E+01
.7678E-02	.1134E+03	.6526E+00	.4779E+02	.3057E+00	.2019E+03	.2346E+01
.8023E-02	.1033E+03	.6899E+00	.4127E+02	.3210E+00	.1892E+03	.2305E+01
.8378E-02	.9699E+02	.7253E+00	.3700E+02	.3348E+00	.1809E+03	.2261E+01
.8710E-02	.9681E+02	.7573E+00	.3665E+02	.3470E+00	.1803E+03	.2255E+01
.9069E-02	.9720E+02	.7923E+00	.3651E+02	.3602E+00	.1804E+03	.2244E+01
.9441E-02	.9363E+02	.8279E+00	.3384E+02	.3733E+00	.1754E+03	.2199E+01
.9787E-02	.8952E+02	.8595E+00	.3103E+02	.3845E+00	.1697E+03	.2155E+01
.1015E-01	.8856E+02	.8919E+00	.3023E+02	.3956E+00	.1681E+03	.2139E+01
.1051E-01	.8690E+02	.9233E+00	.2905E+02	.4063E+00	.1657E+03	.2118E+01
.1087E-01	.8307E+02	.9538E+00	.2667E+02	.4163E+00	.1603E+03	.2077E+01
.1122E-01	.7892E+02	.9827E+00	.2422E+02	.4254E+00	.1544E+03	.2032E+01
.1157E-01	.7335E+02	.1009E+01	.2118E+02	.4333E+00	.1464E+03	.1976E+01
.1192E-01	.6655E+02	.1034E+01	.1774E+02	.4400E+00	.1364E+03	.1908E+01

.1227E-01	.5979E+02	.1056E+01	.1459E+02	.4457E+00	.1261E+03	.1835E+01
.1262E-01	.5403E+02	.1075E+01	.1211E+02	.4503E+00	.1170E+03	.1769E+01
.1296E-01	.4897E+02	.1093E+01	.1010E+02	.4541E+00	.1087E+03	.1708E+01
.1330E-01	.4389E+02	.1109E+01	.8275E+01	.4572E+00	.1002E+03	.1650E+01
.1364E-01	.3933E+02	.1123E+01	.6796E+01	.4598E+00	.9219E+02	.1599E+01
.1398E-01	.3619E+02	.1136E+01	.5858E+01	.4619E+00	.8658E+02	.1563E+01
.1433E-01	.3654E+02	.1148E+01	.5927E+01	.4639E+00	.8725E+02	.1557E+01
.1468E-01	.3752E+02	.1161E+01	.6177E+01	.4661E+00	.8904E+02	.1558E+01
.1504E-01	.3611E+02	.1175E+01	.5767E+01	.4682E+00	.8647E+02	.1543E+01
.1539E-01	.3472E+02	.1187E+01	.5379E+01	.4702E+00	.8389E+02	.1529E+01
.1575E-01	.3371E+02	.1200E+01	.5106E+01	.4721E+00	.8200E+02	.1519E+01
.1611E-01	.3196E+02	.1211E+01	.4652E+01	.4739E+00	.7869E+02	.1503E+01
.1649E-01	.2941E+02	.1223E+01	.4026E+01	.4755E+00	.7377E+02	.1480E+01
.1689E-01	.2607E+02	.1234E+01	.3271E+01	.4770E+00	.6719E+02	.1449E+01
.1730E-01	.2225E+02	.1244E+01	.2500E+01	.4781E+00	.5945E+02	.1414E+01
.1771E-01	.1817E+02	.1252E+01	.1787E+01	.4790E+00	.5093E+02	.1377E+01
.1812E-01	.1422E+02	.1259E+01	.1206E+01	.4796E+00	.4240E+02	.1342E+01
.1853E-01	.1060E+02	.1264E+01	.7710E+00	.4800E+00	.3431E+02	.1310E+01
.1896E-01	.7283E+01	.1268E+01	.4551E+00	.4803E+00	.2666E+02	.1280E+01
.1937E-01	.4476E+01	.1270E+01	.2505E+00	.4804E+00	.1998E+02	.1255E+01
.1976E-01	.1940E+01	.1272E+01	.1169E+00	.4805E+00	.1377E+02	.1233E+01
.2017E-01	-.6224E+00	.1272E+01	.3310E-01	.4805E+00	.7394E+01	.1211E+01
.2060E-01	-.3033E+01	.1271E+01	.9499E-03	.4805E+00	.1264E+01	.1190E+01
.2102E-01	.2229E+02	.1273E+01	.2320E+01	.4807E+00	.5758E+02	.1400E+01
.2143E-01	.2451E+02	.1283E+01	.2686E+01	.4818E+00	.6161E+02	.1415E+01
.2187E-01	.2367E+02	.1293E+01	.2494E+01	.4830E+00	.5955E+02	.1406E+01
.2230E-01	.2264E+02	.1303E+01	.2289E+01	.4840E+00	.5724E+02	.1397E+01
.2272E-01	.2160E+02	.1313E+01	.2095E+01	.4849E+00	.5495E+02	.1388E+01
.2314E-01	.2062E+02	.1321E+01	.1921E+01	.4858E+00	.5279E+02	.1379E+01
.2355E-01	.1971E+02	.1330E+01	.1750E+01	.4865E+00	.5055E+02	.1370E+01
.2398E-01	.1902E+02	.1338E+01	.1538E+01	.4872E+00	.4751E+02	.1362E+01
.2442E-01	.1845E+02	.1346E+01	.1323E+01	.4879E+00	.4418E+02	.1356E+01
.2487E-01	.1678E+02	.1354E+01	.1220E+01	.4884E+00	.4268E+02	.1339E+01
.2532E-01	.1382E+02	.1361E+01	.1261E+01	.4890E+00	.4384E+02	.1312E+01
.2577E-01	.9996E+01	.1367E+01	.1341E+01	.4896E+00	.4580E+02	.1278E+01
.2624E-01	.5812E+01	.1370E+01	.1415E+01	.4902E+00	.4777E+02	.1240E+01
.2671E-01	.3569E+01	.1372E+01	.1795E+01	.4909E+00	.5429E+02	.1218E+01
.2718E-01	.3104E+01	.1374E+01	.2529E+01	.4920E+00	.6467E+02	.1209E+01
.2766E-01	-.1354E+00	.1375E+01	.2722E+01	.4932E+00	.6802E+02	.1177E+01
.2815E-01	-.3886E+01	.1374E+01	.2764E+01	.4946E+00	.6967E+02	.1139E+01
.2863E-01	-.6805E+01	.1371E+01	.2931E+01	.4960E+00	.7277E+02	.1107E+01
.2911E-01	-.9174E+01	.1367E+01	.3165E+01	.4974E+00	.7659E+02	.1079E+01
.2959E-01	-.1147E+02	.1362E+01	.3366E+01	.4990E+00	.8002E+02	.1051E+01
.3008E-01	-.1368E+02	.1356E+01	.3560E+01	.5007E+00	.8340E+02	.1024E+01
.3058E-01	-.1606E+02	.1349E+01	.3680E+01	.5025E+00	.8601E+02	.9949E+00
.3109E-01	-.1810E+02	.1340E+01	.3872E+01	.5044E+00	.8939E+02	.9691E+00
.3159E-01	-.1963E+02	.1331E+01	.4154E+01	.5064E+00	.9364E+02	.9475E+00
.3209E-01	-.2126E+02	.1320E+01	.4382E+01	.5086E+00	.9734E+02	.9248E+00
.3260E-01	-.2298E+02	.1309E+01	.4558E+01	.5108E+00	.1005E+03	.9021E+00
.3312E-01	-.2354E+02	.1297E+01	.5119E+01	.5133E+00	.1072E+03	.8910E+00
.3366E-01	-.2500E+02	.1284E+01	.5388E+01	.5162E+00	.1109E+03	.8758E+00
.3420E-01	-.2742E+02	.1270E+01	.5289E+01	.5191E+00	.1112E+03	.8553E+00
.3475E-01	-.2947E+02	.1254E+01	.5287E+01	.5220E+00	.1124E+03	.8373E+00
.3528E-01	-.3156E+02	.1238E+01	.5197E+01	.5248E+00	.1128E+03	.8171E+00
.3581E-01	-.3390E+02	.1221E+01	.4973E+01	.5275E+00	.1119E+03	.7942E+00
.3633E-01	-.3627E+02	.1202E+01	.4705E+01	.5300E+00	.1105E+03	.7713E+00
.3686E-01	-.3888E+02	.1182E+01	.4337E+01	.5324E+00	.1078E+03	.7468E+00
.3741E-01	-.4157E+02	.1160E+01	.3938E+01	.5347E+00	.1045E+03	.7208E+00
.3795E-01	-.4383E+02	.1137E+01	.3656E+01	.5367E+00	.1024E+03	.6977E+00

FRENCH BLAST SIMULATOR

CASE: MOD.A2--26 -- PLOT 1

$XSTA_i$ = 0.445
V_{drv} = 0.004 m^3
P_4/P_1 = 107.8
L_{ref} = 6.640 m

Offset, Δy = 0.010
Grid Clustered About X_{CLUST} = 0.140

DENSITY vs. DISTANCE

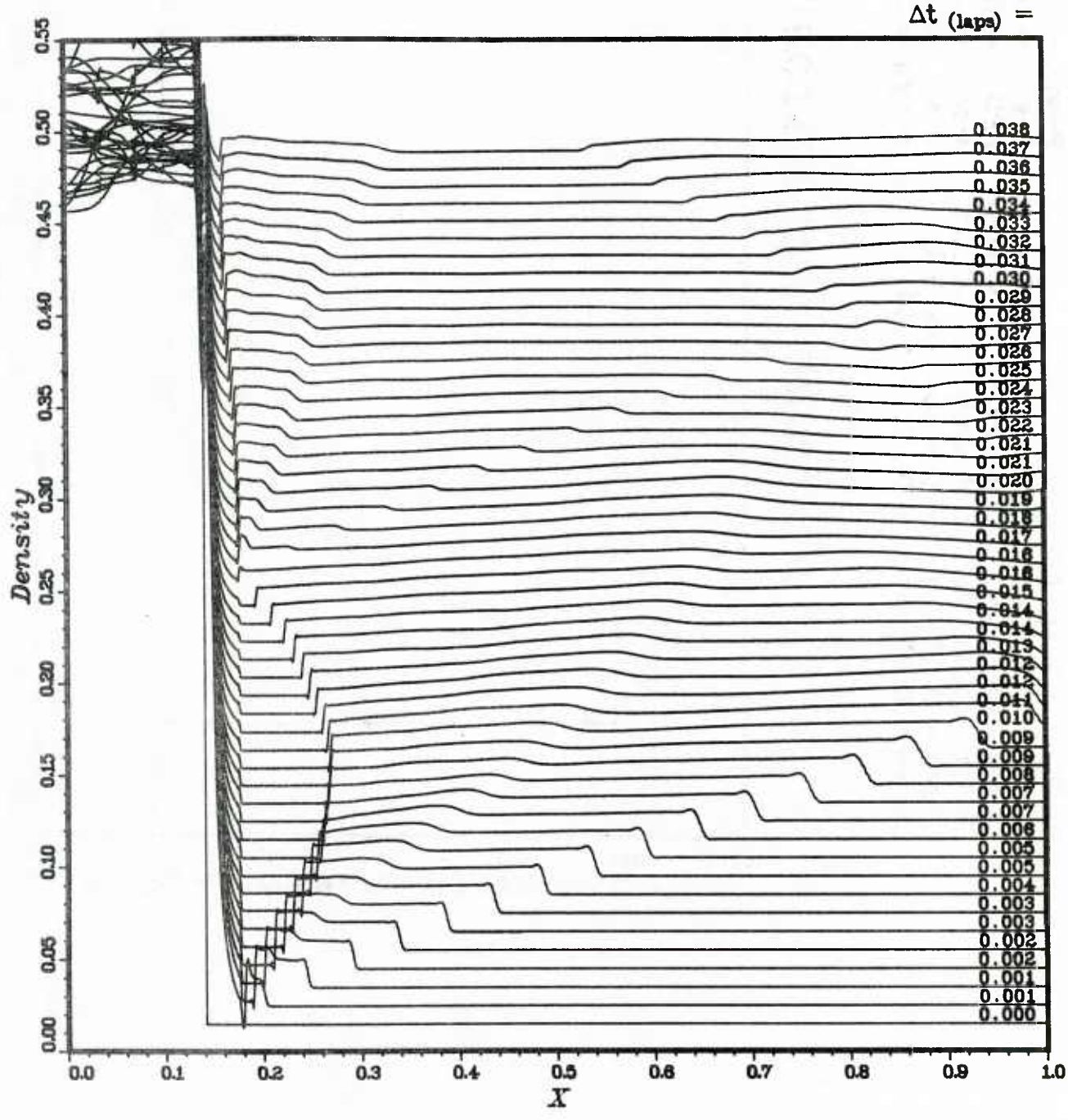

SHOCK TUBE W/STEPPED DRIVER

CASE: = MODEL-A2			P-so	= 197.6 kPa	(28.66 psi)
L-ref = 6.640 m	X-sta = 1.778 m		t-a	= 3.556 ms	
L-drv = 0.884 m	P-drv = 107.8 atm		PPD	= 0.017 s	(0.023 s)
V-drv = 0.004 m^3	P-amb= 101.4 kPa		I-so	= 1.272 kPa-s	(0.003 kT)
L-dvn = 5.461 m	T-amb= 299.8 K		Q-s	= 107.6 kPa	
L-rwe = 0.00 m	T4/T1 = 1.59		I-dyn	= 0.481 kPa-s	(0.002 kT)

PRESSURE-TIME HISTORY

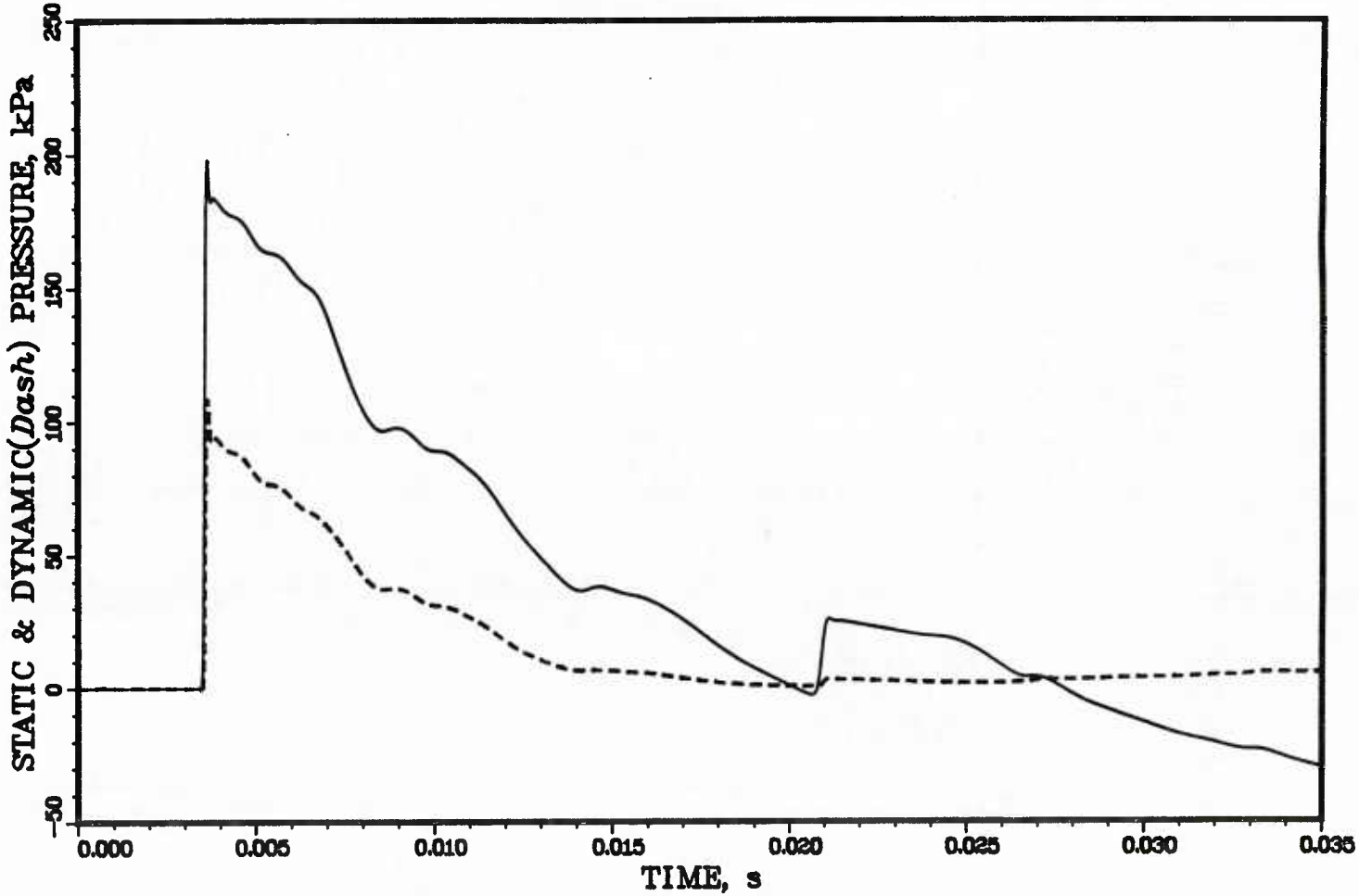

DISTRIBUTION LIST

No. of Copies	Organization
12	Administrator Defense Technical Info Center ATTN: DTIC-DDA Cameron Station Alexandria, VA 22304-6145
1	Director of Defense Research & Engineering ATTN: DD/TWP Washington, DC 20301
1	Asst. to the Secretary of Defense (Atomic Energy) ATTN: Document Control Washington, DC 20301
1	Director Defense Advanced Research Projects Agency ATTN: Technical Library 1400 Wilson Boulevard Arlington, VA 22209
2	Director Federal Emergency Management Agency ATTN: D. A. Bettge Technical Library Washington, DC 20472
1	Director Defense Intelligence Agency ATTN: DT-2/Wpns & Sys Div Washington, DC 20301
1	Director National Security Agency ATTN: E. F. Butala, R15 Ft. George G. Meade, MD 20755
1	Director Joint Strategic Target Planning Staff JCS Offut AFB Omaha, NB 68113
1	Director Defense Communications Agency ATTN: 930 Washington, DC 20305
9	Director Defense Nuclear Agency ATTN: DDST TIPL/Technical Library SPSS/K. Goering SPTD/T. Kennedy SPAS/P.R. Rohr G. Ullrich STSP/COL Kovel NATD NATA Washington, DC 20305
2	Commander Field Command, DNA ATTN: FCPR FCTMOF Kirtland AFB, NM 87117
1	Commander Field Command, DNA Livermore Branch ATTN: FCPRL P.O. Box 808 Livermore, CA 94550
1	HQDA DAMA-ART-M Washington, DC 20310
10	Central Intelligence Agency Office of Central Reference Dissemination Branch Room GE-47 HQS Washington, DC 20502
1	Program Manager US Army BMD Program Office ATTN: John Shea 5001 Eisenhower Avenue Alexandria, VA 22333
2	Director US Army BMD Advanced Technology Center ATTN: CRDABH-X CRDABH-S Huntsville, AL 35807

DISTRIBUTION LIST

No. of Copies	Organization
1	Commander US Army BMD Command ATTN: BDMSC-TFN/N.J. Hurst P.O. Box 1500 Huntsville, AL 35807
1	Commander US Army Engineer Division ATTN: HNDED-FD P.O. Box 1500 Huntsville, AL 35807
2	Deputy Chief of Staff for Operations and Plans ATTN: Director of Chemical & Nuclear Operations Technical Library Department of the Army Washington, DC 20310
3	Commander US Army Engineers Waterways Experiment Station ATTN: Jim Watt Jim Ingram Technical Library P.O. Box 631 Vicksburg, MS 39180
1	Commander US Army Materiel Command ATTN: AMCDRA-ST 5001 Eisenhower Avenue Alexandria, VA 22333-0001
3	Commander Armament R&D Center US Army AMCCOM ATTN: SMCAR-TDC SMCAR-TSS W. Reiner Dover, NJ 07801
1	Commander US Army Armament, Munitions and Chemical Command ATTN: SMCAR-ESP-L Rock Island, IL 61299-7300
1	Director Benet Weapons Laboratory Armament R&D Center US Army AMCCOM ATTN: SMCAR-LCB-TL Watervliet, NY 12189
1	Commander US Army Aviation Research and Development Command ATTN: AMSAV-E 4300 Goodfellow Boulevard St. Louis, MO 63120
1	Director US Army Air Mobility Research and Development Laboratory Ames Research Center Moffett Field, CA 94035
1	Commander US Army Communications - Electronics Command ATTN: AMSEL-ED Fort Monmouth, NJ 07703
1	Commander US Army Communications - Research and Development Command ATTN: DRSEL-ATDD Fort Monmouth, NJ 07703
1	Commander U.S. Army Communications - Electronics Command (CECOM) CECOM R&D Technical Library ATTN: AMSEL-IM-L, B 2700 Fort Monmouth, NJ 07703-5000
2	Commander US Army Electronics Research and Development Command ATTN: DELEW-E, W. S. McAfee DELSD-EI, J. Roma Fort Monmouth, NJ 07703-5301

DISTRIBUTION LIST

No. of Copies — Organization

7 Director
US Army Harry Diamond Labs
ATTN: Mr. James Gaul
Mr. L. Belliveau
Mr. J. Meszaros
Mr. J. Gwaltney
Mr. Bill Vault
Mr. R. J. Bostak
Dr. W. J. Schuman, Jr.
2800 Powder Mill Road
Adelphi, MD 20783

4 Director
US Army Harry Diamond Labs
ATTN: DELHD-TA-L
DRXDO-TI/002
DRXDO-NP
DELHD-RBA/J. Rosado
2800 Powder Mill Road
Adelphi, MD 20783

1 Commander
US Army Missile Command - Research, Development and Engineering Center
ATTN: AMSMI-RD
Redstone Arsenal, AL 35898

1 Director
US Army Missile and Space Intelligence Center
ATTN: AIAMS-YDL
Redstone Arsenal, AL 35898-5500

2 Commander
US Army Natick Research and Development Center
ATTN: DRXRE/Dr. D. Sieling
STRNC-UE/J. Calligeros
Natick, MA 01762

1 Commander
US Army Tank Automotive Research and Development Command
ATTN: AMSTA-TSL
Warren, MI 48397-5000

1 Commander
US Army Foreign Science and Technology Center
ATTN: Research & Concepts Br
220 7th Street , NE
Charlottesville, VA 22901

1 Commander
US Army Logistics Management Center
ATTN: ATCL-O,
Mr. Robert Cameron
Fort Lee, VA 23801

3 Commander
US Army Materials Technology Laboratory
ATTN: DRXMR-ER, Joe Prifti
Eugene de Luca
Technical Library
Watertown, MA 02172

1 Commander
US Army Research Office
P.O. Box 12211
Research Triangle Park
NC 27709

4 Commander
US Army Nuclear & Chemical Agency
ATTN: LTC Finno
ACTA-NAW
MONA-WE
Technical Library
7500 Backlick Rd, Bldg. 2073
Springfield, VA 22150

1 Commander
US Army TRADOC
ATTN: DCST&E
Fort Monroe, VA 23651

2 Director
US Army TRADOC Systems Analysis Activity
ATTN: LTC John Hesse
ATAA-SL
White Sands Missile Range
NM 88002

DISTRIBUTION LIST

No. of Copies	Organization
2	Commandant US Army Infantry School ATTN: ATSH-CD-CSO-OR Fort Benning, GA 31905
1	Commander US Army Development & Employment Agency ATTN: MODE-TED-SAB Fort Lewis, WA 98433
1	Commandant Interservice Nuclear Weapons School ATTN: Technical Library Kirtland AFB, NM 87115
1	Chief of Naval Material ATTN: MAT 0323 Department of the Navy Arlington, VA 22217
2	Chief of Naval Operations ATTN: OP-03EG OP-985F Department of the Navy Washington, DC 20350
1	Chief of Naval Research ATTN: N. Perrone Department of the Navy Arlington, VA 22217
1	Director Strategic Systems Projects Office ATTN: NSP-43, Technical Library Department of the Navy Washington, DC 20360
1	Commander Naval Electronic Systems Command ATTN: PME 117-21A Washington, DC 20360
1	Commander Naval Facilities Engineering Command Washington, DC 20360
1	Commander Naval Sea Systems Command ATTN: SEA-62R Department of the Navy Washington, DC 20362
3	Officer-in-Charge(Code L31) Naval Construction Battalion Center Civil Engineering Laboratory ATTN: Stan Takahashi R. J. Odello Technical Library Port Hueneme, CA 93041
1	Commander David W. Taylor Naval Ship Research & Development Center ATTN: Code 522, Library Div Bethesda, MD 20084
1	Commander Naval Surface Weapons Center ATTN: DX-21, Library Br. Dahlgren, VA 22448-5000
2	Commander Naval Surface Weapons Center ATTN: Code WA501/Navy Nuclear Programs Office Code WX21/Technical Library Silver Spring, MD 20902-5000
1	Commander Naval Weapons Center ATTN: Code 533, Technical Library China Lake, CA 93555-6001
1	Commander Naval Weapons Evaluation Facility ATTN: Doc Control Kirtland AFB, NM 87117
1	Commander Naval Research Laboratory ATTN: Code 2027, Technical Library Washington, DC 20375

DISTRIBUTION LIST

No. of Copies	Organization
1	Superintendent Naval Postgraduate School ATTN: Code 2124, Technical Reports Library Monterey, CA 93940
1	AFSC/SDOA Andrews Air Force Base, MD 20334
1	ADTC/DLODL, Technical Library Eglin AFB, FL 32542
1	AFWL/SUL Kirtland AFB, NM 87117
1	Air Force Armament Laboratory ATTN: AFATL/DLODL Eglin AFB, FL 32542-5000
1	AFESC/RDCS ATTN: Paul Rosengren Tyndall AFB, FL 32403
1	AFATL (DLYV) Eglin AFB, FL 32542
1	RADC (EMTLD/Docu Libray) Griffiss AFB, NY 13441
1	AFWL/NTES ATTN: R. Henny Kirtland AFB, NM 87117-6008
1	AFWL/NTED ATTN: J. W. Aubrey Kirtland AFB, NM 87117-6008
2	Commander-in-Chief Strategic Air Command ATTN: NRI-STINFO Library Offutt AFB, NB 68113
1	AFIT ATTN: Library Bldg. 640, Area B Wright-Patterson AFB Ohio 45433
1	FTD/NIIS Wright-Patterson AFB Ohio 45433
1	Director Lawrence Livermore Lab. ATTN: Technical Info Dept L-3 P.O. Box 808 Livermore, CA 94550
2	Director Los Alamos Scientific Lab. ATTN: Doc Control for Reports Library P.O. Box 1663 Los Alamos, NM 87544
2	Director Sandia Laboratories ATTN: Doc Control for 3141 Sandia Report Collection L. J. Vortman P.O. Box 5800 Albuquerque, NM 87185
1	Director Sandia Laboratories Livermore Laboratory ATTN: Doc Control for Technical Library P.O. Box 969 Livermore, CA 94550
1	Director National Aeronautics and Space Administration Scientific & Technical Info Facility P.O. Box 8757 BWI Airport Baltimore, MD 21240
1	Director NASA-Ames Research Center Applied Computational Aerodynamics Branch ATTN: MS 202-14, Dr. T. Holtz Moffett Field, CA 94035

DISTRIBUTION LIST

No. of Copies	Organization
3	Aberdeen Research Center ATTN: N.H. Ethridge J. Keefer Library P.O. Box 548 30 Diamond Street Aberdeen, MD 21001
1	Aerospace Corporation ATTN: Technical Info Services P.O. Box 92957 Los Angeles, CA 90009
1	Agbabian Associates ATTN: M. Agbabian 250 North Nash Street El Segundo, CA 90245
1	The BDM Corporation ATTN: Richard Hensley P.O. Box 9274 Albuquerque International Airport Albuquerque, NM 87119
1	Black & Veatch Consulting Engineers ATTN: H. D. Laverentz 1500 Meadow Lake Parkway Kansas City, MO 64114
1	The Boeing Company ATTN: Aerospace Library P.O. Box 3707 Seattle, WA 98124
2	California Research and Technology ATTN: M. Rosenblatt F. Sauer Suite B 130 11875 Dublin Blvd Dublin, CA 94568
1	Carpenter Research Corporation ATTN: H. Jerry Carpenter Suite 424 904 Silver Spur Road Rolling Hills Estates, CA 90274
1	Dynamics Technology, Inc. ATTN: D. T. Hove Suite 300 21311 Hawthorne Blvd. Torrance, CA 90503
1	Goodyear Aerospace Corporation ATTN: R. M. Brown, Bldg 1, Shelter Engineering Litchfield Park, AZ 85340
6	Kaman AviDyne ATTN: Dr. R. Reutenick (4 cys) Mr. S. Criscione Mr. R. Milligan 83 Second Avenue Northwest Industrial Park Burlington, MA 01830
3	Kaman Sciences Corporation ATTN: Library P. A. Ellis F. H. Shelton 1500 Garden of the Gods Road Colorado Springs, CO 80907
2	Kaman-TEMPO ATTN: DASIAC Don Sachs P.O. Drawer QQ 816 State Street Santa Barbara, CA 93102
1	Kaman-TEMPO ATTN: E. Bryant, Suite UL-1 715 Shamrock Road Bel Air, MD 21014
1	Lockheed Missiles & Space Company ATTN: J. J. Murphy, Dept. 81-11, Bldg. 154 P.O. Box 504 Sunnyvale, CA 94086
1	Martin Marietta Aerospace Orlando Division ATTN: G. Fotieo P.O. Box 5837 Orlando, FL 32805

DISTRIBUTION LIST

No. of Copies	Organization
2	McDonnell Douglas Astronautics Corporation ATTN: Robert W. Halprin K.A. Heinly 5301 Bolsa Avenue Huntington Beach, CA 92647
1	New Mexico Engineering Research Institute (CERF) ATTN: J. Leigh P.O. Box 25 UNM Albuquerque, NM 87131
2	Physics International Corporation 2700 Merced Street San Leandro, CA 94577
2	R&D Associates ATTN: Allan Kuhl Technical Library P.O. Box 9695 Marina del Rey, CA 90291
1	R&D Associates ATTN: G.P. Ganong P.O. Box 9330 Albuquerque, NM 87119
2	Science Applications, Inc. ATTN: W. Layson John Cockayne P.O. Box 1303 1710 Goodridge Drive McLean, VA 22102
1	Science Applications, Inc. ATTN: Technical Library 1250 Prospect Plaza La Jolla, CA 92037
1	Sparta, Inc. ATTN: I. B. Osofsky Suite 250 23293 So. Pointe Dr. Laguna Hills, CA 92653
1	Sverdrup Technology, Inc. ATTN: R. F. Starr P. O. Box 884 Tullahoma, TN 37388
1	SRI International ATTN: Dr. G. R. Abrahamson 333 Ravenswood Avenue Menlo Park, CA 94025
2	Systems, Science and Software ATTN: C. E. Needham Lynn Kennedy PO Box 8243 Albuquerque, NM 87198
3	Systems, Science and Software ATTN: Technical Library R. Duff K. Pyatt PO Box 1620 La Jolla, CA 92037
1	Texas Engineering Experiment Station ATTN: Dr. D. Anderson 301 Engineering Research Center College Station, TX 77843
1	Thermal Science, Inc. ATTN: R. Feldman 2200 Cassens Dr. St. Louis, MO 63026
1	TRW - Ballistic Missile Division ATTN: H. Korman, Mail St. 526/614 P.O. Box 1310 San Bernadino, CA 92402
2	TRW Systems Group ATTN: Benjamin Sussholtz Stanton Fink One, Space Park Redondo Beach, CA 90278
1	Battelle Memorial Institute ATTN: Technical Library 505 King Avenue Columbus, OH 43201

DISTRIBUTION LIST

No. of Copies | Organization

1 California Institute of Technology
ATTN: T. J. Ahrens
1201 E. California Blvd.
Pasadena, CA 91109

2 Denver Research Institute
University of Denver
ATTN: Mr. J. Wisotski
Technical Library
PO Box 10127
Denver, CO 80210

1 Massachusetts Institute of Technology
Aeroelastic and Structures
Research Laboratory
ATTN: Dr. E. A. Witmer
Cambridge, MA 02139

1 Massachusetts Institute of Technology
ATTN: Technical Library
Cambridge, MA 02139

1 Northrop University
ATTN: Dr. F. B. Safford
5800 W. Arbor Vitae St.
Los Angeles, CA 90045

2 Southwest Research Institute
ATTN: Dr. W. E. Baker
A. B. Wenzel
8500 Culebra Road
San Antonio, TX 78228

1 Stanford University
Durand Laboratory
ATTN: Dr. D. Bershader
Stanford, CA 94305

Aberdeen Proving Ground

Dir, USAMSAA
ATTN: AMXSY-D
AMXSY-MP, H. Cohen

Cdr, USATECOM
ATTN: AMSTE-TO-F

Cdr, CRDC, AMCCOM
ATTN: SMCCR-RSP-A
SMCCR-MU
SMCCR-SPS-IL

USER EVALUATION SHEET/CHANGE OF ADDRESS

This Laboratory undertakes a continuing effort to improve the quality of the reports it publishes. Your comments/answers to the items/questions below will aid us in our efforts.

1. BRL Report Number_____ Date of Report_____

2. Date Report Received_____

3. Does this report satisfy a need? (Comment on purpose, related project, or other area of interest for which the report will be used.)_____

4. How specifically, is the report being used? (Information source, design data, procedure, source of ideas, etc.)_____

5. Has the information in this report led to any quantitative savings as far as man-hours or dollars saved, operating costs avoided or efficiencies achieved, etc? If so, please elaborate._____

6. General Comments. What do you think should be changed to improve future reports? (Indicate changes to organization, technical content, format, etc.)

CURRENT ADDRESS

Name

Organization

Address

City, State, Zip

7. If indicating a Change of Address or Address Correction, please provide the New or Correct Address in Block 6 above and the Old or Incorrect address below.

OLD ADDRESS

Name

Organization

Address

City, State, Zip

(Remove this sheet along the perforation, fold as indicated, staple or tape closed, and mail.)

FOLD HERE

Director
U.S. Army Ballistic Research Laboratory
ATTN: SLCBR-DD-T
Aberdeen Proving Ground, MD 21005-5066

NO POSTAGE
NECESSARY
IF MAILED
IN THE
UNITED STATES

OFFICIAL BUSINESS
PENALTY FOR PRIVATE USE, $300

BUSINESS REPLY MAIL
FIRST CLASS PERMIT NO 12062 WASHINGTON, DC
POSTAGE WILL BE PAID BY DEPARTMENT OF THE ARMY

Director
U.S. Army Ballistic Research Laboratory
ATTN: SLCBR-DD-T
Aberdeen Proving Ground, MD 21005-9989

FOLD HERE